CLOSED-FORM SOLUTION FOR STRESS INTENSITY FACTORS OF SEMI-ELLIPTICAL SURFACE CRACKS WITH DIFFERENT INCLINATIONS IN A CYLINDER BAR UNDER PURE TENSION AND PURE TORSION

MOHAMMADKAZEM RAMEZANI

FACULTY OF ENGINEERING
UNIVERSITY OF MALAYA
KUALA LUMPUR

2018

CLOSED-FORM SOLUTION FOR STRESS INTENSITY FACTORS OF SEMI-ELLIPTICAL SURFACE CRACKS WITH DIFFERENT INCLINATIONS IN A CYLINDER BAR UNDER PURE TENSION AND PURE TORSION

MOHAMMADKAZEM RAMEZANI

THESIS SUBMITTED IN FULFILMENT OF THE REQUIREMENTS FOR THE DEGREE OF DOCTOR OF PHILOSOPHY

FACULTY OF ENGINEERING
UNIVERSITY OF MALAYA
KUALA LUMPUR

2018

UNIVERSITI MALAYA

ORIGINAL LITERARY WORK DECLARATION

Name of Candidate: MOHAMMADKAZEM RAMEZANI [redacted])

Registration/Matric No: KHA130039

Name of Degree: DOCTOR OF PHILOSOPHY (PHD)

Title of Project Paper/Research Report/Dissertation/Thesis ("this Work"):

CLOSED-FORM SOLUTION FOR STRESS INTENSITY FACTORS OF SEMI-ELLIPTICAL SURFACE CRACKS WITH DIFFERENT INCLINATIONS IN A CYLINDER BAR UNDER PURE TENSION AND PURE TORSION

Field of Study:

I do solemnly and sincerely declare that:

(1) I am the sole author/writer of this Work;
(2) This Work is original;
(3) Any use of any work in which copyright exists was done by way of fair dealing and for permitted purposes and any excerpt or extract from, or reference to or reproduction of any copyright work has been disclosed expressly and sufficiently and the title of the Work and its authorship have been acknowledged in this Work;
(4) I do not have any actual knowledge nor do I ought reasonably to know that the making of this work constitutes an infringement of any copyright work;
(5) I hereby assign all and every rights in the copyright to this Work to the University of Malaya ("UM"), who henceforth shall be owner of the copyright in this Work and that any reproduction or use in any form or by any means whatsoever is prohibited without the written consent of UM having been first had and obtained;
(6) I am fully aware that if in the course of making this Work I have infringed any copyright whether intentionally or otherwise, I may be subject to legal action or any other action as may be determined by UM.

Candidate's Signature Date

Subscribed and solemnly declared before,

Witness's Signature Date

Name:
Designation:

Abstract

Surface flaws could occur as internal or external semi-elliptical cracks in cylinder or round bars along the axial or circumferential direction. Fracture analysis has been widely implemented to predict failure of cylinder bars and engineering components caused by preexisting small cracks so that precautionary measures could be taken to either prevent future crack propagation or to determine the remaining life of the components. In order to achieve this, the Stress Intensity Factors (SIFs) must be evaluated accurately for the different Modes of fracture and crack geometries. Many approaches and models have been proposed in the literatures to evaluate the SIFs of cracks based on finite element analysis. However, very little works has focused on using the Dual-Boundary Element Method (DBEM) which is a more reliable and robust tool to evaluate the SIFs for a wide range of cracks. In this research, a systematic study was undertaken to use DBEM-based software BEASY to analyze the SIFs of semi-elliptical surface cracks with different inclination angle in cylinder bar subjected to pure tension and pure torsion. The main parameters being considered in this work to evaluate the SIFs were the crack depth to cylinder diameter ratio $\left({}^{a}/_{d}\right)$, the crack aspect ratio $({}^{a}/_{c})$, crack inclination angle (θ). Different mesh sizes have been implemented in order to achieve the optimum accuracy of the results obtained from the software. The results were validated as follows; firstly, the DBEM results obtained for each loading conditions were compared with available analytical solutions proposed by other researchers. In the second stage, the DBEM results were compared with other numerical works which have been reported in the literature. The general closed-form solutions were developed to evaluate the corresponding SIFs for Mode I, Mode II and Mode III fracture types. The solutions were obtained through a systematic curve fitting approach on the SIFs produced by BEASY. The solutions confirmed that Mode I fracture in the cylinder bar under pure tension was maximum when

the crack front was perpendicular to the load direction (crack inclination angle of 0^o) and it was minimum when crack inclination angle was 45^o. However, Mode II and Mode III fractures were negligible at the crack inclination angle of 0^o and they reached to their maximum at an inclination angle of 45^o. On the other hand, when the cylinder was subjected to pure torsion it was vice versa and Mode I fracture was negligible at the angle of 0^o where Mode II and Mode III fractures were at their peak. This research has demonstrated the viability of using DBEM-based software BEASY to evaluate the SIFs of inclined semi-elliptical surface cracks in cylinder bar subjected to pure tension and pure torsion.

Key words: stress intensity factor; surface crack; solid cylinder; closed-form solution; dual boundary element method

Abstrak

Kelemahan permukaan boleh terjadi sebagai retakan semi-elips dalaman atau luaran di silinder atau bar bulat sepanjang arah paksi atau lilitan. Analisis keretakan telah dilaksanakan secara meluas untuk meramalkan kegagalan bar silinder dan komponen kejuruteraan yang disebabkan oleh retakan kecil yang telah wujud sebelum ini supaya langkah berjaga-jaga dapat diambil untuk sama ada mencegah penyebaran retak masa depan atau untuk menentukan jangka hayat komponen. Untuk mencapai matlamat ini, Faktor Intensiti Stres (SIFs) mesti dinilai dengan tepat untuk pelbagai mod retakan dan geometri retak. Banyak pendekatan dan model telah dicadangkan dalam literatur untuk menilai keretakan SIF berdasarkan analisis unsur finite. Walau bagaimanapun, tidak banyak kajian yang telah memberi tumpuan kepada menggunakan Kaedah Elemen Sempadan Sempadan (DBEM) yang merupakan alat yang lebih dipercayai dan mantap untuk menilai SIFs untuk pelbagai keretakan. Dalam kajian ini, kajian sistematik telah dijalankan untuk menggunakan perisian BEASY berasaskan DBEM untuk menganalisis SIF retak permukaan semi-elips dengan sudut kecenderungan yang berbeza di bar silinder yang menumpukan ketegangan tulen dan kilasan tulen. Parameter utama yang dipertimbangkan dalam kajian ini untuk menilai SIF ialah kedalaman retakan ke nisbah diameter silinder $\left({}^{a}/_{d}\right)$, nisbah aspek retak $({}^{a}/_{c})$, sudut kecenderungan retak (θ). Saiz mesh yang berbeza telah dilaksanakan untuk mencapai hasil ketepatan optimum yang diperoleh daripada perisian. Keputusan telah disahkan sebagai berikut; Pertama, hasil DBEM yang diperolehi untuk setiap keadaan pemuatan dibandingkan dengan penyelesaian analisis yang tersedia yang dicadangkan oleh penyelidik lain. Di peringkat kedua, hasil DBEM dibandingkan dengan kerja-kerja statistik lain yang telah dilaporkan dalam kajian lepas. Penyelesaian bentuk tertutup umum telah dibangunkan untuk menilai SIF yang berkaitan untuk jenis retakan Mod I, Mod II dan Mod III. Penyelesaian

diperoleh melalui pendekatan pemasangan lengkung yang sistematik pada SIF yang dihasilkan oleh BEASY. Penyelesaiannya mengesahkan bahawa retakan Mod I di bar silinder di bawah ketegangan tulen adalah maksimum apabila retakan hadapan adalah perpendikular dengan arah beban (retak sudut kecondongan 0^o) dan ia adalah minimum apabila sudut retak kecenderungan adalah 45^o. Manakala, retakan Mod II dan Mod III adalah kecil di sudut retak kecenderungan 0^o dan ia mencapai maksimum pada sudut kecondongan 45o. Sebaliknya, apabila silinder tertumpu kepada kilasan murni, sebaliknya dan retakan Mod I diabaikan pada sudut 0^o di mana retakan Mod II dan Mod III berada di maksimum. Kajian ini telah menunjukkan daya maju menggunakan perisian Beasy berasaskan DBEM untuk menilai SIFs kecenderungan retakan permukaan semi-elips dalam bar silinder yang ditumpukan kepada ketegangan tulen dan kilasan tulen.

Kata kunci: tekanan faktor keamatan; retakan permukaan; silinder solid; penyelesaian bentuk tertutup; kaedah unsur sempadan dual.

Acknowledgments

I would like to express my great appreciation for those who supported me along this path, both in research and life.

To my better half and love of my life, my wife, Bita; I owe it all to you. Many thanks. In addition, I would like to thank my family for their moral and financial support during my studies.

I would like to express my sincere gratitude to my supervisors as follows:

Prof. Judha Purbolaksono for the continuous support of my PhD study and research, for his patience, motivation, enthusiasm, and immense knowledge.

A very special gratitude goes out to Prof. Ramesh Singh who have provided me moral and technical support in my research. He thought me the value of being patient and trust those who have comprehensive knowledge in research. It is evident without his support, I could not finish my research. I could not have imagined having a better advisor and mentor for my PhD study.

My thanks goes to Dr. Andri Andriyana and Dr. Liew Haw Ling for sharing their knowledge and also their helpful suggestions and supports during my research.

Lastly, I wish to thank the Ministry of Higher Education, Malaysia, for providing the financial supports through the High Impact Research Grant

(UM.C/625/1/HIR/MOHE/ENG/33).

Table of Contents

List of Figures

List of Tables

List of Symbols and Abbreviations

a	Depth of crack
b	Width or half-width of cracked plate
c	Half-length of crack
φ	Parametric angle of ellipse
σ_0	Applied tension to the cylinder bar
Q	Shape factor for elliptical crack
t	Thickness or one-half plate thickness
g	Curve fitting function
f_φ	Angular function
f_w	Finite-width correction factor
J	*J*-Integral
K_I	Mode I, SIF
K_{II}	Mode II, SIF
K_{III}	Mode III, SIF
$W(\Gamma)$	Energy Density
$\mathbf{t}$	The work-conjugate of traction
$\mathbf{u}$	Displacement
d	Diameter of Cylinder bar
L	Length of Cylinder bar
E	Modulus of Elasticity

ν	Poisson's ratio
τ_0	Applied shear to the cylinder bar
k	elliptical modulus
$K(k)$	Incomplete elliptic integral of the first kind
$E(k)$	Incomplete elliptic integral of the second kind
θ	Crack face inclination
σ_0	Applied stress to the cylinder bar
s	Crack front arc-length
F_{JM}	Boundary-correction factor for surface crack in the cylinder
f_S	Maximum value for SIFs
f_θ	Inclination-correction factor

CHAPTER ONE: INTRODUCTION

1.1 Background and Motivations

Fracture is a problem that society has faced for as long as there have been man-made structures. Due to this fast growing complex technology, this problem even got worse today than previous centuries. There are plenty of factors which can cause structural failure but from investigation on fallen structures, engineers found that microscopic cracks are the most common defect which lead to failure. It is evident that materials is never flawless and external loading or fatigue in service develops the flaw until becomes the critical crack size and finally lead to failure, the same as dislocation and impurities, etc (Kou & Burdekin, 2006).

All engineering components and structures contain geometrical discontinuities-threaded connections, windows in aircraft fuselages, keyways in shafts, teeth of gear wheels, etc. The shape and size of these features are crucial due to their impact on the strength of the artifact. If these discontinuities may not be properly designed or perfectly assembled then sharp corners, grooves, nicks, voids, etc. will emerge which cause stress concentration and lead to structure failure.

Moreover, damages like impact, fatigue, unexpected loads and so on usually happen in service. Since the maintenance of structures during their service may be poor or not proper, these damages can cause microscopic cracks and most of them are arrested inside the materials but it takes one run-way to destroy the whole structure (Beer & Johnston, 1981).

In order to avoid brittle fractures, relationship among stresses, cracks and fracture toughness is being analyzed. Systematic scientific rules were developed to characterize cracks and their effects to predict if and when the structure or their components containing

crack(s) may become unsafe during the service lives of the structure. This science is called fracture mechanics (Beer & Johnston, 1981; Zerbst et al., 2014).

Fracture mechanics is a set of theories characterizing the behavior of solids or structures with geometrical discontinuity at the scale of the structure. The discontinuity characteristic may be in form of line discontinuities in two-dimensional media like plates or shells and surface discontinuities in three-dimensional media. Fracture mechanics has developed to a mature discipline in science and engineering, and completely changed our understandings about behavior of engineering materials.

Conventional failure criteria have been evolved into strength failure of load-bearing structures which can be classified as ductile or brittle failures (Elices et al., 2017). When breakage of a structure is preceded by large deformation which occurs over a relatively long time and may be associated with yielding or plastic flow, it is considered as ductile failure. On the other hand, brittle failure is usually sudden and preceded by small deformation (Pineau et al., 2016).

Based on this failure classification, fracture mechanics can be divided into Linear-Elastic Fracture Mechanics (LEFM) and Elastic-Plastic Fracture Mechanics (EPFM) (Beer & Johnston, 1981; Song et al., 2018). For brittle-elastic materials like high-strength steel, glass, ice, concrete, etc. LEFM give ideal results. However, for ductile materials like low-carbon steel, stainless steel, certain aluminum alloys and polymers, EPFM is suited for failure evaluations.

Cylindrical components have been used widely in engineering structures such as aerospace, offshore structures, vehicle motors, power transition shafts, etc. Under the action of mechanisms such as cyclic loading, propagation of fatigue cracks may occur. One result of this propagation could be the failure of the component. In the worst case, a catastrophic collapse of a whole structure is also possible. Consequently, prediction of the propagation of an existing or postulated crack becomes an important part of a safe

design and maintenance of a structure. To predict the crack propagation life and the residual life of structure, it is necessary to know the severity of the crack, especially in terms of the crack tip conditions. In fracture mechanics, this severity can be measured by several parameters, of which the most widely used is the stress intensity factors (SIF) which depends on the crack size, geometry of cracked member and mode of loading (Irwin, 1957; Fu et al., 2017). Therefore, with the stress intensity factor known, prediction of crack propagation can be done.

The three-dimensional nature of this kind of cracks results in a stress intensity which is not only varying along the crack front but is also highly sensitive to the crack shape. Numerical techniques or approximations are often implemented to study the SIF for this problem (Newman & Raju, 1981; Chen, 2016A).

SIF was introduced by Irwin (1957) based on his previous research on Westergaard's (1939) work. He proposed SIFs as a description of the stress field ahead of crack front. Irwin has also shown that SIF is uniquely related to the energy release rate, proposed by Griffith (1920), so can be used to define fracture phenomenon (Erdogan, 1983).

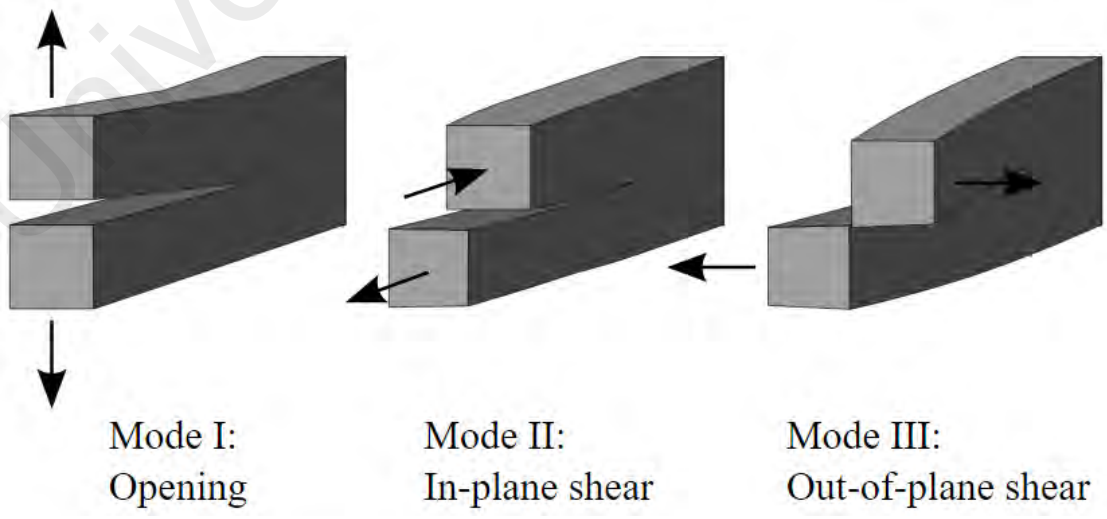

Figure 1-1: Three different crack modes in fracture mechanics (Beer & Johnston, 1981).

Three different crack modes in fracture mechanics are illustrated in Figure 1-1. Mode I or opening mode occurs when the crack is subject to tensile stresses normal to the crack plane. Displacement of the crack faces is perpendicular to the crack plane. Mode II or sliding mode results from in-plane shear loading in the crack plane. Displacement occurs in the plane and normal to the crack front. Mode III or tearing mode results from out-of-plane shear loading (Lawn & Wilshaw, 1975; Rozumek et al., 2018). Fracture propagation is controlled by the stress intensity at the crack tip, computed using SIFs for each mode of propagation, and fracture toughness. If the stress intensity at the crack tip exceeds the fracture toughness, the fracture will propagate.

A detailed assessment of crack behavior in a cylinder bar under repeated loadings is necessary, especially for long deep cracks. Solutions for stress intensity factors for surface cracks in cylinder are available in the literature for a wide range of cracks. Researchers have been evaluating SIFs of flaws in solid bodies by using different methods and practical solutions were proposed to predict stress intensity distributions along the crack front (Toribio et al., 1991; Livieri and Segala, 2016).

Lebahn et al. (2013) evaluated SIFs of semielliptical surface crack on the round bar subjected to cyclic tension and bending. SIFs were obtained from crack propagation tests and solutions were validated both numerically and experimentally. Experimental results are also available from Freitas et al. (1995) and Fonte and Freitas (1994; 1997), where fatigue crack growth tests were carried out in round bars subjected to cyclic bending and steady torsion stresses.

However, in doing an analysis of 3D crack problem, the complexities of the experimental setup is greatly concerned. Thus, a numerical analysis is always sought to reduce the experimental work. Raju and Newman (1986) evaluated the SIFs of a semi-elliptical crack using the three-dimensional finite element method. They proposed SIF closed-form solutions for cracks in plates and round bars.

Madia et al. (2011) reported SIF solutions of cracks in solid or hollow round bar subjected to mixed mode loading. They used FEM to evaluate SIFs in shafts and proposed imperial solutions for different crack sizes. Li et al. (2016) used a combined *J*-integral and Finite Element Method (FEM) to evaluate SIFs for inclined external surface cracks in pressurized pipes.

Based on the literatures, many researchers evaluated cracks on round bar with only one inclination. However, in reality, cracks may occur at any different inclinations. A comprehensive empirical stress intensity factor solution for an inclined semi-elliptical surface crack in the cylinder under pure tension or pure torsion is not provided in the literature. The lack of this solution for such a critical components in mechanical structures, led to this research reported in this thesis to find a closed-form solutions of SIF of a semi-elliptical surface cracks with different inclinations in the round bar subjected to pure tension and pure torsion.

As reported by Cisilino and Ortiz (2005), the Boundary Element Method (BEM) is found to be preferably suited for quantifying the conservation integrals. This is because the high accuracy of the displacements and stresses including their derivatives at the internal points can be obtained in BEM through their boundary integral representations, as opposed to other numerical techniques, like FEM.

For three-dimensional analyses, the conservation integrals are usually used in their so-called surface- or domain-independent form. While adopting the surface-independent form of conservation integrals, the integration can be carried out along a contour in a plane perpendicular to the crack front and also over the surface enclosed by the contour. A number of works on surface cracks by the boundary element method (BEM) have also been reported in literature.

For examples, Mi and Aliabadi (1994; 1992) presented the dual boundary element method (DBEM) for evaluating general 3D crack problems. BEASY software is based on Dual-

boundary element method (DBEM) which is developed by Mi and Aliabadi (1994) to treat the crack boundaries. The DBEM and in general BEM can be a faster and more reliable method than FEM. For example, if the same model is evaluated in both methods, DBEM needs less elements than FEM to model the crack and assess the SIF which means that it needs less computational time. On the other hand, singularity on the crack corners are well-treated in BEASY (Mi & Aliabadi, 1992; Guiggiani et al., 1991; Aliabadi et al., 1985; Citarella et al., 2016).

DBEM is excessively implemented by various researchers including Joseph et al. (2014), Chandra et al. (2014) and Siow et al. (2016) to evaluate SIFs in different models. Results proved that this method and BEASY software are accurate and reliable to be implemented for stress intensity evaluations.

In addition, in order to prove the accuracy of SIFs, obtained results from BEASY in this study have been compared and validated by popular analytical solutions such as He and Hutchinson (2000) and Newman and Raju (1981) and numerical solutions like He and Hutchinson (2000).

1.2 Aim and Objectives

The aim of this research was to develop a comprehensive closed-form solutions for Mode I, Mode II and Mode III stress intensity factors of a semi-elliptical surface cracks with different inclinations in a cylinder bar subjected to pure tension and pure torsion. To achieve this goal, followings are the objectives of the research:

- To evaluate the Stress Intensity Factors (SIFs) of semi-elliptical surface crack with different inclinations in the cylinder bar under pure tension and pure torsion by using dual-boundary element method using the software of BEASY.

- To validate the DBEM results in this research by comparing them with available analytical and numerical solutions in the literature.
- To develop a general set of closed-form solutions to evaluate the corresponding SIFs for Mode I, Mode II and Mode III of semi-elliptical surface crack by using the curve-fitting approaches.

1.3 Thesis Outline

The thesis consists of six chapters. These can be summarized as follows:

In chapter 1, introduction of fracture mechanics is briefly discussed and importance of SIFs evaluations in engineering components design is provided as well. In addition, objectives and outlines of present work are presented in this chapter.

Literature review on fracture mechanics, general SIFs studies, different methods for SIFs evaluations and closed-form solution for SIFs are discussed in Chapter 2. A brief introduction on basic equations and DBEM in BEASY is given in this chapter as well.

Research methodology used in this study is discussed in chapter 3. Modelling techniques, mesh evaluations in BEASY, variables and methods to derive the solution are main topics of this chapter.

Results and discussions are provided in chapter 4. BEASY validation in each loading, collected data from SIF evaluations and proposed closed-form solutions to evaluate the corresponding SIFs for Mode I, Mode II and Mode III of semi-elliptical surface crack in the cylinder bar under pure tension and pure torsion are proposed in this chapter.

Chapter 5 consists of conclusion and recommendations for further work.

CHAPTER TWO: LITERATURE REVIEW

2.1 History of Stress Intensity Factors

The cylindrical bars are often found in machine components and structures for various applications. Due to applied cyclic loads, material defects and improper manufacturing processes, the components may contain flaws such as surface cracks. Under cyclic loadings, a crack or flaw may propagate into a critical stage, leading to an undesirable shattering failure (Jia et al., 2016; Datta et al., 2018). Scheduled inspections shall be well planned and performed to ensure the safety of the component to be fit in service.

In doing so, understanding of the crack behaviors in components is paramount important. In particularly, quantifying the severity of a surface flaw or crack is a part of developments of the fatigue life prediction. Linear elastic fracture mechanics (LEFM) approach has been widely adopted in engineering design process to particularly evaluate the crack behaviors (Beer & Johnston, 1981).

The stress intensity factors are the quantitative values commonly used to evaluate the elastic stress-strain field in the vicinity of a crack front. Thus, the evaluation of the stress intensity factors has been a major task in LEFM since decades ago and becomes more essential, especially the possibility of the use of the data in a preliminary design stage (Song et al., 2018).

SIF have been implemented as a key factor in various criteria and models of fracture and crack growth equations (Anderson et al., 1961; Fu et al., 2017). Fracture toughness which expresses the material's resistance to brittle fracture is defined in terms of the SIF. In order to calculate the SIF, the crack problem has to be formulated as a boundary value problem of linear elasticity and solved in terms of displacement field and/or the stress field. The SIF can be subsequently obtained from Irwin's expansion of stress field (or the displacement field) in the vicinity of a crack tip (Irwin, 1957).

The SIFs have been investigated by many researchers due to its importance in LEFM. Toribio et al. (1991) evaluated SIFs of a cracked bolt subjected to tension, bending and residual stresses. The stress intensity factor is obtained by using an energetic technique, the Stiffness Derivative Method, based on the computation of the energy release rate upon a virtual crack extension. Two modifications are introduced into the computation in order to improve the accuracy of the results. It is shown that the influence of residual stress on SIFs were negligible. Kim et al. (1998) evaluated SIFs for composites with an inter-laminar crack subjected to normal loading. They applied Fourier integral transform method and a Fredholm integral equation of the first kind to evaluate Mode I SIFs for various crack ratios. Their finding were in agree with past findings in literature and confirmed that SIFs are influenced by number of layers and volume of fibers in each layer.

Dong et al. (2003) presented stress intensity factors for notch cracks by using conventional finite element method approach. The estimation method is based on a separation of an actual notch stress state into two parts. One part is a far-field stress in the form of membrane and bending components that satisfy far-field equilibrium conditions, and the other is a self-equilibrating part that provides an effective measure of the notch stress state. Their solutions not only captured the singular characteristics as the notch tip is asymptotically approached, but also recovered the far-field (or nominal) stress state.

Jiang et al. (2015) obtained SIFs of a crack in a thin pre-stressed layer. They studied the effects of tensile initial T-stress and compressive initial stress on SIFs by means of numerical calculations. It is confirmed that fracture toughness is increased by tensile initial T-stress and decreased when compressive pre-stress is applied.

Chauhan et al. (2016) presented SIF solutions at the deepest points on hypocycloidal hole in anisotropic finite plate subjected to in-plane loading. Their method can predict SIFs or

infinite plate by considering large plate size. It is shown that the whole geometry, material properties, loading angle and plate size will significantly influence the values of SIFs.

Mangalgiri et al. (1984) evaluated SIFs at the cracks emanating from circular holes in the rectangular plate under uniaxial tension along the edges. They used FEM approach to analyze the stress intensity factors. It is shown that non-linear behavior is arising due to varying contact at pin-hole interface with increasing load and it was treated by using a virtual crack closure concept of stress field at the crack tip. Lin and Smith (1999) studied on SIFs of two symmetric quarter-elliptical corner cracks in a plate subjected to remote tension. They used both quarter-point displacement and J-integral methods to calculate stress intensity factors on the cracks emanating from circular fastener holes in plates. Obtained results were compared with some other results found in the literature and their accuracy have been demonstrated in the study.

Cirello et al. (2008) developed a numerical approach by combining of two hybrid finite element formulations to analyze the stress intensity factors in cracked perforated plates with a periodic distribution of holes and square representative volume elements. The accuracy of this method was proved by experimental measurements and conventional FEM calculations. As expected the results show a strong dependence of the SIF on the crack tip location with respect to the positions of the holes; in particular, the hole is a shield for the crack when the tip is located in front of its centroid.

Moreira et al. (2009) proposed a calibration to the stress intensity factor in a cracked stiffened plate subjected to remote uniform traction by using three-dimensional finite element analyses. This method has been validated by FEM and DBEM results collected from literature. It is concluded that in a three-dimensional analysis, stress intensity factor has different values through the thickness. Thus, a two-dimensional stress intensity factor analysis is only an approximation of the exact solution. Moreover, a non-uniform stress intensity factor distribution through the thickness was obtained which justifies the non-

straight crack front of advancing fatigue cracks in stiffened panels subjected to cyclic loading.

Saimoto et al. (2010) proposed Mode I SIFs for for cracks initiated from a hole which is located in the center of a finite plate with applied tensile uniform stress was calculated by using the program of the versatile method of two-dimensional elastic problem by Body Force Method. It was investigated whether the stress intensity factors for cracks initiated with unsymmetrical lengths from both sides of the hole edges could be approximated to the stress intensity factor of a center-cracked plate with practical allowable accuracy. They concluded that, depending on crack length conditions the approximation of the stress intensity factor by using the center-cracked plate would have better results.

Livieri and Segala (2012) calculated SIF solutions of elliptical crack in a finite plate. Results obtained numerically and evaluated analytically under mixed mode loading. They proved that existing cracks in a finite body can be replaced by an ellipse and calculation of equivalent J-integral on the edge of ellipse would be easier and more accurate. Zhao et al. (2012) introduced an analytical method for calculating the stress intensity factor of an infinite plate containing multiple hole-edge cracks by using approximate superposition method. They checked the reliability of their approach by comparing their results with available FEM ones. They used an equivalent crack in plate instead of multiple one and calculate the SIFs for that one. They concluded their approach would be faster and more reliable than available conventional ones.

Kondo et al. (2014) investigated on generalized SIFs of sharp V-notched plates under transverse bending using developed Mindlin's plate theory. They performed experiments on V-notched plate subjected to singular strain field around a crack and used strain gages to study the results. They have also analyzed the same model by Finite Element Method (FEM) and compared collected data from experiments with those obtained from FEM

which were in acceptable range. It was also shown that both experimental and numerical results were in agreement with the past numerical investigations.

Uslu et al. (2014) reported SIFs of surface cracks in finite-thickness plates subjected to thermal or displacement-controlled loads. Same studies had been performed on hollow cylinders to assess SIFs subjected to thermal shock (Fillery & Hu, 2010; Nabavi & Ghajar, 2010). They proved that temperature changes do not influence on stress intensity factors. They also confirmed that SIFs of cracks subjected to thermal loadings are smaller than the same cracks under mechanical loadings. In other words, when the same thermal loads are applied to a cracked structure, it would yield higher fatigue crack growth lives than when there is no crack there. Chen (2015) used Reissner–Mindlin plate theory to investigate SIFs for cracks in plates subjected to both the bending stress singularities due to concentrated moments at boundaries and transverse shear stress singularities due to concentrated transverse shear forces at boundaries. The application of inverse Mellin transform gave the exact forms of singular stress fields near the corner, including the stress singularity orders and the generalized stress intensity factors. He used FEM results to validate hi approach and comparison proves that his approach was reliable.

Weißgraeber et al. (2016) used closed-form analytical Finite Fracture Mechanics approach to study crack initiation at elliptical holes in plates under uniaxial tension. Comparison of proposed approach with other available numerical results in the literature indicated the accuracy of the solution. Employing this stress intensity factor and the closed-form solution of the stress field in the notched plate, a Finite Fracture Mechanics (FFM) solution to the problem of crack initiation is proposed. In this FFM solution two coupled stress and energy criteria are considered. Both only require a strength and a fracture toughness parameter for evaluation and no empiric length parameters are introduced.

Iida and Hasebe (2016) presented SIF solutions for an infinite thin plate with a rhombic hole subjected to bending. They proposed approximate expressions of the stress intensity factor using the stress distribution before the crack initiation. Stress intensity factors for short cracks can be obtained precisely by implementation of these expressions. The importance of their proposed solutions is they can give the stress distribution even before crack initiation.

Dunn et al. (1997) presented closed form solutions for SIFs of cracked I-beams subjected to bending. They combined Herrmann and Sosa (1986), coupled with dimensional considerations and a finite element calibration approaches to extract expressions for SIFs. They measured fracture loads for cracked polymethyl methacrylate (PMMA) I-beams in four-point flexure. Their method was accurate and within 5% of FEM results.

Cheng (1999) proposed Mode I SIF solutions of an edge-cracked beam with fixed ends. Their approach was independent to the loading since it involves only the concept of material strength. Their proposed solution was validated by previous numerical investigation in the literature. In addition, they studied sharp cracks close to beam ends and concluded that SIFs would greatly reduce for cracks which located close to the ends.

Xie et al. (2007) studied SIFs of cracked multi-channel beams. They applied G^*-integral theory in an extremely simple manner to the infinite boundary problem such as multi-channel structures to generate closed-form SIF solutions for structural beams. Ghafoori and Motavalli (2011) presented an analytical method to calculate SIFs of cracked I-beams subjected to mixed mode bending and axial loading. Their solution was an extension to the Kienzler and Hermann (1986) and validated by experimental results. They applied an elementary beam theory estimation of strain energy release rate as the crack is widened into a fracture band and confirmed that their solution is more accurate than previous one.

Cortinez and Dotti (2013) obtained general analytical Mode I SIFs solutions for thin-walled beams. Their solution was an extension to a previous proposed solution by (Xie

et al., 1998) and claimed that their technique is more accurate other methods in the open literature up to that time. They studied the effect of wrapping effect, a very common feature in thin-walled beams on Mode I SIFs. Similar study on thin-walled composite beams have been performed by Dotti et al. (2013). Their solution was a correction to their previous proposed solution (Cortinez & Dotti, 2013) and they validated the accuracy of their formula by FEM and other available data in the literature. It was shown that approached derived for isotropic materials can be used without major problems for laminated composites thin-wall beams.

Yin et al. (2017) studied SIFs for an L-shaped corner crack in steel members with rectangular hollow section subjected to tension and bending loading. They used J-integral method based on finite element analysis to evaluate SIFs for L-shaped corner cracks with different combinations of flange and web crack lengths. It was found that the stress intensity factor at either crack tip is dependent not only on the crack length of the same side but also on the ratio of the flange and web crack lengths. The shorter side of the L-shaped corner crack tends to have larger SIF value.

Weili and Finnie (1989) evaluated SIFs for round bars and other simply closed cylindrical bodies with internal or external radial cracks. They used plane strain solutions to calculate stress intensity factors and their results were in agreement with numerical data in the literature. Peng et al. (2005) provide an assessment on a Mode I SIF solution of circumferential surface cracks in pressure vessels and pipes. They have implemented FEM to calculate the SIFs and validated their technique with both Newman's and Bergman's solutions. They have implemented FEM to calculate the SIFs and their solutions. Ricci and Viola (2006) studied on SIFs of cracked beams and bars subjected to a bending moment, shear forces and a torsion. They proposed an extension to an existing analytical solution from Kienzler and Herrman (1986). This method was based on an elementary beam theory estimation of the strain energy release as the crack is widened

into a fracture band. Moreover, they addressed the coupled bending-torsional vibration of cracked T-beams within the context of the dynamic stiffness matrix method of analyzing structures.

Dao and Sellami (2012) studied SIFs of a circumferential semi-elliptical surface crack in a hollow cylinder under mixed mode bending and tensile loading. They believed that fatigue crack growth study must cover the final crack shape as well as the initial shape. Crack propagation during each cycle must be studied and their changes have to be considered in S-N curves. Tao et al. (2015) investigated on Mode I SIFs of a crack in a nanoscale cylindrical inhomogeneity subjected to remote load. Their findings show residual interface tension has negative effect on SIF and it is influenced by inhomogeneity radius in the specimen. Liu et al. (2016) evaluated SIFs of an axial crack in cylindrical shell experimentally using optical caustic method. They proved that increasing the shell thickness or decreasing the shell radius would result in a larger caustic spot at the crack tip. In addition, their results have been compared with other numerical results which shows the accuracy of their proposed method.

Fu et al. (2017) determined stress intensity factors for mixed mode fracture induced by inclined external surface cracks in pipes under axial tension and bending, using a combined J integral and 3 dimensional finite element method. It was concluded that, for given wall thickness to internal radius ratio and crack depth to half crack length ratio, the absolute values of the influence coefficients of all three modes I, II and III stress intensity factors along the whole crack front increase with the increase of the relative depth for all inclination angles of the surface cracks. It is also found that the crack propagation angles in depth of the inclined cracks increases in magnitude along the whole crack front with the decrease of the crack inclination angle defined as the angle between the crack and pipe axial direction.

Dhakad et al. (2017) investegiated the fatigue crack growth behaviour of surface cracked piping, pressurized base straight component (PBSC) and pressurized base straight weld component (PBWC) are performed on the basis of the linear elastic fracture mechanics principles. It is concluded that the available open literature SIF solutions like ASM and Bergman for external surface cracked straight pipe case having the semi-elliptical crack profile predicts the fatigue life of the component when having constant crack depth profile.

Gintalas et al. (2017) provided mid-wall stress intensity factor and normalized T-stress solutions for through-wall cracked pipes under bending for a range of crack sizes and pipe radius to wall thickness ratios by using an extensive series of finite element calculations. These solutions have been fitted by polynomial equations enabling their use for practical assessments for a range of crack sizes and pipe radius to thickness ratio.

Mahbadi (2017) evaluated tress intensity factors of rotating solid disks or cylinders with a radial crack subjected to a uniform tension at their outer surface and a uniform temperature change through the body. The stress intensity factors are obtained applying an approximate method and using the proper geometric functions for combination of the thermomechanical stresses. Results showed good agreement with numerical data collected from literature.

Rubio et al. (2017) proposed SIF expressions of an open crack with sickle shape, located at the central section of a shaft, as a function of the relative depth of the crack, the shape factor and the relative position on the crack front. They used a 3D numerical FEM analysis considering different elliptical geometries of the crack to determine SIFs along the crack front. Results have been validated by other numerical investigations in the literature. Finally, the sickle crack propagation has been analyzed using a developed algorithm based on the Paris Law and the expression for sickle cracks proposed. The

results obtained with the propagation method indicate that, regardless of the initial geometry, the sickle crack becomes straight with growth.

2.2 Different Methods to Evaluate SIFs

2.2.1 Experimental Evaluations

Researchers executed many experimental investigations, theoretical studies and numerical analysis to obtain SIF solutions for surface cracks in a smooth round bar. He et al. (2016) developed an experimental procedure for accurate evaluation of mode I SIFs of a surface crack in the plate. They have studied the effect of non-singular displacement terms in the area close to crack tip and proved that their method is much more accurate than existing experimental methods. They suggested that this method can be applied to other structures subjected to different loadings. Deschenes et al. (2017) studied a new experimental method to evaluate the influence of welding residual stresses (RS) on fatigue crack propagation rate (FCPR) in mode I SIFs. They works led to the development of a novel specimen geometry, named CT-RES, in which RS are introduced by weld bead deposition far from the region in which fatigue crack propagation (FCP) occurs. As a consequence, the effect of factors influencing FCPR other than RS such as microstructural changes or plastic deformation, often introduced by welding processes, can be avoided.

Chakraborti et al. (2017) introduced a robust technique for experimental determination of mode I stress intensity factor in orthotropic materials using only a single strain gage. The reliability of this method is established by theoretical foundation and finite element based analysis. They confirmed that accurate values of Mode I SIFs are achievable if strain gage locations are selected as per the criteria set by the proposed approach.

Kazarinov et al. (2017) presented experimental data on dynamic crack propagation in square PMMA plates of two types – 3.5 and 20 mm thick. Samples were loaded dynamically (mode I loading type) and crack tip position was registered using high speed camera. Explosion of a copper wire due to high electrical current was used to load faces of the initially prepared cracks. Mode I SIFs were obtained by application of caustics method. Thick samples demonstrated considerably higher values of final crack travel distance and higher crack velocity values. Additionally, it is shown that stress intensity factor were dependet on crack velocity. Saboori et al. (2017) conducted a series of fracture experiments on PMMA U-notched samples using an improved loading configuration, which was redesign of the apparatus recently presented for doing fracture tests under combination of tensile and out-of-plane shear loading. In order to assess the effect of notch tip radius, the tested specimens are fabricated with three different radii. Consequence of comparing the theoretical and experimental results for different notch tip radii reveals that both criteria are accurate enough to predict the fracture behavior of the U-notched engineering members subjected to mixed mode I/III loading. It is not found any considerable difference between the curves of fracture initiation angle and fracture resistance resulted from the PS and MS criteria. The criteria also show that the out-of-plane fracture angle due to pure mode III loading is constant and independent of the notch tip radius. Gonzales et al. (2017) used Digital image correlation (DIC) techniques to obtain the SIF via experimental J-integral evaluations in an AISI 4340 steel disk-shaped compact-tension (DCT) specimen subjected to mode I loading conditions. The proposed analytical-experimental hybrid approach was then applied to investigate the influence of crack closure on SIF measurements under constant amplitude loading conditions, after and before the application of overloads. It was concluded that the use of linear-elastic equations to calculate the SIF values from the DIC measurements can lead to improper

conclusions if the effects of phenomena such as crack closure, crack tip blunting or residual strains are not taken in account in the analyses.

Rozumek et al. (2017) investigated on experimental results of the crack path and description of fatigue crack growth in plane specimens made of S355 steel under tension and bending with torsion. Specimens with rectangular cross-sections and stress concentrator in the form of external one-sided sharp notch were used. They concluded that under mixed mode condition Mode I + Mode II the fatigue lifetime increase with the loading angle value due to decreasing of the Mode I. In addition, increasing in the angle of alpha - determining a ratio of the torsional moment to the bending moment – will lead to decrease of the fatigue life and for alpha equal to 45^{o} a higher crack growth rate is observed for mode I, which goes into mode III domination.

James and Anderson (1969) described a simple procedure of performing an experimentation to determine the stress intensity factor of an internally pressurized cylinder with a through-the-wall longitudinal crack for which no analytical solution was available. Experimental results are available from Freitas et al. (1995) and Fonte and Freitas (1994; 1997), where fatigue crack growth tests were carried out in round bars subjected to cyclic bending and steady torsion stresses. Lebahn et al. (2013) evaluated SIFs of semielliptical surface crack on the round bar subjected to cyclic tension and bending. SIFs were obtained from crack propagation tests and solutions were validated both numerically and experimentally. They proposed solutions for SIFs of elliptical and straight front cracks and proved that those solutions are in agreement with previous investigations.

Stacker and sander (2017) evaluated fatigue life of a round bar under constant and variable amplitude loadings in the very high cycle fatigue regime. They compared collected data from experiments with three-dimensional FEM modelling and available analytical approaches in the literature. Fractographic investigations of the fracture

surfaces and the common crack initiating imperfections are performed by means of optical microscopy and scanning electron microscopy. The evaluation of the cyclic stress intensity factors on the basis of the inclusion size shows smaller values for increasing stress ratios. Also, with increasing number of cycles to failure the stress intensity factor range decrease. Roiko et al. (2017) studied growth of small cracks initiated from microscopic notches and loaded near the growth threshold in round bar under different stress ratios experimentally. The results of in-situ optical measurements during high cycle fatigue testing show that small cracks initiate and grow quickly after which there is a long period of slow growth until the large crack growth threshold is reached. The crack growth rate data from different loading ratios indicates that the positive portion of the stress amplitude or the maximum stress intensity factor can be used to compare crack growth rates. The test data also shows that increasing only the compressive stress portion of the loading will cause an arrested small crack to grow again.

Ozturk et al. (2017) developed an experimentally calibrated and validated crystal plasticity finite element model with a probabilistic crack nucleation model for predicting dwell and cyclic fatigue crack nucleation in polycrystalline microstructures of titanium or Ti alloys. Experimental characterization of failed samples reveal that crack initiation on planes are highly inclined away from the stress axis. At higher peak stresses, time-dependent load shedding mechanism dominates, introducing a significant dwell debit, while limited dependence on stress hold is observed at lower peak stresses.

Campagnolo et al. (2017) evaluated the fatigue criterion based on the average value of the strain energy density (SED) to re-analyse some experimental results reported in the recent literature and obtained by fatigue testing notched bars under pure torsion and under torsion with superimposed static tension loadings. The tested specimens were characterized by different notch tip radii and were made of stainless and carbon steels. The fatigue crack initiation and propagation phases of each tested specimen were

monitored by adopting the electrical potential drop method. It has been observed that by adopting a definition of the crack initiation life in correspondence of an initiated crack depth about equal to the structural volume size, the SED-based syntheses could have been improved.

Yang et al. (2017) investigated the effect of stress ratio on the very high cycle fatigue (VHCF) behaviors of titanium alloy by implementation of ultrasonic fatigue tests. Based on fractography and fracture mechanics, the fatigue failure process was congruously divided into four stages: (1) crack initiation induced by cleavage of primary α grains and its coalescence; (2) microstructure-sensitive slow crack propagation; (3) microstructure-insensitive fast crack propagation; and (4) final fatigue failure. For surface crack initiation, less than 3% of the total fatigue life was consumed in fatigue crack propagation stage in the VHCF regime. Furthermore more than 95% of the total crack growth life contributed to microstructure-sensitive crack propagation stage in the HCF and VHCF regimes. The effect of the stress ratio on fatigue crack propagation life was not found.

Li et al. (2017) performed axial loading tests with variable stress ratio to evaluate the very high cycle fatigue property of TC4 titanium alloy, and a life prediction approach associated with failure mechanism was proposed. The interior failure process is characterized as: (1) occurrence of slip lines or bands on partial α grains, (2) nucleation of micro-cracks within some α grains, (3) coalescence of micro-cracks and formation of granular bright facets, (4) stable macro-crack growth within fisheye (5) unstable crack growth outside fisheye and (6) momentary fracture. The fatigue life prediction method associated with crack nucleation and growth is valid on the basis of the good agreement between the predicted and experimental results, especially in the VHCF regime.

2.2.2 Numerical Evaluations

2.2.2.1 Finite Element Method

The analysis of 3D crack problem, the complexities of the experimental setup is of great concern. Thus, a numerical analysis is always considered to reduce the experimental work. Raju and Newman (1986) generated the SIFs of a semi-elliptical crack by using the three-dimensional finite element method and proposed a closed-form solution by implementation of curve-fitting approach on obtained data from FEM. Their solutions works for surface cracks in infinite body, corner cracks and embedded cracks accurately. These solutions are fundamental closed-form solutions for stress intensity factors in research history. These solutions are used, validated and modified by many researchers later.

Carpinteri (1992A; 1992B) proposed SIF solutions for straight-front and semi-elliptical cracks in round bars under tension. He used FEM to produce SIFs and validated his results by comparing them with previous investigations such as Raju and Newman (1986). In his approach, he shifted the finite element midside nodes near the crack front to quarter-point positions. Levan and Royer (1993) reported the SIFs for transverse circular cracks in round bars subjected to tension, bending and twisting by using the boundary integral equation method. They proposed SIF solutions for Mode I, Mode II and Mode III SIFs along the crack front for a wide range of crack geometries. The reliability of their method was proven by comparing obtained results with analytical, experimental and numerical results available in the literature.

Fonte et al. (1999A; 1999B) studied the behavior of surface flaws in a round bar subjected to bending and torsion loading. They used three-dimensional FEM approach to obtain the SIFs. They confirmed that in the round bar subjected to the bending only Mode I SIFs are non-zero. Firstly, they validated their model for Mode I with available results in the literature. Then they proceed to the torsional loading and found that Mode III SIFs are

maximum at the deepest point in the crack where Mode II SIFs are zero and Mode II SIFs are maximum where crack front intercepts the free surface.

Rajaram et al. (2000) proposed a new method to obtain fracture mechanics singularity strength such as J-integral, SIFs, fatigue life, etc. by using CAD packages which can create complicated 3D models and "automatically" mesh them with tetrahedral elements. The created model in CAD can be analyzed in FEM for further evaluations. The practicality of the proposed method lies in its ability to obtain accurate results from rather irregular tetrahedral meshes readily obtained from commercially-available CAD packages possessing fairly good meshing capabilities. They applied their method to different 2D and 3D cracks in plates, prismatic and round bars and achieved to high accuracy in analysis.

Shih and Chen (2002) proposed the dimensionless Mode I SIFs of an embedded elliptical crack in a round bar by introducing collapsed singular elements in the ANSYS finite element software. They also used curve-fitting approach on results obtained by FEM to formulate the SIFs of elliptical cracks. Their results showed that SIFs are positively influenced by crack depth ratio but crack aspect ratio has negative effect on them. Guo et al. (2003) evaluated SIFs of elliptical surface cracks in notched round bars under tension and proposed an empirical equation for the SIF of surface cracks in notched round bars. They used three-dimensional Finite Element Analysis (FEA) models to study SIFs at the crack front. They validated their results by comparing them with available numerical and experimental results in the literature. It is shown that SIFs are strongly affected by the theoretical stress concentration coefficient.

Noda and Takase (2003) studied V-shaped notched round bar under tension, bending and torsion and introduced generalized SIFs K_{I,λ_1}, K_{II,λ_2} and K_{III,λ_3} by using the singular integral equation of the body force. They compared their results with Benthem-Koiter's formula (Benthem & Koiter, 1973) and confirmed that their results is more accurate than

them. Dyja et al. (2004) studied experimentally and numerically rolling round reinforcement rod. They used FEM simulations of the process of rolling round helical-ribbed rods to determine the specific Mode flow within the gap. They also did experimental study to validate their findings from FEM. Shin and Cai (2004) evaluated the SIFs of a semi-elliptical surface crack in a rod subjected to tension and pure bending for different crack aspect ratios by the experiments and numerical modeling using the ABAQUS FEA codes. They provided SIF solutions along the crack front in terms of crack aspect ratio, crack depth ratio and place ratio. They compared their results with other available results in the literature and concluded that their proposed SIF values at the deepest point on the crack are in good agreement with other results. However, SIF trends and values at the surface interception is a little bit different with other results due to singularity and stress intensity there.

Courtin et al. (2005) proposed SIF distribution by using the energetic method which consists in calculating the J-integral values on rings surrounding the crack tip in the FEM based-software ABAQUS. They compared their proposed method with the displacement extrapolation technique which requires orthogonal meshes and singular elements are not automatically accessible in all finite element codes for it. It is shown that the J-integral method shows some advantages compared to the displacement extrapolation one. First of all, this method may be applied automatically with the ABAQUS code. Then, the knowledge of the exact displacement field in the vicinity of the crack tip is not required, and the use of singular finite elements is not essential anymore. Besides, non-orthogonal meshes are without effect on the SIF calculations. The user has just to be sure that a convergent value is obtained on the different rings.

Shahani and Habibi (2007) studied the problem of mixed mode fracture induced by a semi-elliptical circumferential crack lying at the outer surface of the cross-section of a hollow cylinder subjected to bending moment and torsion. Stress intensity factors in

mixed mode condition were determined using three-dimensional finite element modeling with 20 node-isoparametric elements and the singular form of these finite elements at the crack front. Results were proven to be reliable by comparing against available data in literature. However, when torsion is added to tension and bending moment, a non-symmetrical distribution of stress intensity factor along the crack front is observed which can cause non-symmetric fatigue crack propagation.

Madia et al. (2011) reported SIF solutions of cracks in solid or hollow round bar subjected to mixed mode loading using FEM approach. They proposed closed-form analytical as well as table geometry functions for various cracks on the solid or hollow axle body. Ismail et.al (2012) reported various SIF results for a surface crack in a round bar under tension, bending, torsion and mixed-mode loadings. They used FEM to obtain SIF for each single loading and mixed mode loading. Then, they proposed a solution for SIFs which can predict the combined SIF by using FEM results. However, they found some differences between two methods due to crack face interceptions and deformations. Predan et al. (2013) used FEM to evaluate SIFs for circumferential semi-elliptical surface cracks in a hollow cylinders under torsion. They proposed SIF solutions for Mode II and III by using polynomial approximation formulas. It is shown that Mode II is acquired higher values in shallow cracks than deep ones. It is also confirmed that higher values of SIFs were achieved at the interception points than other points along the crack front for fatigue crack growth in hollow cylinder under pure torsion. They confirmed that Mode II SIFs are dominant in crack propagation.

Sodeifi and Hosseini (2015) studied the effect of three important parameters including the notch length and width and confining pressure on the mode I critical SIF using a thick-walled hollow cylindrical marly specimen. A triaxial stress was applied on the specimen and the pressure required for the propagation of the artificial notches was measured. Three tests were conducted to investigate the effect of each parameter on the mode I

critical SIF. The experimental critical SIF was compared with the average critical SIF obtained from ABAQUS and ANSYS. It was found that the mode I critical SIF decreased with increasing in the notch width and increased with increasing in the notch length. The critical SIF nonlinearly increased with increasing in confining pressure.

Zhao et al. (2016) studied dynamic SIFs of cracked rail shafts at high speed by a 3D explicit FEM model. Their results showed that static solutions of the crack face contact are different from dynamic ones and crack propagation is a dynamic phenomenon. In addition, during movement, vertical cracks are completely closed by bending loading which indicates the absence of Mode I SIFs along the crack front where Mode II and Mode III SIFs got increased. Findings showed that vertical crack in the absence of lubricant and lower traction efforts will probably not propagate. Li et al. (2016) used a combined *J*-integral and Finite Element Method (FEM) to evaluate SIFs for inclined external surface cracks in pressurized pipes subjected to mix mode loadings. Their results showed that increasing in crack inclination will lead to deacrease of Mode I SIFs. However, Mode II and Mode III will increase and reach to their maximum values at the angle of 45^{o}. It is also found that the influence coefficients of all three modes increase with the increase of crack relative depth along the whole crack front.

Isidoro and Martins (2016) used FEM and FEA together with LEFM concepts to investigate on SIFs of semi-elliptical surface crack on round bar subjected to bending and torsion. Results proved that when bending loading is dominant only Mode I SIF values are high in the component. However, in pure torsion, Mode II and Mode III values become dominant ay crack tip. Hashimoto et al. (2017A; 2017B) conducted the rolling contact fatigue (RCF) test by using a specimen with a small drilled hole. In the first step, they quantified the crack-growth threshold according to fracture mechanics principles by using the finite element method to analyze the Mode II stress intensity factor. Then they correlate the obtained values of Mode II SIFs with values of penny-shaped cracks in an

infinite body under uniform shear. It was concludeded that the crack-size dependency of the threshold SIF range, well-known for Mode I fatigue cracks, also exists for Mode II fatigue cracks, as produced after rolling contact. The values of the threshold SIF range obtained by the RCF tests were in good agreement with those obtained in the torsional fatigue tests under static compression.

Pourheidar et al. (2018) evaluates SIFs for the semi-elliptical surface cracks, applicable in the geometrical transitions and axle body of railway axle by using FEM. The stress intensity factor were estimated applying analytical solutions for two different non-linear stress state (bending,press-fit). Comparing the results with finite element solutions revealed that Wang-Lambert weight function gives the best approximation where the maximum difference was found to be less than 5% for the deepest point and 8% for the surface point. The impact of stress intensity factor approximation in residual life time prediction were investigated through series of crack propagation simulations considering realistic load spectra and a comparison with the available experimental results in the literature.

Zhang and Guo (2018) proposed a singular Voronoi cell finite element model (SVCFEM) for estimation of the mixed-mode stress intensity factors of crack tip. Formulation of a singular Voronoi cell finite element is based on a modified complementary energy principle. To satisfy the stress singularity at the crack tip, they enriched stress solution in assumed stress hybrid model. In addition to polynomial and reciprocal terms, singular stress terms of Williams's expansion were added for elliptical crack to capture crack-tip stress concentrations. After obtaining the stress, SIFs of model I and model II were calculated using linear least-squares method. Comparisons of SVCFEM solution with analytical solution for crack are made to demonstrate the efficiency of SVCFEM.

2.2.2.2 Boundary and Dual-Boundary Element Method

As reported by Cisilino and Ortiz (2005), the BEM is found to be preferably suited for quantifying the conservation integrals. This is because the high accuracy of the displacements and stresses including their derivatives at the internal points can be obtained in BEM through their boundary integral representations, as opposed to other numerical techniques, like FEM. For three-dimensional analyses, the conservation integrals are usually used in their so-called surface- or domain-independent form. While adopting the surface-independent form of conservation integrals, the integration can be carried out along a contour in a plane perpendicular to the crack front and also over the surface enclosed by the contour. A number of works on surface cracks by the boundary element method (BEM) have also been reported in literature.

For examples, Mi and Aliabadi (1994; 1992) presented the dual boundary element method (DBEM) for evaluating general 3D crack problems. BEASY (BEASY 10 Release 14) software is based on Dual-boundary element method (DBEM) which is developed by Mi and Aliabadi (1994) to treat the crack boundaries. This method is based on the displacement and the traction integral equations that can be written, respectively, as (Mi & Aliabadi, 1994):

$$C_{ij}(\mathbf{x}')u_j(\mathbf{x}') = \int_S U_{ij}(\mathbf{x}',\mathbf{x})t_j(\mathbf{x})dS - \int_S T_{ij}(\mathbf{x}',\mathbf{x})u_j(\mathbf{x})dS \qquad \text{Eq. 2-1}$$

$$\frac{1}{2}t_j(\mathbf{x}') + n_i(\mathbf{x}')\int_S S_{kij}(\mathbf{x}',\mathbf{x})u_k(\mathbf{x})dS = n_i(\mathbf{x}')\int_S D_{kij}(\mathbf{x}',\mathbf{x})t_k(\mathbf{x})d\Gamma(\mathbf{x}) \qquad \text{Eq. 2-2}$$

Where $\mathbf{x}$ and $\mathbf{x}'$ are boundary and source point, respectively. i and j represent Cartesian components, the coefficient C_{ij} is given by δ_{ii} (Kronecker delta function) for a smooth boundary at $\mathbf{x}'$, $T_{ij}(\mathbf{x}',\mathbf{x})$ and $U_{ij}(\mathbf{x}',\mathbf{x})$ denote the Kelvin traction and displacement fundamental solutions, respectively, S_{kij} and D_{kij} contains derivatives of $T_{ij}(\mathbf{x}',\mathbf{x})$ and $U_{ij}(\mathbf{x}',\mathbf{x})$, n_i is the outward normal vector and S represents the domain surface.

These fundamental integrals in Eq. 2-1 and Eq. 2-2 are regularly provided for $\boldsymbol{R} \neq 0(\boldsymbol{R} = |\mathbf{x} - \mathbf{x}'|)$. Since these solutions are order of $1/\boldsymbol{R}$ in U_{ij}, $1/\boldsymbol{R}^2$ in T_{ij} and D_{kij} and $1/\boldsymbol{R}^3$ in S_{kij}, they will exhibit singularities when the distance $\boldsymbol{R}$ tends to zero. Accurate integration procedures for these singular integrals have been reported in References (Mi & Aliabadi, 1992; Guiggiani et al., 1991; Aliabadiet al., 1985).

Gao et al. (1992) studied SIFs of cracks in an elastic elliptic inclusion using 2D BEM. They used quadratic quarter-point crack-tip elements method to directly evaluate stress intensity factors of cracks which lie along the interface between dissimilar materials. They have also considered the effects of the mismatch of the shear modulus of the inclusion and that of the matrix in their presented results.

Zamani and Sun (1993) obtained an analytical SIF solution at crack tip elements using BEM. In their approach they proposed an algorithm which employs singular crack tip elements where SIF appears as a degree of freedom. Their solution can predict SIF accurately along the crack front. Olsen (1994) used BEM to determine Mode I and Mode II SIFs. He utilized the conservation laws on the circular path around the crack tip and crack face to evaluate SIFs. In order to show the accuracy of the proposed method, they tested results numerically and confirmed that total computed energy release rate showed the highest accuracy where Mode I and Mode II SIFs were less accurate. However, calculate T-term in this method was not accurate.

Guozhong et al. (1995) proposed SIFs of semi-elliptical surface cracks in plates and cylindrical pressure vessels using Hybrid BEM. Firstly, they used a hybrid boundary element method to model a three-dimensional linear elastic fracture analysis and extracted the first and the second kind of boundary integral equations. Then, they presented the discretization of boundary integral equations, the divisions of different boundary elements, and the procedures for the calculations of singular and hypersingular

integrals in detail. Finally, SIFs have been proposed for surface cracks in finite thickness plates and cylindrical pressure vessels. Results indicated high accuracy of proposed method for the analysis of surface cracks.

Man et al. (1995) studied SIFs of symmetrical and non-symmetrical cracks emanating from lugs in the presence of contact stresses. They used BEM and special techniques to model the problem and solved it in a systematic way. The technique used based on an efficient boundary element contact analysis with iterative and fully incremental loading procedures. This technique is applicable to the solution of non-linear frictional contact problems in cracked structures. Obtained results are shown to be dependent on the coefficient of friction.

Rigby and Aliabadi (1997) evaluated SIFs of cracks at attachment lugs using BEM and *J*-integral. In their study, they investigated on the single and two symmetrical corner elliptical cracks in the shanked lug. Results were in good agreement with available data in the literature. Wearing and Ahmadi-Brooghani (1999) evaluated SIFs of cracks in plate subjected to bending loading using BEM. Different combinations of boundary conditions, crack configurations and loading conditions were considered in their study to illustrate the effectiveness of BEM. To calculate the stress intensity factors, the J-integral method, the displacement extrapolation method, the quarter point approach and the stress extrapolation method were implemented and final results from each method have been compared with either FEM or analytical results available in the literature. Findings confirmed that proposed method showed good agreement in all cases.

Matsumto et al. (2000) evaluated SIFs of biomaterial interface cracks based on interaction energy release rate and BEM sensitivity analysis. They proved that their method can give more accurate results with a coarse mesh than displacement extrapolation method used in BEM analysis to compute the SIF and the computation cost required for this method is small due to small differential extension of the crack. Dirgantara and Aliabadi (2002)

introduced stress intensity factor solutions for several crack configurations in plates subjected to internal pressure, and also combined bending and tension by using DBEM. SIFs were obtained by a crack surface displacement extrapolation technique and the J-integral technique and several new results for edge crack and cracks emanating from a hole were also presented.

Cisilino and Ortiz (2005) and Ortiz et al. (2006) extensively reported the computations of SIFs of three-dimensional crack problems using the BEM. They implemented bi-quadratic variation approach to obtain SIFs. Their method gives better results at the deepest point on the crack than crack interception with free surface where this method fails.

Mavrothanasis and Pavlou (2007) developed a suitable Green's function for the infinite elastic solid, containing internal penny-shaped crack and loaded by a singular co-axial tensile and radial ring-shaped source acting outside or on crack faces. The corresponding boundary integral equation (BIE) is solved by the BEM for the calculation of the mode-I stress intensity factor of cracked axisymmetric finite bodies under tension. The proposed technique has three advantages: (a) it does not require discretization of the crack surface, (b) it does not require multiregion modeling and (c) it reduces the 3-D discretization of the solid to 1-D, resulting in substantially reduced effort. Numerical results are derived for the case of a cylindrical bar with a central penny-shaped crack located in a plane normal to its axis, loaded by tensile force. The accuracy of the SIF results was guaranteed due to the fact that the singularity at the crack tip was included in the Green's function

Purbolaksono et al. (2009) used DBEM to study SIFs of multiple semi-elliptical cracks in bi-material tubes under internal pressure. They proved that when Young’s modulus of the inner part is greater than of the outer part, SIFs for the internal surface cracks would be higher than those of free scale tubes. However, for external surface cracks it is vice versa. Barroso et al. (2012) studied generalized SIFs of corner cracks in multi-material

plates using BEM. They applied a simple least squares fitting approach to the numerical results obtained from BEM along the boundary edges in a multimaterial corner. The tool has been shown to be useful in the computation of generalized SIFs in complicated practical situations, as is the case of an adhesively bonded double-lap joint between aluminum and a unidirectional 0° CFRP laminate.

Alatawi and Trevelyan (2014) introduced a method to evaluate SIFs for 2D problems by using Extended Boundary Element Method (XBEM). Their solutions give Mode I and II directly in contrary to BEM equations which need post-processing like J-integral for SIF calculations. Their results converge to the same values as those from the J-integral. They validated their solutions with numerical available data. Joseph et al. (2014) reported SIFs of a corner crack emanating from a pinhole in a cylinder subjected to cyclic tension. Results confirmed that smaller cracks show higher stress intensity factors and cracks at the pinhole edge tends to grow faster than those at cylinder edge.

Chandra et al. (2014) studied SIFs and fatigue crack growth of a corner crack in the prismatic bar under combined cyclic torsion-tension loads. They confirmed that for larger cracks Mode II SIFs at crossed surface points have larger values but Mode I SIFs acquired less values. Initial crack aspect ratio of $a/c \neq 1$ was evolving to a unity at a number of cycles before fracture. High values of Mode III SIFs observed at larger torsional loading for cracks with aspect ratio of $a/c \neq 1$. Siow et al. (2016) studied SIFs of a corner crack in metallic prismatic bars subjected to multi-axial fatigue loading. They used DBEM to evaluate SIFs in prismatic bar under cyclic bending and torsional loading. Their findings indicate that corner cracks in prismatic bars tend to grow along their depth direction than their front direction. In addition, larger cracks acquire higher values of SIF due to higher stress concentrations at the sharp tip of crack ends.

Cui et al. (2017) proposed contour integral approaches to calculate SIFs for two-dimensional cracks. The proposed approaches are derived from the conservative J- and I-

integrals, in which constant elements of the displacement discontinuity method (DDM) are employed. Two numerical examples, a horizontal straight crack and a slanted straight crack under uniaxial tension at infinity, were conducted to demonstrate the validation of the approaches. Numerical results confirm that highly accurate SIFs can be extracted by integral contours remote from crack tip and increasing the total number of DDM elements can improve accuracy significantly.

Yan et al. (2017) established a novel boundary type meshless method called continuous–discontinuous hybrid boundary node method in which the enriched discontinuous shape function is developed to solve linear elastic crack problems. Both single mode and mixed mode problems can be solved by this method. A number of examples are calculated by this method, and comparisons are made between the stress intensity factors obtained by this method and some published results in the literature to endorse the accuracy of this method. The numerical examples are shown that the present method is effective and can be widely applied in practical engineering.

2.2.3 Analytical and Closed-Form Solutions

Analytical and Closed-form SIF solutions are also reported excessively in literature. One-dimensional crack problems have already been evaluated excessively in analytical and numerical ways (Murakami, 1987), including cracks in anisotropic and orthotropic materials (see for example Arnold and Binienda, 1995 and Delale et al., 1991) and the interaction of multiple cracks (Tan et al, 1993). However, most factual cracks are in embedded shapes or surface breaking planar cracks and subjected to complex two-dimensional stress fields. Unfortunately, for most planar cracks and applied loadings exact SIF-solutions cannot be obtained.

Since analytical solutions are the most general and ready to use in any engineering applications, they are likely the most wanted ones. An embedded circular crack in an infinite body was the first analytically evaluated crack. Sneddon (1946) has analyzed a simplified case of this problem when the load direction was parallel to the center of the crack. In order to solve the unknown crack opening displacement, the mixed boundary conditions in the crack plane can be transformed into a pair of dual integral equations. This set of equations can be analytically solved. The stress field and the displacement field can be obtained in the form of special integral representations when the crack opening displacement has been solved.

Kassir and Sih (1975) developed Sneddon's solution for the problem of a circular crack under arbitrary applied normal loading. The modified method was based on the Fourier expansion of the applied stress field, the unknown crack opening displacement and the SIF in polar coordinates. For each term of the SIF expansion, a set of dual integral equations was derived and analytically solved. Fabrikant (1989) investigated on another method for the circular crack problem. His method was based on a special integral representation of the distance between two arbitrary points and subsequent integral transforms.

Analytical SIF-solutions for planar cracks with more complicated geometries have been derived only for certain special cases of the applied stress fields. The first contribution concerning the analysis of a stress field near an elliptical crack was made by Galin (1961) who derived the solution for a contact problem for a punch of elliptical cross-section acting against a semi-infinite elastic body. His solution was adopted later for an inverse problem of a pressurized crack which is presently known as Galin's theorem. It states that if an elliptical crack is opened up by the applied pressure in the form of a polynomial, the form of the crack opening displacement also includes a polynomial of the same type.

Sih and Kassir (1975), Kobayshi and Shah (1971), Nishioka and Atluri (1983) and Martin (1986) obtained SIF-solutions for an elliptical crack subjected to various polynomial stress fields. They used the same method based on the representation of the displacement field and the stress field around an elliptical crack by means of one harmonic function. This function satisfies the mixed boundary conditions in the plane of the crack and can be represented by a system of potential harmonic functions in ellipsoidal coordinates. If the applied pressure has the form of a polynomial, then the boundary condition in the crack domain can be transformed into the system of algebraic equations with unknown coefficients. The main difficulty of this method is the calculation of the derivatives in ellipsoidal coordinates. Also, this approach cannot be used for an arbitrary applied stress field.

Martin in (1986) used the method of expansion of the applied stress field and the unknown crack opening displacement into the system of orthogonal Gegenbauer polynomials. The boundary condition in the crack domain is transformed into a system of linear algebraic equations. In general it is a system with an infinite number of equations, but it can be truncated in the case of a polynomial applied stress field. The SIF-solutions were obtained for constant, linear and quadratic stress fields.

Pommier et al. (1999) obtained a set of Mode I SIF solutions of semi-elliptical surface crack subjected to various stress distributions. They used body force method (Nisitani & Murakami, 1974) to evaluate SIFs. The method allows the prediction of the crack shape and stress intensity factor during the growth of the crack. The stress intensity factor equations presented herein should be useful for correlating fatigue crack growth rates of «mechanically» short cracks.

Guo et al. (2007) derived the stress intensity factor for a single edge crack originating from the T-plate weld toe from a general weight function form and two reference stress intensity factors. The weight function together with the stress distribution on the crack

plane was used to obtain the stress intensity factor solutions. The validity of the weight function for the T-plate was verified by the comparison with the numerical data available in the literature. Through these analyses, it has been demonstrated that for the padded plate geometries considered, the stress intensity factor for a cracked padded plate can be obtained using the weight function of a T-plate together with the actual stress distribution on the crack plane for the uncracked padded plate geometry.

Lin and Pan (2008) introduced the theoretical framework and closed-form stress intensity factor solutions in terms of the structural stresses for spot welds under various types of loading conditions based on elasticity theories and fracture mechanics. The loading conditions of interest were the resultant loads on the inclusion with respect to the center of the inclusion in a finite or infinite plate and the surface tractions on the lateral surface of a finite or infinite plate. Based on the J integral for a strip model, closed-form analytical stress intensity factor solutions for spot welds joining two sheets of equal thickness are derived in terms of the structural stresses around a rigid inclusion in a plate under various types of loading conditions.

Xu et al. (2010) found analytical solutions for SIFs and T-stresses near crack tip. They used Hamiltonian formalism in elasticity to investigate on edge-cracked cylinder under various loading conditions. They provided all three SIFs Modes and showed they are depend on the boundary conditions as well as the external loading directions. Numerical results were obtained to show the accuracy of the proposed method.

Likeb et al. (2014) studied on a new pipe-ring specimen as ring for fracture toughness testing. The pipe-ring specimen with through thickness crack was subjected to bending loading. In this case the bending and share stresses occurred in critical pipe-ring sections. In order to ensure transferability between standard and proposed pipe-ring specimen the compendia for stress intensity factor and limit loads for pipe-ring specimens with different crack aspect ratio has been proposed. The results of stress intensity factor and

limits load are obtained by using finite element modelling in ABAQUS software. Results showed that three point bended pipe-ring specimen exhibit similar fracture behaviour with single notch bend specimen and the solution of SIF and limit load is possible to be normalized with standard one.

Peng and Jones (2016) proposed a simple solution to calculate Mode I SIFs for through-the-thickness flaws with an oblique elliptical crack front. They used finite element method to generate SIFs and compared obtained results from FEM to those collected from proposed approach which proves the accuracy of their method. It is claimed that their method is simple to use and will help researchers to calculate engineering estimates for fatigue and fracture related problems.

Chapuliot (2016) presented the development of stress intensity factor compendia for defects in nozzle corners. For that purpose, a large set finite element modeling were performed in order to cover the geometries, the defect sizes, the loading situations where encountered by large nuclear components. Then, based on that set of finite element modeling, an approximate solution relying on a fit of the stress field along the bisector line of the nozzle corner was proposed. This solution allows determining accurately the mean and maximum stress intensity factor along the crack front for pressure loading and at the maximum of cold thermal shock loading. It was validated through a comparison to existing solutions or finite element modeling results.

Paolo Livieri (2016) simplified a procedure to evaluate stress intensity factors of cracks by means of an equivalent hole. In this method, the crack would be replaced by an equivalent size hole and hoop stress on the free border will be evaluated. To prove the accuracy of this method, model have been studied experimentally and numerically which confirmed that the technique of the equivalent hole is applicable to both thick plates (and thin plates. This method can predict Mode I SIFs more accurate than Mode II.

Ribeiro and Hill (2016) provided a solution for 2D eigenstrain problem in the rectangular domain which can serve as a benchmark for validation of fracture mechanics analysis methods. This method can estimate the stress intensity factor due to residual stress in cracked components. They validated their method by comparing them with available analytical and numerical solutions. FEM Models are used to assess the validity of the principle of superposition, using crack face tractions, relative to the SIF calculation for this specific problem.

Meneghetti et al. (2016) introduced a method to rapidly estimate the averaged the strain energy density (SED) the tip of cracks under in-plane mixed mode I + III loading by using the peak stress method (PSM) in FEM. the proposed approach has two advantages: Firstly, there is no need of mesh refinement in the close neighborhood of the points of singularity, so that coarse FE meshes can be adopted; Secondly, geometrical modeling the control volume in FE models is no longer necessary. The reliability of proposed method have been proven by comparing results with accurate values calculated directly from the FE strain energy by adopting very refined FE meshes.

Hammond and Fawaz (2016) proposed a non-dimensional geometric correction factor for SIF calculations by using finite element analysis. Numerical results collected from literature for loaded single-edge cracked plates with rotationally free and constrained loaded edges typically used in fatigue crack growth experiments. Comparison between data collected from literature and those obtained by proposed method was satisfactory.

Sung and pan (2017) proposed a new analytical solutions for structural stress and stress intensity factors of similar and dissimilar spot welds in lap-shear specimens. They studied a rigid inclusion in a finite square thin plate under counter bending, central bending, in-plane shear and tension are developed. Their solution can predict SIFs on magnesium/steel spot welds in lap-shear specimens of equal thickness under pinned

loading conditions with less than 6% differences with computational results obtained from three-dimensional finite element analyses.

Pachoud et al. (2017) studied SIF for axial semi-elliptical surface cracks and embedded elliptical cracks at longitudinal butt welded joints of steel liners by means of the finite element method. At first the applicability of published parametric equations for SIF of elliptical cracks in plates was validated. Then the influence of the weld shape was assessed through a systematic parametric study. It was shown that the weld profile has a significant influence on SIF for semi-elliptical surface cracks while it has no significant influence on SIF for embedded elliptical cracks within the studied range of relative crack depth. Finally, a new parametric equation was proposed to estimate the weld shape correction factor for semi-elliptical surface cracks. It was found that the weld shape has a major influence on small semi-elliptical surface cracks relative depth *a/t,* i.e., when they are located in the weld reinforcement region. It results in a mitigation of the SIF due to the local redistribution of major principal stresses. On the contrary, embedded elliptical cracks were not significantly affected by the weld shape within the relative crack sizes of interest for fatigue crack growth in the scope of LEFM. Finally, an empirical parametric equation was derived to estimate weld shape correction factors for SIF at the deepest point of axial semi-elliptical surface cracks at longitudinal butt welded joints of steel.

Perl and Steiner (2017) evaluated distributions of the combined 3-D Stress Intensity Factor due to both internal pressure and autofrettage along the front of radial crack arrays emanating from the bore of an overstrained spherical pressure vessel. The 3-D analysis was performed using the finite element (FE) method employing singular elements along the crack front. A novel realistic autofrettage residual stress field incorporating the Bauschinger effect was applied to the vessel. The residual stress field was simulated using an equivalent temperature field in the FE analysis and numerous radial crack array configurations were analyzed. The results clearly demonstrated the favorable effect of

autofrettage which may considerably reduce the prevailing effective stress intensity factor, thus delaying crack initiation and slowing down crack growth rate, and hence, substantially prolonging the total fatigue life of the vessel. Furthermore, the results emphasized the importance of properly accounting for the Bauschinger effect including re-yielding, as well as the significance of the three dimensional analysis herein performed.

Zhao et al. (2017) introduced the strain gradient and the internal length scales into the basic equations of mode III crack by the modified gradient elasticity (MGE). By using a complex function approach, the analytical solution of stress fields for mode III crack problem was derived within MGE. When the internal length scales vanish, the stress fields can be simplified to the stress fields of classical linear elastic fracture mechanics.

Mokhtarishirazabad et al. (2017) proposed new methodology for evaluating overload effect in biaxial fatigue cracks by evaluation of mixed-mode (Mode I and Mode II) stress intensity factor and the COD for samples with and without overload cycle under biaxial loading. In this hybrid method experimental displacement data are fitted to analytical solutions based on Williams' series development so they can be used for studying the biaxial fatigue cracks. Hou et al. (2017) combined the XFEM and interaction integral methods to investigate the effects of confining pressure on SIFs and T-stress on CCBD specimens. Three Kind of CCBD specimens with different properties were studied, which were assumed as homogeneous and isotropic material, functionally graded material (FGM) and discontinuous material with a material interface, respectively. They confirmed that by increasing in confining pressure Mode I and Mode II will decrease but T-stress is increasing.

Lan et al. (2017) obtained stress intensity factors of a crack by using a general finite element procedure based on the proportional crack opening displacements. They have tested this method on the nonsingular 3-node linear, 4-node linear, 8-node parabolic, 8-

node axisymmetric elements and 8-node hexahedral solid elements. It is shown that the current method exhibits good element type adaptability and significantly less mesh dependency, and accurate results can be obtained effectively using rather coarse meshes. The accuracy of proposed method is proved by comparing results obtained from this approach by those collected from previous works in the literature.

Gupta et al. (2017) studied on the accuracy and robustness of three stress intensity factor extraction methods for the Generalized/eXtended Finite Element Method (G/XFEM): the Cutoff Function Method (CFM), the Contour Integral Method (CIM), and the Displacement Correlation Method (DCM). It is shown that the DCM, with proper enrichment of the G/XFEM approximation, has an accuracy and robustness comparable to the CFM at a fraction of the computational cost.

Imachi et al. (2018) evaluated mixed-mode dynamic stress intensity factors (DSIFs) for two-dimensional (2D) elastic cracked solids by employing ordinary state-based peridynamics (OSPD) theory. The interaction integral is adopted in the evaluation of the DSIFs. Since the displacement derivative cannot be evaluated in the standard OSPD theory, the derivative components in the interaction integral are derived based on the moving least-squares approximation (MLSA). In addition, the diffraction method is introduced in the MLSA to accurately evaluate the field variables around the crack. High accuracy and path-independent mixed-mode DSIFs are achieved by this present formulation and discretization. In general, the developed proposed approach offered high accuracy of the DSIFs and more importantly the path-independence of the DSIFs is obtained. The DSIFs evaluation can be adopted for dynamic crack propagation problems considering crack speed.

Elfakhakhre et al. (2018) used complex potential method into singular integral equation to formulate SIFs of single and multiple curved cracks in an elastic half plane with free boundary condition. Gauss quadrature formulas have been implemented to sole the

singular integral equation numerically. It is shown that SIFs are influenced by the position of the cracks, the distance between the cracks, and the distance between the cracks and the boundary of the half plane. Moreover, when cracks are closer to each other or to the boundary, SIFs values increase.

Shah and Kobayashi (1971), Kassir and Sih (1975) have solved the problems of a penny-shaped crack and an elliptical crack near the boundary of a semi-infinite elastic solid using the alternating method. The main difficulty in using this method for a problem of an elliptical crack was that the first solution - the SIF and the stress field for an elliptical crack in an infinite body - was restricted by the case of a polynomial applied pressure. Therefore, Kobayashi and Shah (1973) and Kassir and Sih (1975) used the polynomial approximation of the correcting stress over the crack domain due to a free surface, which lead to the certain inaccuracy in results.

Sung et al. (1996) construct a model to evaluate the mode II SIF for the layered material with a center crack under an arbitrary shear crack surface loading. The mixed boundary value problem is formulated by the Fourier integral transform method and a Fredholm integral equation is derived. The integral equation is numerically solved and the effects of the mode II SIF on the ratio of the shear modulus between each layer, Poisson's ratio and crack length to layer thickness are analyzed.

He and Hutchinson (2000) presented SIF solutions for Mode II and III for semi-circular and semi-elliptical surface cracks subjected to the remote shear stress. They studied the influence of Poisson’s ratio on SIFs and provided correction equations to an existing analytical solution (Kassir & Sih, 1966; Sih & Liebowitz, 1998; Tadaet al., 2000). They validated their findings with data collected from FEM generated by ABAQUS software. It is shown that their approach is more accurate than existing ones especially at the interception points where stress concentration is significantly influenced by singularity.

Atroshchenko et al. (2009) introduced the boundary value problem of three-dimensional classical elasticity for an infinite body containing an elliptical crack. They applied the method of simultaneous dual integral equations for a problem of elliptical crack subjected to the arbitrary normal loading and stress intensity factor is obtained in the form of the Fourier series expansion. Results are compared with collected data from similar methods and it is proven that proposed approach is easier and more reliable than previous ones.

Livieri and Segala (2016) presented an accurate approximation of the SIF for embedded elliptical cracks which lies in the longitudinal plane with its major axis inclined with respect to the radial direction in cylindrical and spherical vessels. A polynomial weight function of a planar flaw which is known as O-integral given by Oore and Burns (1980) have been implemented. For torsion loading of shafts with cracks (Mode II & Mode III), solutions are less common than for Mode I loading, due to difficulties in obtaining accurate analytical or numerical solutions. Chen (2016A) proposed a solution for SIFs of an embedded crack in an elliptical inclusion. He replaced a crack with slender ellipse and used available equations to evaluate stress concentrations on the ellipse. Results obtained by this method are compared with available data in literature to prove the accuracy of the approach.

In different work, Chen (2016B) provided a solution for a crack embedded in thermal dissimilar elliptic inclusion using the same approach. He claimed that the stress intensity factor depends on (a) the geometry of the medium, (b) the elastic constants on different portions of the medium and (c) the temperature distribution on different portions of the medium. They studied crack propagation through calculation of propagation angle and tensile critical stress. It is found that crack inclination affects the initial propagation significantly but the influence of the ply angle of the outer sub laminates is negligible. It is shown that crack propagation is highly influenced by its size, place and inclination in the composite and composite material.

Noury and Eriksson (2017) employed the finite element method to gain an understanding of the behaviour of a cracked bridge roller bearing in service. The cracked roller is considered as a two-dimensional edge-cracked disk subjected to a radial compressive line load. The crack parameters Mode I and Mode II SIFs were calculated for the relevant load configuration and angle of disk rotation. The calculated data were also used to check the accuracy of approximate SIF solutions reported in previous works. It was found that Mode II dominates and that the Mode I and Mode II SIFs are strongly influenced by crack length ratio $a/(2R)$ and the angle of rotation α.

Li and Wang (2018) obtained a solution for an inclined intera-laminar crack in the central layer of angle-ply composite subjected to a unidirectional tensile stress. Results showed that SIFs are primarily determined by the ply angle of the outer constraining sublaminates and the crack orientation angle when the thickness of the outer constraining sublaminates is more than twice that of the central layer. however, for a large crack when its tips are close to the interfaces, an inclined crack may corresponds to a minimum propagation stress in composites with a large ratio of the longitudinal modulus to the transverse modulus.

Li et al. (2018A) proposed a method for estimating the stress intensity factors (SIFs) of kinked crack with finite kink length. This method is based on an estimation expression which is derived from the work of Cotterell and Rice (1980) from the stress field series of the original (unkinked) crack tip to the second order by using weight function. In order to increase the estimation accuracy for the kinked crack with finite kink length, the third order coefficients of the stress field series of the original crack tip are introduced into this expression and these parameters can be obtained by a fitting procedure. Application of this modified expression to the cases of singly-kinked, edge kinked and doubly-kinked cracks reveals a good approximation with the finite element (FE) results of SIFs and showed that the accuracy is increased.

In the different work, Li et al. (2018B) proposed a method to estimate the mode III stress intensity factor (SIF) of kinked crack under anti-plane load. The SIF of the kinked crack can be estimated by an expression derived from the stress field series of the original crack include first three order terms by the weight function (WF) method. The coefficients of the WFs were obtained by a fitting procedure based on the solutions of the weight function problem, which were solved by a conformal mapping method. The influence of the WFs in the estimation was evaluated as a function of the kink angle and the kink length ratio. The application to the case of a kinked crack shows good agreement with the analytical results. This method can be used to approximate the SIF result based on the analytical solution for the original crack. This approach is also suitable for studies of multi-kinked cracks or the process of fatigue crack growth.

Anderson et al. (2018) evaluate stress intensity factors from the asymptotic displacement (or stress) fields at a crack front by using commercial FE-codes, also when approaches such as XFEM are employed. The proposed methodology can deal with multiaxial loading of curved crack fronts in three-dimensional bodies. In addition, it is shown that new approach found to perform better than the J-integral under compressive loading. It is demonstrated that results converge with respect to mesh size and that the method is capable of separating the SIFs also under mixed mode loading conditions. It is finally shown that the method provides reasonable results for a three-dimensional problem with a Hertzian contact load traversing a cracked rail head. This problem features both large compressive loading and a non-proportional multiaxial state of stress.

Crack problems formulated and solved for an infinite elastic solid are based on the assumption that the crack is sufficiently far away from the boundaries of the body. However, in practical applications the effect of free boundaries may significantly affect the stress distribution near the crack front. In order to account for the free boundary effect, the alternating method can be used. The (Schwarz-Newmann) alternating method was

introduces by Kantorovich and Krylov (1964). The method includes the successive, iterative superposition of two solutions in order to satisfy the boundary conditions. The first solution is the stress intensity factor and the stress field in an infinite body, containing a crack. The second solution is for the stress field in a semi-infinite or finite body subjected to the stress field applied to the boundary plane. This solution for a semi-infinite body has been derived analytically (see for example, Love, 1929 and Kupradze, 1979). For finite bodies the stress field can be obtained numerically using the finite element method (see for example, Smith, 1976 and Nisioka and Atluri, 1983).

A wide class of crack problems are problems of surface breaking planar cracks in semi-infinite and finite bodies. Sih and Hartranft (1973) analyzed the problem of a semi-circular crack in a semi-infinite body by the alternating method. The SIF and the stress field solutions were obtained in the integral form with Bessel kernels. The stress field solution in a semi-infinite body loaded on the boundary plane was taken from (Love, 1929).

Wang and Zhang (1999) investigated on closed-form SIF solutions of 3D cracks in finite body. They implemented the energy release rate method and combined with relevant 2D SIFs and obtained a new analytical solutions for Mode II and Mode III SIFs. They concluded that their method is relatively fast and can calculate SIFs within seconds. They established a Pythagorean Theorem to show the relationship among the three-dimensional crack surface displacements and the crack sliding displacements of longitudinal section and the crack tearing displacements of transversal sections in the vicinity of the crack front.

Kastratovic et al. (2015) introduced a modification to an existing SIF solutions for two unequal cracks in an infinite body under remote uniform stress. The validation of the proposed solution was obtained by two different methods of FEM and Extended Finite

Element Method (X-FEM). The strength of new solution was its capability to evaluate multiple cracks in the thin plate subjected to uniform uniaxial tensile stress.

Alizadeh and Saeidi (2018) provided SIFs for a semi-circular surface crack in arbitrary elastic finite and infinite bodies by using General Point Load Weight Function (GPLWF) concept. An explicit expression is derived to determine SIFs for semi-circular cracks subjected to uniform, linear, and nonlinear loads. They have evaluated their proposed solution in special cases like semi-circular cracks in a finite thickness plate subjected to complicated loadings, central and non-central semi-circular cracks in finite-length thick-walled cylinders subjected to a uniform internal pressure, and central semi-circular cracks in an infinite-length thick-walled cylinder subjected to a non-uniform internal pressure are compared with the available results in the literature and those obtained through FEM and proved the accuracy of it.

During last 40 years, several variational and potential methods which investigate on existence and uniqueness of crack problem solutions have been developed by many researchers such as (Constanda, 1990), (Chudinovich & Constanda, 2002). Ciarlet (1988) proposed to use Sobolev spaces for the investigation of the displacement traction problem in three-dimensional linear elasticity. Kupradze (1979) has introduced a special form of elastic displacements by means of single-layer and double-layer potentials with unknown distributed densities. Stephan and Costabel (1987) transformed the variational Dirihlet and Neumann problems to a system of boundary equations and proved the existence, uniqueness and stability of solutions in a special weighted Sobolev space.

Petroski and Achenbach (1978) employed a simple representation for the crack-face displacement to compute the weight function for stress intensity factors subjected to tensile loading. It is shown that crack face displacements given by the representation were in good agreement with analytical results and stress intensity factors computed from the

weight function agree well with those for edge cracks in half planes, radial cracks from circular holes, and radially cracked rings.

Wu (1984) proposed general expressions of stress intensity factors for center cracks, collinear cracks and edge cracks in finite plates, with the cracks subjected to arbitrary stresses by using weight function methods. He studied the influences of finite dimension and boundary constraint and results proved that approximate weight functions were powerful, efficient and simple to use in determining stress intensity factors with very satisfactory accuracy for 2-D cracks in finite bodies under load or displacement control. Also Wu (1992) used weight function approach to obtain closed-form solution for stress intensity factors of various finite plane cracked bodies. In addition, he presented accurate crack face displacement expressions for center and edge cracks which used to derive analytical weight functions, whose accuracy was critically assessed using the related Green's functions. He proposed SIFs or a number of basic load cases including concentrated forces, polynomial as well as a band of linearly varying stress. He indicated that his proposed solutions were versatile, very cost-saving, easy-to-use, and accurate.

Anderson and Glinka (2006) highlighted that the exact or closed-form solutions, for an example by the weight function method, would greatly reduce the need for finite element or boundary element models for the crack problems. They proposed Mode I stress intensity factor solutions for surface cracks in plates using weight function integration methods. Their approach can predict stress distribution (1) constant stress over each integration interval, (2) a piecewise linear representation, and (3) a piecewise quadratic fit. The quadratic method for treating the stress profile is the most efficient and accurate, but it is the most difficult to implement. A piecewise linear representation of the stress profile gives good results for a modest number of stress data points. The constant-stress approximation is considerably less accurate than the other two methods considered, and is not recommended. A number of analytical and closed-form solutions for the SIFs of a

surface crack have been reported in literature. The exact analytical solutions utilizing the weight function method for calculating the SIFs of a surface crack were also reported in (Moftakhar & Glinka, 1992; Shen & Glinka, 1991; Zheng et al., 1997; Shahani & Nabavi, 2006).

Freese and Baratta (2006) proposed stress intensity factors for several classic two-dimensional linear elastic single edge-crack by using weight function approach. The model has been evaluated subjected to the three and four-point bend, pure bending, eccentrically loaded tension, and other boundary condition problems are extracted from the solution to the uniformly loaded single edge-cracked configuration. They confirmed that their approach is applicable and accurate by validating their results with available investigations in the literature.

Bao et al. (2010) studied residual stress intensity factors in welded test samples by application of the weight function and finite element methods. Results obtained from both methods are compared with each other and FEM showed good accuracy on results. They indicated that for complicated geometries FEM can be implemented. For cracks located in compressive residual stress field, external stress should be applied simultaneously to the residual stress field to make the crack surface completely open for calculating the total SIF. The residual SIF can then be found by the superposition principle.

Jing and Wu (2015) developed complex Taylor series expansion method for computing more accurate weight functions of arbitrary 2D crack geometry. They evaluated four different cracks (a) a periodic array of collinear cracks in an infinite sheet, (b) an edge crack in a finite with plate, (c) a single radial crack in a circular disc and (d) double cantilever beam specimen and it is confirmed that proposed approach accurately performed on each of them. They concluded the new approach and conventional weight function method are mutually complementary and the mix of them can be significantly effective for fracture and crack growth analyses.

Jin et al. (2016) calculated Mode-I stress intensity factor (SIF) for symmetrical radial cracks emanating from hollow cylinder in an infinite plane under complex nonlinear loadings by using weight function method. The validity of their proposed solutions was confirmed by comparing results obtained from their method by those collected from literature. They applied their method to evaluate SIFs of (1) horizontal fracture with non-constant pressure inside it; (2) inclined fracture with constant pressure; and (3) inclined fracture with non-constant pressure. They concluded that their approach exhibits its advantages over other methodologies in solving SIFs of fractures emanating from borehole.

Jin et al. (2017) applied the same weight function parameters to evaluate SIF for single radial cracks emanating from borehole in an infinite plane. The weight function based SIF is validated against available boundary collocation based SIF in the literature and they are in good agreement with each other. This time they applied their method to (1) horizontal and inclined cracks with different applied loadings on it; and (2) radial crack with only pressure loadings and calculate the SIFs.

However, Wu et al. 2018 critically verified Jin et al.'s (2016; 2017) weight functions for or single and double edge cracks emanating from a circular hole in an infinite plate through comparisons of Green's functions and stress intensity factors obtained by different weight function approaches. They concluded that proposed solution by Jin et al. is in disagreement with previous analytical solutions and their validation approach is not accepted since they merely compared SIFs for some load cases which is not sufficient to reveal the true quality of weight functions and can be misleading. The only way for accuracy evaluation of weight functions is through point-by-point examination of the corresponding Green functions.

Sorensen and Smith (1976) analyzed the semi-elliptical crack in a plate under uniform tension using the alternating method. The stress field due to the free surface was

approximated by the polynomial of the third degree and Shah and Kobayashi's solution (1971) was used to obtain the corresponding SIF and the stress field. The polynomial representation of the applied stress field lead to certain underestimation of the SIF-solution. Holdbrook and Dover (1979) proposed SIF solutions for semi-elliptical surface cracks in infinite width plate subjected to tension and bending. They considered the effects of free front area, finite area and finite second moment of area in their equations. It has been shown that using this new stress intensity factor solution it is possible to correlate fatigue crack growth data measured on surface cracked plate specimens with conventional through crack data. Scott and Thorpe (1981) combined curve fitting approach and best available solutions to obtain SIFs for cracks in plates subjected to tension or bending loadings. Several crack tip SIF solution have been proposed where did not agree with each other particularly. It was not confirmed which one was more accurate but they could give good prediction on fatigue crack growth calculations.

Raju and Newman (1979) used the finite element method to calculate stress intensity factors for semi-elliptical cracks in finite thickness plates subjected to tension. Later they fitted their results for elliptical, semi-elliptical and quarter-elliptical cracks into an empirical equation (Newman & Raju, 1981) for the SIF as a function of the parametric angle, crack depth and length, plate thickness and width for tension and bending loads. Their solution is applicable to a wide range of crack and plate parameters and is widely used in engineering applications.

Nishioka and Atluri (1983) used the alternating method with the finite element stress field solution for a problem of a semi-elliptical crack in a plate under remote tension and bending. A fifth degree polynomial was used to fit the stress field over the crack surface due to the free surface. That allowed to increase the accuracy of the results in comparison with previous works. Using the finite element solution for a stress field enables to analyze the finite bodies of an arbitrary shape. Isida et al. (1984) found SIF solutions by using

fitted polynomials in crack aspect ratio a/c and crack size ratio a/t to their results. Their solutions showed good accuracy with Newmwn-Raju's (1981) over the range of 0.125 $\leq a/c \leq$ 1.0, $0 \leq a/t \leq$ 0.8 but they only give values on Corner points on ellipse where crack meets the surface (CPE) or Deepest Point on Ellipse (DPE) unlike Newman-Raju's which is able to provide all SIF values along the crack front.

Carpinteri (1992B; 1994; 1996A; 1996B) presented SIFs for part-through cracks in round bars under cyclic combined axial and bending loading. He used FEM approach to calculate the SIFs and validated those results by Newman-Raju's Method. Newman-Raju's solutions also verified by Hosseini and Mahmoud (1985; 1986) experimentally and they indicated that proposed solution by Newman-Raju is reliable. They performed different set of experimental tests on cracks with different aspect ratio to evaluate both SIFs and fatigue life of specimen under fatigue loadings.

Lin and Smith (1999) presented SIFs and fatigue crack growth lives for crack plates by using a two degree of freedom methods. They showed that their results had good agreement with those obtained by Newman-Raju. However, they claimed that when crack depth is larger than 90% of the plate thickness Newman-Raju's solution would not be accurate. In order to predict the accurate values of SIFs at any given aspect ratio, they proposed a correction to Newman-Raju's approach.

Sripichai and Pan (2012) introduced closed-form structural stress solutions with equivalent and numerical coefficients for a rigid inclusion in a square plate under opening and bending loading by using the results of three-dimensional finite element analyses. The results indicated that the computational mode I stress intensity factor solutions agree well with those based on the structural stress solutions. Next, accurate closed-form stress intensity factor solutions with fitting coefficients for spot welds in the square overlap parts of cross-tension specimens were presented.

Wang et al. (2012) proposed dimensionless stress intensity factors of cracked chevron notched Brazilian disc specimen is the coefficient in the crucial formula for calculating the fracture toughness. This method can be conveniently obtained by the analytical method based on the straight through crack assumption proposed by Munz et al. (1980). It is shown that obtained results from proposed solution is in agreement with results obtained by Munz et al. (1980) and it was also explained physically through comparison of the load bearing capacity between CCNBD and the corresponding CSTBD specimen based on stress intensity factor concept.

Dempsey and Mu (2014) determined a stress intensity factor weight function for edge-cracked rectangular plate. They used crack opening displacement (COD) Green's function to evaluate SIFs. The accuracy of the weight function that has been developed is assessed by treating the case of an edge crack in an infinite strip subjected to pure bending, an edge-cracked rectangular plate subjected to pure bending, and an edge-cracked rectangular plate subjected to self-equilibrated concentrated loads at the crack mouth.

Nagai et al. (2015) developed a solution for the stress intensity factor of a semi-elliptical surface crack in plates with high-aspect-ratio up to 8.0 subjected to a fifth-order-polynomial stress distribution by using the influence function method. Their method advantage to other previous ones in the literature is no one had proposed solutions to cracks with aspect ratio higher than one since they are characterized as semicircular cracks. Their solution can predict crack propagation with high aspect ratio accurately which is crucial for work-life estimations.

Okada et al. (2016) evaluated SIF solutions for semi-elliptical cracks with high aspect ratios in plate and thick wall cylinder. They used Virtual Crack Closure-Integral Method (VCCM) for SIFs evaluations. They compared their method with available analytical and FEM numerical data in the literature and confirmed that their approach is accurate. They

claimed their approach needs less time and effort to calculate SIFs. In addition, they established that maximum values of SIFs do not occur at the deepest point in cracks with higher aspect ratios.

Seitl et al. (2017) introduced normalized stress intensity factors for three- and four-point bending specimens with a chevron notch by varying the chevron notch angle and length. The three- and two-dimensional models of bent chevron notched specimens in the software ANSYS were prepared by using possible symmetrical conditions. The 2D model was used with variable thicknesses of the layers representing the characteristic shape of the chevron notch (with the plane stress boundary condition). The numerically obtained results from the 2D and 3D solutions are compared with data from literature. The numerical study showed good concordance between 3D and the known literature data. This contribution also showed the influence of Poisson's ratio on the SIF calculated from a 3D numerical model. This effect can be seen on both types (Plane strain and Plane stress) of 2D models. However, a 2D model with non-uniform thicknesses showed a major difference from the 3D solution. This effect should be taken into account in cases when the SIF value is calculated using a 3D numerical model.

Kolitch et al. (2017) studied stress intensity factors of semi-elliptical surface cracks in plates under bending and tension loading. They used FEM to generate SIFs and proposed an approximate solutions by introducing a correction to Newman-Raju's (1981) solutions. It is shown that new proposed solution show more accuracy than Newman-Raju's one in comparison with obtained FEM results. In addition, they claimed that their solution can predict SIFs even if the crack depth and width are close to the specimen thickness and width, respectively.

He et al. (2018) developed a wide range of Mode I SIF solution for an eccentrically cracked middle tension specimen with clamped ends. In the derivation of the solution, an equivalent model was developed; weight functions for eccentric cracks in a finite-width

strip were utilized, with approximate closed-form and plate-end displacement solutions obtained. Good agreements between the approximate solutions and corresponding FEM results were observed over a wide range of eccentricities and crack lengths.

Meshii and Watanabe (1998) studied on SIFs for an inner circumferential surface crack in the hollow cylindrical shell under bending and derived closed-form equations for SIFs and inclination angles at the cylinder edges. These equations can appropriately evaluate the effects of cylinder length and crack location on the stress intensity factor Solutions are compared and validated with FEM results and it is shown that the stress intensity factor increases as the cylinder length decreases, and as the crack gets near the cylinder edge.

Predan et al. (2013) calculate the SIFs for the circumferential semi-elliptical surface cracks in a hollow cylinder's cross section under torsion using a finite-element technique. The configuration of standard semi-elliptical surface cracks is described using the outer surface crack-lengths and the crack depths. They show that the magnitude of the *Mode II* SIFs near the free surface becomes more significant for stable crack-initiation than that of *Mode III* at any point along semi-elliptical crack.

Zareei and Nabavi (2016) studied on Non-dimensional SIFs solution which gives SIFs at the deepest point of an internal circumferential semi-elliptical crack in the pipe under any arbitrary loading. They proposed a solution by using the weight function method which is validated by FEM and other available data in the literature. The closed-form expression was implemented to solve the stress intensity factor of the crack by representation of the stress distribution for the uncracked pipe using a nth-order polynomial to provide a more accurate fitting of highly non-linear stress distributions.

Wang et al. (2017) evaluated SIFs sharp corrosion pits in pipes. They proposed a three-dimensional FEM model and used domain integral method to derive SIFs. In addition, they developed an expression for maximum SIFs of corrosion pits in cast iron pipes by

evolutionary polynomial regression. It is shown that assuming corrosion pits as surface crack will result in an overestimation of the stress intensity factor, causing inaccurate prediction of risk of pipe failures imposed by pitting corrosion.

Keprate et al. (2017) have proposed a computationally inexpensive adaptive Gaussian process regression model (AGPRM) which may be utilized as an alternative to FEM for prediction of SIF to assess fatigue degradation in offshore pipeline. SIF values were evaluated using FEM by carefully accounting for the discretization error emanating due to the finite mesh size in the FEM simulation. It is concluded that AGPRM method is much faster than FEM which SIF of 50 test points is reduced from 50 min (for FEM) to 12 s with the help of the proposed AGPRM, thus making remnant fatigue life assessment less laborious and time consuming.

Valiente (1980) obtained two different SIF solutions of a straight-fronted semi-elliptical surface crack in the cylinder bar subjected to tension. The first solution is derived by using the energy release rate on crack front and is applicable to the entire crack front as a whole.

$$Y = \left(0.473 - 3.286\left(\frac{a}{D}\right) + 14.797\left(\frac{a}{D}\right)^2\right)^{\frac{1}{2}}\left(\left(\frac{a}{D}\right) - \left(\frac{a}{D}\right)^2\right)^{\frac{1}{4}} \quad \text{Eq. 2-3}$$

However, the second solution is based on virtual crack extension and uses the stiffness derivative technique to calculate the energy release rate and only gives the value at DPE.

$$Y = 1.4408 - 3.6364\left(\frac{a}{D}\right) + 19.35\left(\frac{a}{D}\right)^2 - 34.7849\left(\frac{a}{D}\right)^3 + 36.8446\left(\frac{a}{D}\right)^4 \quad \text{Eq. 2-4}$$

Astiz (1986) also evaluated dimensionless SIF solutions of semi-elliptical surface cracks in the round bar under tensile loading using FEM. Crack configurations in Astiz's work is provided in Figure. 2-1.

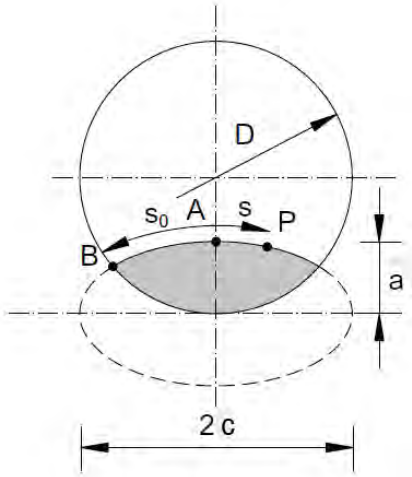

Figure. 2-1: Crack configurations in Astiz's work (Astiz, 1986).

For $s/s_0 = 0$ a polynomial fitting on the results has been performed and the following expression was proposed for dimensionless SIF

$$Y = \sum_{\substack{i=0 \\ i\neq 1}}^{4} \sum_{j=0}^{3} C_{ij} \left(\frac{a}{D}\right)^{i} \left(\frac{a}{c}\right)^{j} \qquad \text{Eq. 2-5}$$

Where the coefficients C_{ij} are presented in Table 2-1.

Table 2-1: Coefficients C_{ij} in Astiz's dimensionless SIFs.

i	$j = 0$	$j = 1$	$j = 2$	$j = 3$
0	1.118	-0.171	-0.339	0.13
2	1.405	5.902	-9.057	3.032
3	3.891	-20.37	23.217	-7.555
4	8.328	21.895	-36.992	12.676

Shiratori et al. (1987) and Murakami et al (1987) present some solutions for semi-elliptical surface cracks round bar subjected to tension and bending. Their method is based on the concept of choosing two referential two-dimensional problems and two

geometrically similar three-dimentional problems, the ratio of SIF in the in the three-dimensional problem is approximately equal to that in the two-dimensional one. They applied their method to the surface cracks in the plate and collected the data. Then, obtained results where compared by available data in the literature. When it is confirmed that the approach is accurate they applied it on round bar.

James and Milles (1988) reported SIF solution of straight-fronted semi-elliptical cracks in round bars under tensile loading by polynomial fitting on previous experimental (Daoud et al., 1978; Bush, 1981) and numerical results (Daoud et al., 1978; Blackburn, 1976; Salah el din & Lovegrove, 1981; Mattheck et al., 1984). The equation is valid for $0.01 < a/D < 0.65$.

$$Y = 0.926 - 1.771\left(\frac{a}{D}\right) + 26.421\left(\frac{a}{D}\right)^2 - 78.481\left(\frac{a}{D}\right)^3 + 87.911\left(\frac{a}{D}\right)^4 \quad \text{Eq. 2-6}$$

They also offered a solution for circular surface crack by using results from Forman and Shivakumar (1986). This equation is valid for $a/D < 0.6$

$$Y = \frac{\frac{1.84}{\pi}\left[\frac{\tan\left(\frac{\pi a}{2D}\right)}{\left(\frac{\pi a}{2D}\right)}\right]^{0.5}}{\cos\left(\frac{\pi a}{2D}\right)}\left(0.752 + 2.02\frac{a}{D} + 0.37\left(1 - \sin\left(\frac{\pi a}{2D}\right)\right)^3\right) \quad \text{Eq. 2-7}$$

Levan and Royer (1993) found a solution for round bars with transverse circular cracks by using the boundary integral equation method. Figure. 2-2 shows all parameters used in their equation and the parameter $\alpha = (B_0B/B_0B_1)$ shows the curvature of the crack front.

$$Y = \sum_{i=0}^{3}\sum_{j=0}^{3}\sum_{k=0,2,4,6} C_{ijk}\left(\frac{a}{R}\right)^{i}\alpha^{j}\left(\frac{s}{s_m}\right)^{k} \qquad \text{Eq. 2-8}$$

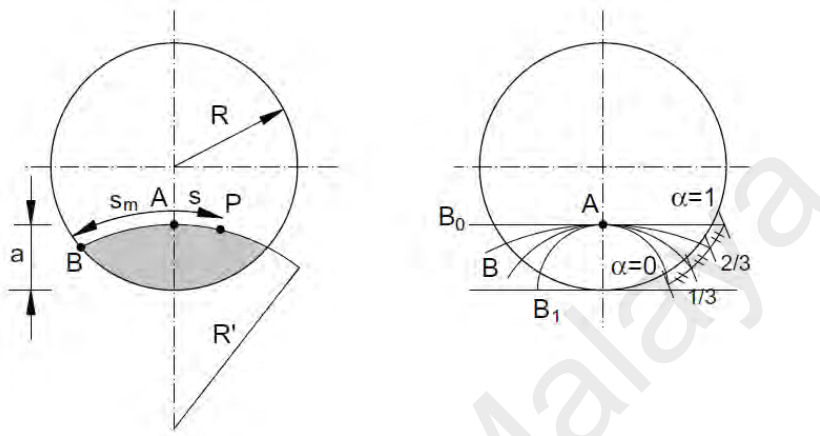

Figure. 2-2: Crack configurations in Levan and Royer's work (Levan & Royer, 1993).

Royer and Levan also (1994) also extracted K_I, K_{II}, K_{III} SIFs for circular-fronted cracks in a round bar under tensile loading, bending and torsion. These factors are expressed in terms of the crack geometrical parameters and the abscissa on the crack front. The results will allow one to predict the mechanical behavior of the crack subject to combined loads.

As it discussed before, Carpinteri (1992A; 1992B) proposed dimensionless SIF solution of straight-fronted semi-elliptical surface cracks in round bars. Values at point B in Figure. 2-3 are associated with those obtained at $\zeta/h = 0.1$, which is very close to the surface. Shih and Chen (2002) proposed a solution for SIF values at the crack center A and the crack end B by numerical fitting to results of Carpinteri's work.

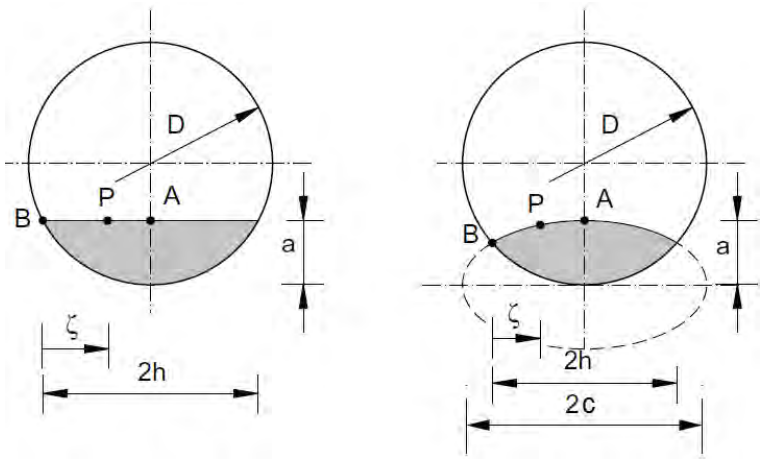

Figure. 2-3: Crack Configurations in Carpinteri's work (Carpinteri, 1992A; Carpinteri, 1992B).

$$Y_A = 0.67 - 0.033\left(\frac{a}{c}\right) + 5.73\left(\frac{a}{D}\right) - 0.29\left(\frac{a}{c}\right)^2 - 2.943\left(\frac{a}{c}\right)\left(\frac{a}{D}\right) \quad \text{Eq. 2-9}$$

$$-22.692\left(\frac{a}{D}\right)^2 + 2.41\left(\frac{a}{c}\right)^2\left(\frac{a}{D}\right) + 10.684\left(\frac{a}{c}\right)\left(\frac{a}{D}\right)^2 + 49.34\left(\frac{a}{D}\right)^3$$

$$-8.82\left(\frac{a}{c}\right)^2\left(\frac{a}{D}\right)^2 - 10.16\left(\frac{a}{c}\right)\left(\frac{a}{D}\right)^3 - 21.43\left(\frac{a}{D}\right)^4$$

$$Y_B = 0.455 - 0.233\left(\frac{a}{c}\right) + 4.893\left(\frac{a}{D}\right) + 0.113\left(\frac{a}{c}\right)^2 + 0.197\left(\frac{a}{c}\right)\left(\frac{a}{D}\right) \quad \text{Eq. 2-10}$$

$$-21.03\left(\frac{a}{D}\right)^2 + 0.557\left(\frac{a}{c}\right)^2\left(\frac{a}{D}\right) + 3.134\left(\frac{a}{c}\right)\left(\frac{a}{D}\right)^2 + 49.497\left(\frac{a}{D}\right)^3$$

$$-5.415\left(\frac{a}{c}\right)^2\left(\frac{a}{D}\right)^2 - 1.124\left(\frac{a}{c}\right)\left(\frac{a}{D}\right)^3 - 24.702\left(\frac{a}{D}\right)^4$$

Lazzarin and Filippi (2006) proposed a generalized Mode I SIFs of sharp V-notches in round bars subjected to bending. Due to its nature, the new parameter might be useful in all cases where: (a) the effect of stress redistribution due to the notch root radius cannot

be neglected; (b) the root radius, in combination only with the maximum principal stress at the notch tip, is not large enough to control the fracture of brittle or quasi-brittle materials, nor the fatigue crack initiation phase. The accuracy of proposed method have been checked carefully against FEM results available in literature.

Miura et al. (2008) derived approximate stress intensity factor expressions for axially through-wall cracked cylinder subjected to linear stress distribution and for circumferentially through-wall cracked cylinder subjected to bending. Considering that the cylindrical structures are often replaced with flat plates in the evaluation of actual components, the propriety of the replacement was also studied. They also studied the adequacy of the replacement of cracked cylinders with cracked plates. The replacement of semi-elliptical surface cracked cylinders with the semi-elliptical surface cracked plates was found to be generally acceptable, while the replacement of cylinders with an infinite axial or full-circumference surface cracks with the single-edge cracked plates brings about large conservatism in the case of thick cylinders with deep cracks.

Malits (2009) presented exact solutions for calculating the SIFs of a circumferential edge crack in a solid cylinder using the dual Dini series equations and a Fredholm integral equation. His explicit equations for the stress intensity factors of different part-through cracks obtained by the curve fitting approaches on the FEM results which collected from literature (Raju & Newman, 1986; Shih & Chen, 2002; Shivakumar & Newman, 1991).

Niasani et al. (2017) proposed closed-form thermo-elastic stress intensity factor for cracked cylinder subjected to thermomechanical loads using weight function method. This method would lessen the taken time for the analyses compared to other numerical methods such as FEM. Results show that while the load effect on cylinder subjected to thermal load lead to the crack growth in small aspect ratio, in cylinder subjected to mechanical loads, it would lead to the growth of crack in large aspect ratio. The results showed that, apart from load effects, the cylinders containing initial semi-circular crack

have the longest life among the cylinders containing initial semi-elliptical crack with the same initial depth.

Ortega-Herrera et al. (2017) presented the development of a polynomial equation of second degree which allows to predict the value of the stress concentration factor on a flat bar with two notches under to axial load for different rations r/L (notch radio/distance between notches) y W/L (bar width/distance between notches). To obtain the mentioned equation, one hundred simulations were carried out on finite element software to determine maximum stress on the bar and then the stress concentration factor is calculated. The results estimated by the proposed equation for stress concentration factor are compared with the results presented by other authors; a good matching among these approaches is obtained.

Yu et al. (2018) studied Elastic T-stress and stress intensity factor solutions for through-wall-cracked pipes under internal pressures by three-dimensional (3D) finite element (FE) calculations. The distribution of normalized SIFs (mode I and mode II) and T-stresses along the crack front for different crack lengths, crack orientations, thickness ratios and Poisson's ratios has been obtained in detail. Their FE results showed that the T-stresses increase with increasing Poisson's ratio and crack angle, respectively. The normalized Mode I increases while Mode II decreases with increasing Poisson's ratio, respectively. The normalized Mode I decreases with increasing crack angle, while Mode II increases with increasing crack angle from 0° to 45° and then decreases from 45° to 90°. Finally, the empirical formulae of the three-parameter Mode I, Mode II and T-stress have been derived by fitting present FE results with the least-squares method for the convenience of engineering applications.

Various solutions for stress intensity factors obtained from a variety of methods have also been presented in the compendiums or handbooks (Sih & Liebowitz, 1998; Tada et al.,

2000; Sih & Kassir, 1975) and literatures (Yu et al., 2015; Dosiyev & Buranay, 2015; Shlyonnikov, 2016; Seifi, 2015).

2.3 Summary

In summary, this chapter discussed that mechanical components that have a manufacturing discontinuity, defect or flaw which under tough working situation like cyclic loads they may turn into a crack. In other words, cracks may initiate in mechanical components as a result of material problem or boundary forces application on the components. Crack propagation during working life time will lead to a fracture or failure of the component. Thus, it is crucial for designers or engineers to study fatigue life or residual fatigue life of a component in the machine or mechanical structure. One the most significant tools to study crack propagation is stress intensity factor assessment along the crack front.

It is shown that researchers have evaluated SIFs by using different approaches and can be classified as follows:

- General SIF evaluation around the crack tip
- SIF assessment of a crack in arbitrary component subjected to arbitrary loading
- SIF evaluation of cracks in infinite body subjected to different loading
- SIF calculation of cracks in plates under different loading
- And finally SIF assessment of cracks in cylinder bar subjected to different loading

Cylinder and round bars are common component in mechanical machines and play a crucial role in power transition. Many researchers studied crack initiation and propagation in cylinders subjected to different loadings as it is presented in this chapter. In addition,

plenty of analytical and closed-form solutions to predict SIFs of surface-flaws in cylinder bars have been provided.

In order to evaluate SIFs, different approached have been implemented by researchers such as Numerical Method, Analytical Method and Experimental Method. Advantages and disadvantages of each method has been explained comprehensively. In this study, numerical approach has been used to evaluate the SIFs. Finite element method (FEM) and boundary element method (BEM and DBEM) are two most common numerical approach for fracture mechanic analysis but Dual-Boundary Element Method is implemented in this study.

Dual-Boundary Element Method (DBEM) based-software BEASY has been chosen to evaluate the SIFs of cracks in this research due to:

- High accuracy of the displacements and stresses including their derivatives at the internal points
- Less time and efforts are needed for simulations by DBEM than FEM
- Singularity in crack tip and crack interceptions is accurately treated
- Reliability of BEASY has been established by previous works in the literature
- Obtained results in BEASY showed more consistency with analytical solutions than FEM while will be discussed in chapter four of this thesis

The literature have shown that a comprehensive closed-form solution of the SIFs for Modes I, II and III of a semi-elliptical surface crack with different inclination angle in a solid cylinder under pure tension and pure torsion have yet to be developed.

CHAPTER THREE: METHODOLOGY

3.1 Applied Method

This chapter will detail the methodology and techniques repeatedly used in this study to achieve the objectives. As it is discussed, to evaluate SIFs of semi-elliptical cracks in cylinder bars DBEM based-software BEASY has been chosen. BEASY's Crack Growth Simulation tools provide engineers with the ability to quickly solve 3D fracture models in support of damage tolerance analysis and structural integrity assessment. Figure 3-1 is showing the approach adopted in this work to reach final solutions.

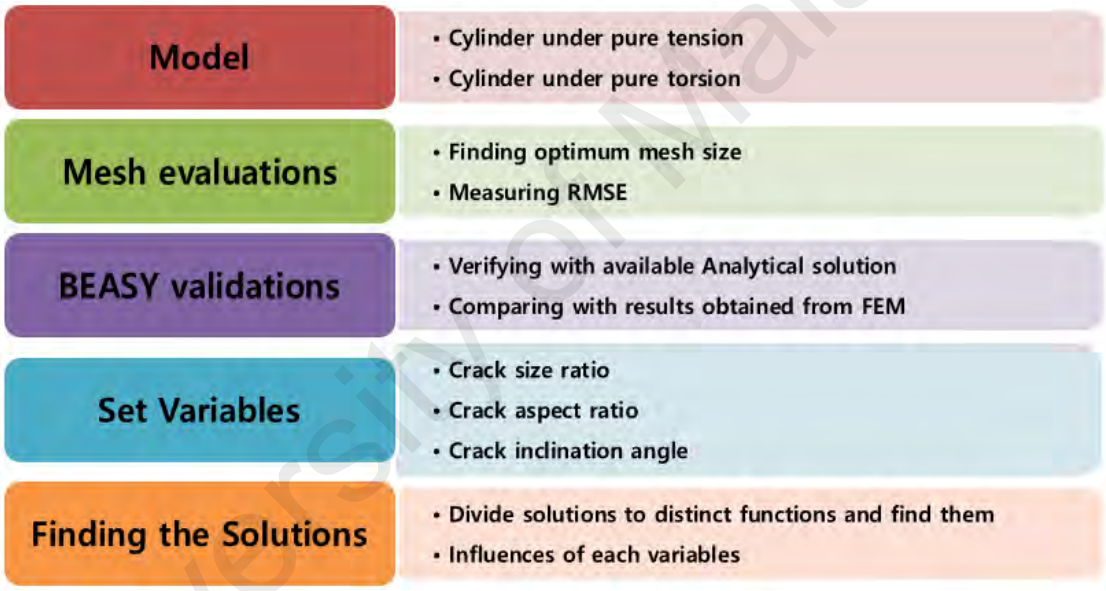

Figure 3-1: Flowchart of applied Methodology in this study

BEASY's Fatigue Crack Growth Simulation technology is easy to use and industry proven. Accurate fracture mechanics solutions are available for predicting:

- Stress Intensity Factors
- Crack Growth Rates
- Crack Growth Paths
- Critical Crack Sizes

BEASY's Crack Growth Simulation software is based on advanced fracture mechanics principles and represents a radically improved approach to computational fracture analysis. BEASY's fracture simulation methodology provides more accurate solutions for those needing to make critical life extension decisions or to determine if an asset can continue to operate safely under existing service loading conditions (BEASY website).

To reach the optimum results in BEASY, a crack is modelled in BEASY with three different mesh sizes of 1.25% , 5% and 10% of crack front arc length in torsion loading and 2.5% , 5% and 10% of crack front arc length in tension loading. Results obtained from BEASY are compared to each other and Root Mean Square Error (RMSE) is calculated respect to each distribution. Findings evidently confirmed that mesh sizes smaller than 5% of crack front arc length do not improve the accuracy of results considerably.

Then to prove the validity of BEASY's results, they have been compared with available analytical solutions in the literature (Newman-Raju's approach (1981) for tension loading and He and Hutchinson (2000) in torsion loading). BEASY showed good agreement with mentioned methods. In addition, results obtained from BEASY have been compared with the same FEM data collected from He and Hutchinson (2000) to endorse the reliability of BEASY.

In order to obtain Empirical Closed-Form SIF Solutions for an inclined semi-elliptical crack in cylindrical bar subjected to pure tension and pure torsion, a well-disciplined approach have been planned and implemented.

Firstly, variables of solutions have been chosen based on their influence on SIFs. From the literature it is found that the most crucial parameter which is highly affected the SIF is crack aspect ratio($^{a}/_{c}$). So this parameter has been opted as a first variable in final solution.

In the cylinder subjected to pure tension five different values of 0.3333, 0.5, 1, 1.5 and 2 have been chosen for crack aspect ratio. However, in the cylinder bar under pure torsion seven values of 0.3333, 0.5, 0.6, 0.75, 1, 1.5 and 2 have been opted due to more complicity of loading and boundary conditions.

Second variable in this study is crack length ratio $\left({}^{a}/_{d}\right)$ since solution would be applicable to cylinder bars at any dimension. To evaluate this study precisely, 2 sets of different assessment have been done.

1- A cylinder with diameter of 10 mm is modelled and cracks with four different sizes of 2.5%, 5%, 7.5% and 10% of cylinder diameter has been modelled with given aspect ratios in each loading.
2- Cracks with size of 2 mm and aspect ratio of 0.75, 1 and 1.5 are modelled in cylinders with diameters from 10mm to 100mm in each loading.

And final parameter is crack inclination angle (θ) which has been chosen 0º (when crack front is normal to cylinder length), 22.5º, 45º, 67.5º and 90º.

After data collection, the solutions are obtained through systematic curve fitting approaches on the SIFs produced by BEASY.

3.2 Model

The three-dimensional analysis is performed to evaluate SIFs of semi-elliptical surface cracks in the cylinder bar subjected to pure tension and pure torsion. The *J*-integral method is used to calculate the SIFs. Main parameters which being considered in this study are Crack size ratio $\left({}^{a}/_{d}\right)$, Crack aspect ratio $({}^{a}/_{c})$ and Crack inclination angle (θ). Three distinct sets of simulations have been performed to study influences of each factor on SIFs, properly.

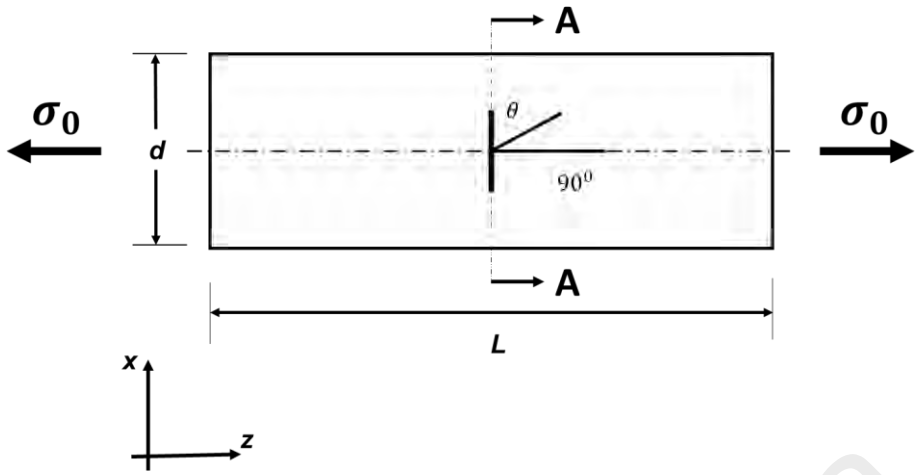

(A)

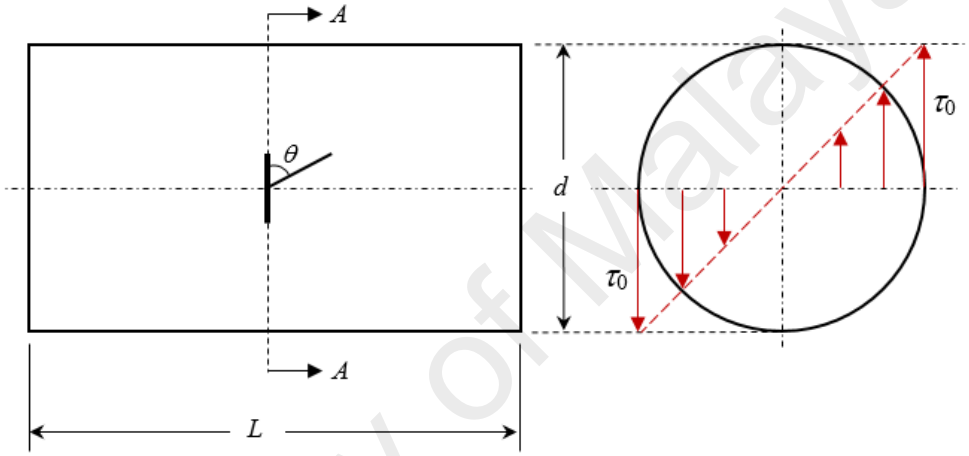

(B)

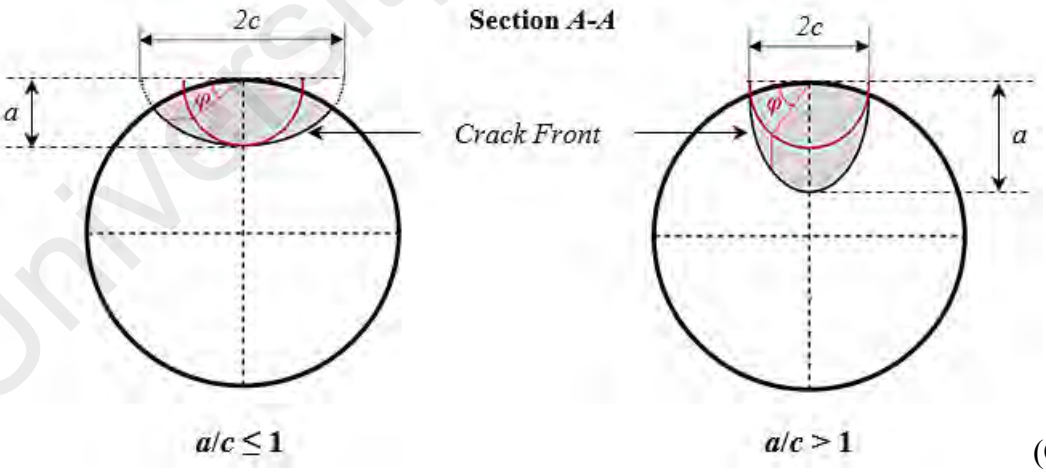

(C)

Figure 3-2: Schematic of specimen, (A) Semi-Elliptical crack on the cylinder bar under pure tension; (B) Semi-Elliptical crack on the cylinder bar under pure torsion; (C) Crack front.

A cylinder bar with diameter of $d = 10$ mm and length of $d = 40$ mm is used in this study (except for that set of simulations performed to evaluate crack size ratio in which cylinders has different dimensions). Crack depth defines by a and its half-length by c at the surface where it is perpendicular to the a. Schematic of the cylinder and its surface crack modelled in BEASY is presented in Figure 3-2. The solid cylinder bar considered in this analysis was a 7000 series aluminum alloy having a yield stress of 500 MPa, modulus of elasticity of 70 GPa and Poisson's ratio ν of 0.33. For a cylinder bar subjected to pure tension, uniform tension of $\sigma_0 = 100$ MPa is applied to the cylinder as a tensile loading and the maximum shear stress of $\tau_0 = 100$ MPa is applied at the outer surface of the cylinder bar as depicted in Figure 3-2 and is within the elastic limit of the cylinder bar. In addition, a typical normal stress distribution on crack face is presented in Figure 3-2C to show that analysis is performed within LEFM and stress values do not exceed the yield stress and go to plasticity zone.

3.2.1 Mesh Evaluation in BEASY

SIF evaluation in BEASY has two distinct stages. At the first stage of analysis, BEASY generally evaluate the model for stress and displacement distributions. Stress distribution for a solid cylinder bar subjected to pure tension and pure torsion are presented in Figure 3-3A & B, respectively. It can be seen that stress at the surface of cylinder is uniformly distributed.

During the second stage, a crack is inserted on the surface of the analyzed model initially and then the updated model will be assessed for SIF values. Since mesh dimensions around crack front is highly sensitive and reaching to accurate results is dependent on perfect meshing in this region, BEASY employs 9-noded quadratic elements at crack front and 6-noded triangular elements for crack face and further area in crack vicinity (Figure 3-3). It can be seen that meshes near crack are fine and they get coarser by getting

further from crack. Boundary of fine and coarse meshes depends on ratio of crack size to the model dimension. The smaller the crack gets, the less distance from crack tip receive fine meshes.

Schematic of meshed model and crack front is given in Figure 3-3. BEASY gives SIF distribution along the crack front based on crack arc length. However, presented results and proposed solutions in this paper are given based on parametric angle along the crack front. Coordinate system to define parametric angle for crack shapes less and higher than one are shown in Figure 3-3B and C, respectively.

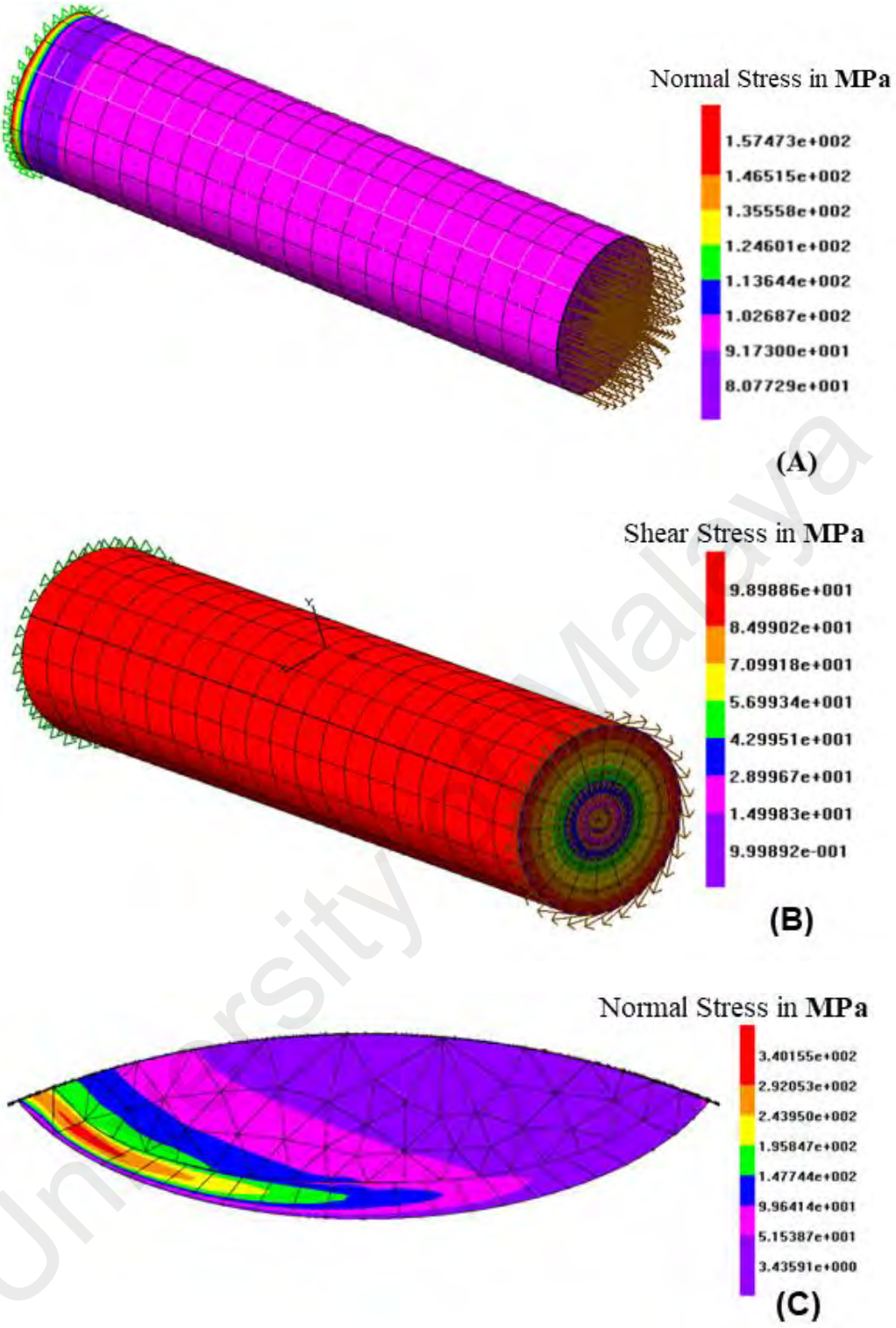

Figure 3-3: Schematic of meshed model; (A) A solid cylinder bar under pure tension and its Von Mises normal stress distribution expressed in MPa; (B) A solid cylinder bar under pure torsion and its shear stress distribution expressed in MPa; (C) Typical Von Mises normal stress distribution on the crack face expressed in MPa.

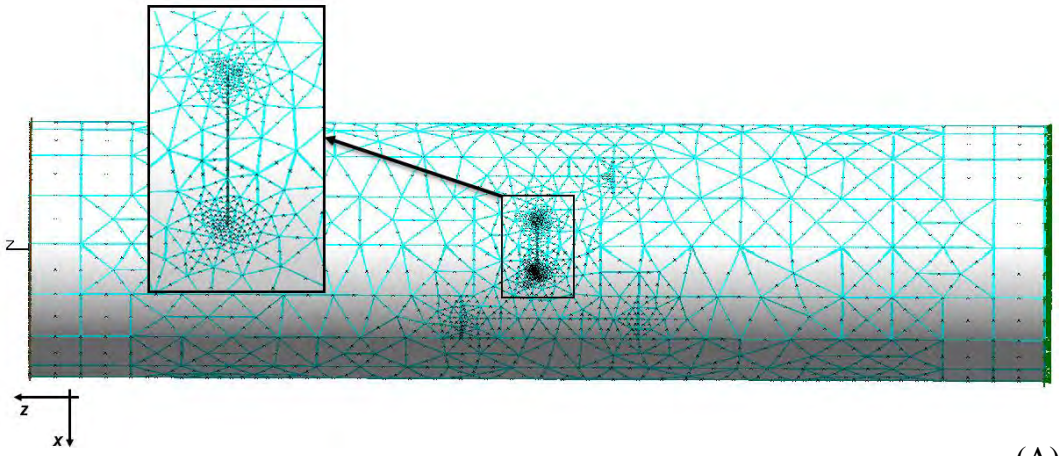

(A)

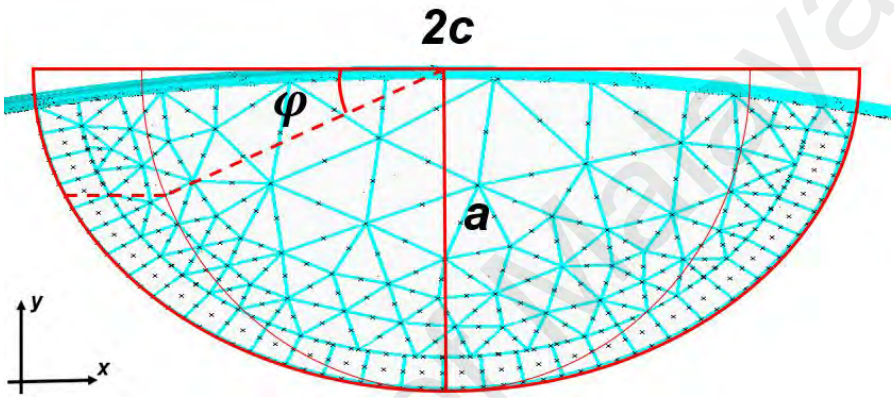

(B)

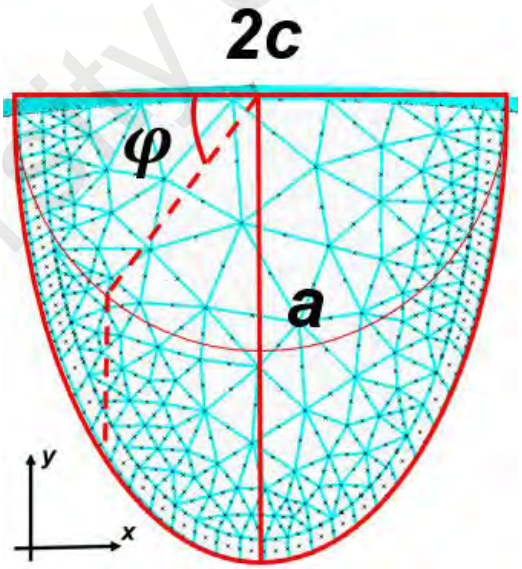

(C)

Figure 3-4: Schematic of Meshed Model, (A) Meshing in the cracked solid cylinder; (B) Crack surface and its parametric angle for cracks with a/c ≤ 1; (C) Crack surface and its parametric angle for cracks with a/c ≥ 1.

3.2.2 Cylinder Bar under Pure Tension

To evaluate the quality of meshes, a crack with size of a/d = 0.05 and shape of a/c = 1 is modelled in the cylinder bar under pure tension with 3 different mesh sizes (h) and SIFs were calculated. Mesh sizes have been chosen almost 10%, 5% and 2.5% of crack arc length (For a crack in this size, arc length is about s = 1.519). Mode I SIF distributions for different mesh sizes are plotted in Figure 3-5A. It can be observed that when mesh size is less than 5%, accuracy does not change considerably. Another exploration on mesh evaluation is measurement of Root Mean-Square Error (RMSE) to have more precise study on mesh sizes. In order to measure RMSE value for different mesh sizes, Eq. 3-1 and Eq. 3-2 have been implemented. RMSE values for Mode I is presented in Figure 3-5B. RMSE results evidently confirm that mesh sizes smaller than 5% of crack front arc length do not improve the accuracy of results considerable so that all mesh sizes to evaluate SIFs in the cylinder bar under pure tension have been chosen maximum 5% of crack front arc-length.

$$\log e = \left\| K^{i+1} - K^{i} \right\|^2 = \frac{1}{|n|} \int_{\varphi_0}^{\pi-\varphi_0} \left(K^{i+1} - K^{i} \right)^2 d\varphi \qquad \text{Eq. 3-1}$$

$$\log e \cong \sqrt{\frac{\sum_{j=1}^{n} \left(K_j^{i+1} - K_j^{i} \right)^2}{n}} \qquad \text{Eq. 3-2}$$

3.2.3 Cylinder bar under Pure Torsion

For cylinder bar under pure torsion, a crack with size of a/d = 0.05 and shape of a/c = 0.5 is modelled in the cylinder bar with 3 different mesh sizes (h) and SIFs were calculated. Mesh sizes have been chosen almost 10%, 5% and 1.25% of crack arc length (For a crack in this size, arc length is about s = 2.2222). SIF distributions for different mesh sizes are plotted in Figure 3-6.

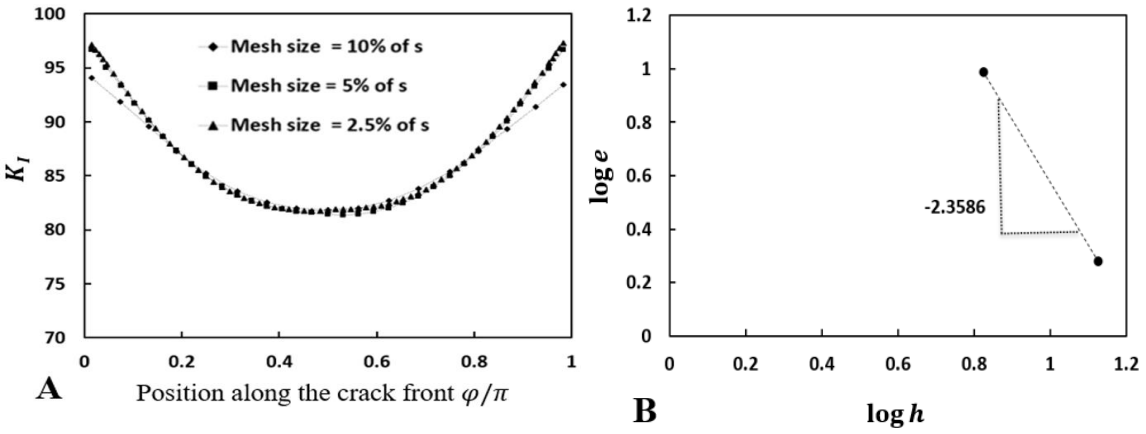

Figure 3-5: (A) SIF distributions for a crack with size of a/d = 0.05 and a/c = 1 in the cylinder bar under pure tension with mesh sizes selected 10%, 5% and 1.25% of its front arc length; (B) Measured RMSE from SIF distributions for respective mesh sizes.

Results prove that Mode III is more affected than Mode II by mesh sizes. It can be observed that when mesh size is less than 5%, accuracy does not change for both Mode II & Mode III. RMSE values for Mode II and Mode III are also calculated and presented in Figure 3-7A & B, respectively. RMSE results evidently confirm that mesh sizes smaller than 5% of crack front arc length do not improve the accuracy of results considerable so that all mesh sizes in cylinder bar under pure torsion also have been chosen maximum 5% of crack front arc-length.

3.3 Applied Technique to Derive Closed-Form Solution

As it discussed, three variables are considered to study SIFs of a semi-elliptical surface crack in the cylinder bar under pure tension and pure torsion and an applicable solution proposed to predict SIF distribution on the crack front. These variables are crack size ratio$\left({}^{a}/_{d}\right)$, crack aspect ratio$({}^{a}/_{c})$ and crack inclination angle(θ). To generate adequate amount of data to evaluate each variable properly, three sets of simulations have been designed.

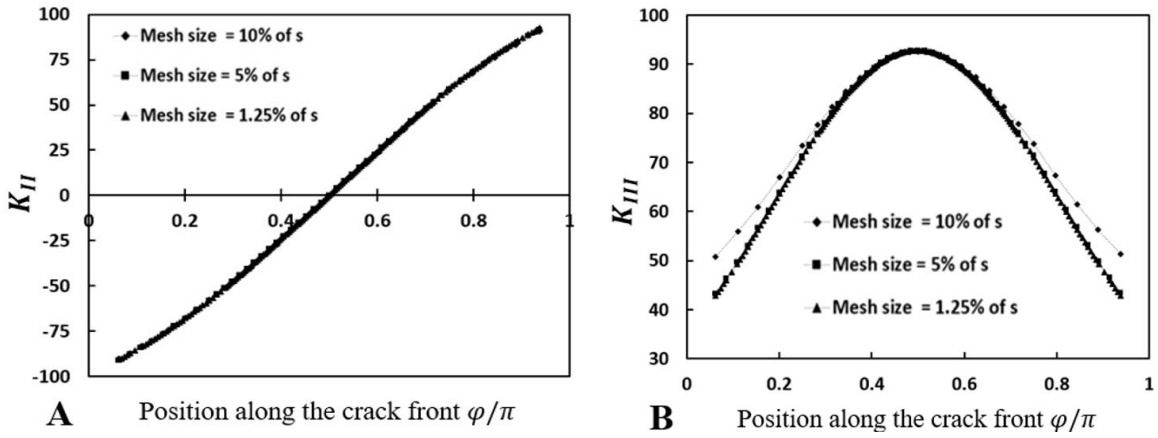

Figure 3-6: SIF distributions for a crack with size of a/d = 0.05 and a/c = 0.5 in the cylinder bar under pure torsion with mesh sizes selected 10%, 5% and 1.25% of its front arc length (A) Mode II; (B) Mode III.

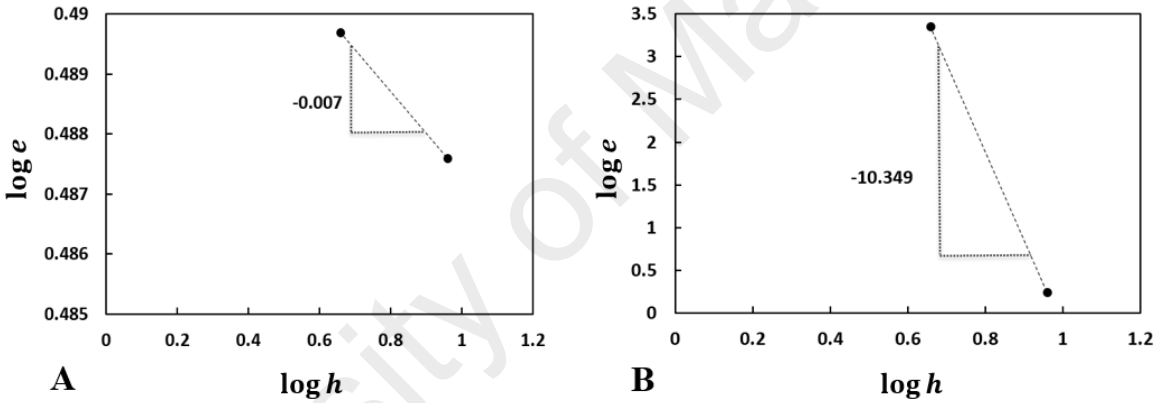

Figure 3-7: Measured RMSE from SIF distributions for mesh sizes selected 10%, 5% and 1.25% of crack front arc length with size of a/d = 0.05 and a/c = 0.5 in the cylinder bar under pure torsion (A) Mode II; (B) Mode III.

In the first set the same crack is modelled in different cylinders and extracted SIFs have been studied to check the crack size ratio and see when cylinders gets infinite body in accordance with the crack. For second set of simulations, cracks with different size and shape ratios modeled in the same cylinder and SIFs were evaluated. Finally, several cases from second set of simulations have remodeled with different inclination respected to load direction to study influence of inclinations on the SIF values.

Researchers adopted different methods from analytical to numerical approximations in order to derive acceptable solution for SIF evaluations. However, in this study a systematic cure-fitting is implemented to reach a decent versatile applicable solution. Proposed solution is composed of three distinct functions. Since maximum values of SIFs are crucial and more concerned in the fracture mechanics, the first function gives Maximum values of Mode II and Mode III SIFs. For Mode I SIFs, first function gives SIF values at $\varphi = \pi/2$ which acquires both the maximum (when crack aspect ratio is less than one) and the minimum (when crack aspect ratio is higher than one) value of SIF. To derive this function, mentioned values from first two sets of simulations are collected and a function fitted to the available data.

Second function deals with inclination influences on SIFs and propose the ratio of first function at expected angle. This function is obtained from stress analysis on the crack face at different inclination except for Mode II which caused additional study on the crack shape.

Last function gives SIF distribution on the crack front. To reach appropriate function, nature of each Mode and rate of changes on respective SIF distribution at the crack front were investigated and closest function to each Mode distribution were introduced.

Two main characteristics of proposed solution which makes it different are nobility and versatility. Different studies have been done by different researchers on surface cracks in infinite body and cylinder bars but no one studied cracks with different inclinations in the cylinder bar under pure tension. No attempts has been done for SIF evaluations in the cylinder bar under pure torsion either. In addition, the proposed solution gives this opportunity to researchers to evaluate any part of function which is needed.

CHAPTER FOUR: RESULTS AND DISCUSSION

4.1 Validation

In order to illustrate the accuracy of results obtained by BEASY, the SIFs of a semi-elliptical crack for different crack sizes have been compared with the available analytical and numerical results collected from literature.

(A)

(B)

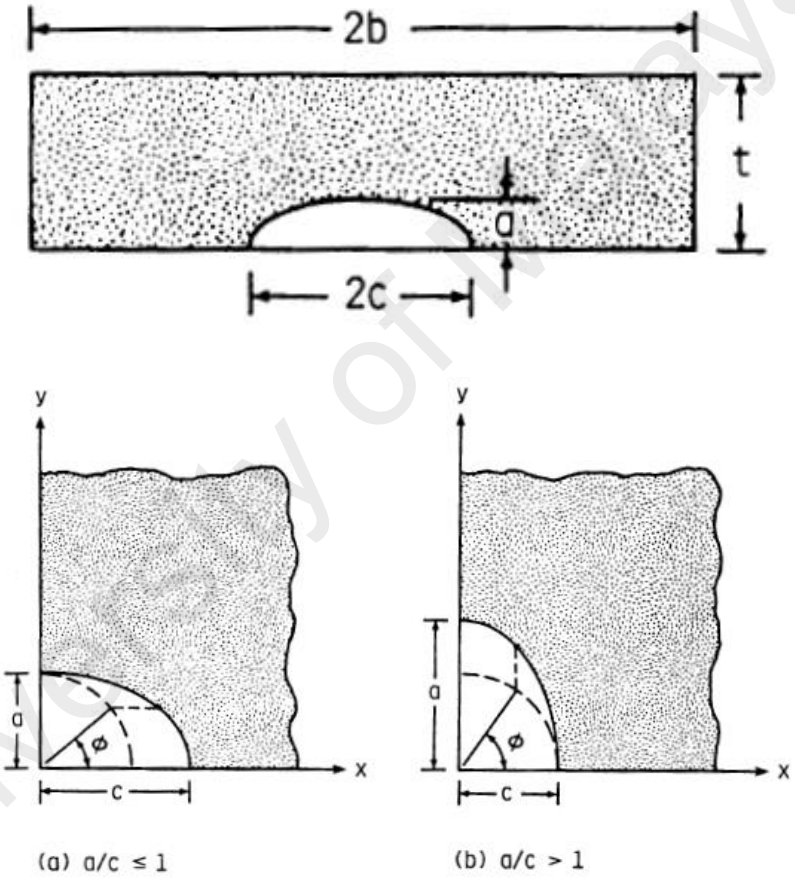

Figure 4-1: (A) Semi-elliptical surface crack in finite plate; (B) Coordinate system used to define parametric angle.

4.1.1 Reference Solution for Cylinder Bar under Pure Tension

Newman-Raju (1981) proposed an empirical equation for the stress intensity factors of a semi-elliptical surface crack in a finite plate subjected to tension (Figure 4-1A). K_I will give Mode I SIFs at any point along the crack front in Eq. 4-1.

$$K_I = S\sqrt{\pi \frac{a}{Q}} F_s \left(\frac{a}{c}, \frac{a}{t}, \frac{c}{b}, \emptyset\right) \quad \text{Eq. 4-1}$$

For $0 \ll {}^{a}/_{c} \ll 2, {}^{c}/_{b} < 0.5, 0 \ll \emptyset \ll \pi$ and ${}^{a}/_{t}$ satisfies Eq. 4-2

$$\left.\begin{array}{ll} \frac{a}{t} < 1.25\left(\frac{a}{c} + 0.6\right) & for\ 0 \ll \frac{a}{c} \ll 0.2 \\ \frac{a}{t} < 1 & for\ 0.2 \ll \frac{a}{c} \ll \infty \end{array}\right\} \quad \text{Eq. 4-2}$$

Where

$$Q = 1 + 1.464\left(\frac{a}{c}\right)^{1.65} \qquad for\ \frac{a}{c} \ll 1 \quad \text{Eq. 4-3}$$

$$Q = 1 + 1.464\left(\frac{c}{a}\right)^{1.65} \qquad for\ \frac{a}{c} > 1 \quad \text{Eq. 4-4}$$

Function of F_s accounts for the influence of crack shape $({}^{a}/_{c})$, crack size $\left({}^{a}/_{t}\right)$, finite width $\left({}^{c}/_{b}\right)$ and parametric angle φ, and was chosen as

$$F_s = \left[M_1 + M_2\left(\frac{a}{t}\right)^2 + M_3\left(\frac{a}{t}\right)^4\right] g f_{\emptyset} f_w \quad \text{Eq. 4-5}$$

For ${}^{a}/_{c} \ll 1$:

$$M_1 = 1.13 - 0.09\left(\frac{a}{c}\right) \quad \text{Eq. 4-6}$$

$$M_2 = -0.54 + \frac{0.89}{0.2 + \left(\frac{a}{c}\right)}$$ Eq. 4-7

$$M_3 = 0.5 - \frac{1}{0.65 + \left(\frac{a}{c}\right)} + 14\left(1 - \frac{a}{c}\right)^{24}$$ Eq. 4-8

$$g = 1 + \left[0.1 + 0.35\left(\frac{a}{t}\right)^2\right](1 - \sin\emptyset)^2$$ Eq. 4-9

$$f_\emptyset = \left[\left(\frac{a}{c}\right)^2 \cos^2\emptyset + \sin^2\emptyset\right]^{1/4}$$ Eq. 4-10

And for $a/c > 1$:

$$M_1 = \sqrt{\frac{c}{a}}\left(1 + 0.04\frac{a}{c}\right)$$ Eq. 4-11

$$M_2 = 0.2\left(\frac{c}{a}\right)^4$$ Eq. 4-12

$$M_3 = -0.11\left(\frac{c}{a}\right)^4$$ Eq. 4-13

$$g = 1 + \left[0.1 + 0.35\left(\frac{c}{a}\right)\left(\frac{a}{t}\right)^2\right](1 - \sin\emptyset)^2$$ Eq. 4-14

$$f_\emptyset = \left[\left(\frac{a}{c}\right)^2 \cos^2\emptyset + \sin^2\emptyset\right]^{1/4}$$ Eq. 4-15

The finite width correction, f_w, can be used for all range of a/c

$$f_w = \left[sec\left(\frac{\pi c}{2b}\right)\sqrt{\frac{a}{t}}\right]^{1/2}$$ Eq. 4-16

4.1.1.1 Comparison Results Obtained from BEASY with Analytical Solution

Three different semi-elliptical surface cracks with depth of a/t = 0.025, 0.05 & 0.1 and shapes of a/c = 0.5 & 1 are modelled in the square bar subjected to pure tensile loading of 100 MPa in BEASY and results are compared with the same cracks evaluated in Eq. 4-1. To calculate the SIFs in BEASY, cracks are modelled in a square bar with dimensions of 10 $mm \times 10\ mm$ and length of $L = 40\ mm$ made of Aluminum with the Modulus of elasticity E = 70 GPa and Poisson's ratio ν = 0.33. Schematic of the model is presented in Figure 4-2.

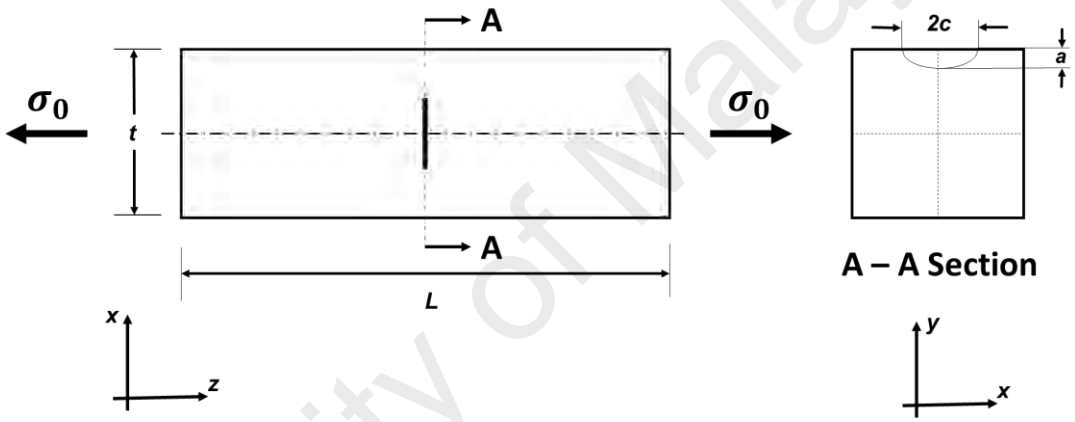

Figure 4-2: Schematic of a semi-Elliptical crack on the square bar.

Comparison of two methods for the stress intensity distributions are presented in Figure 4-3. It can be seen that both BEASY and analytical solution are in good agreement on maximum values of Mode I SIFs which are crucial in fracture mechanics.

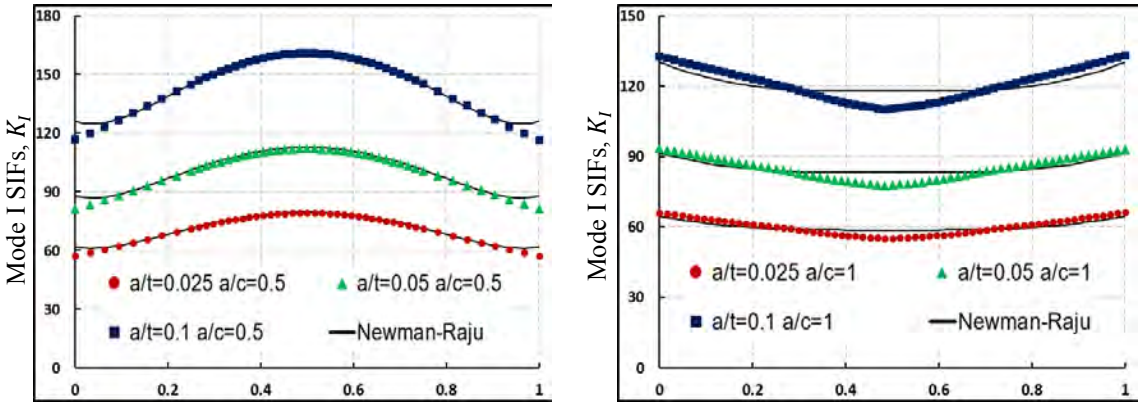

(A) Parametric angle along the crack front φ/π (B) Parametric angle along the crack front φ/π

Figure 4-3: Mode I SIF distributions of semi-elliptical surface cracks on the square bar under pure tension calculated by BEASY and that obtained by analytical solution proposed by Newman and Raju (1981) (A) for a/c=0.5; (B) for a/c=1.

4.1.1.2 Comparison Results Obtained from BEASY with FEM Results

A comparison between DBEM and Finite element Method (FEM) is executed to endorse the reliability of BEASY. SIFs obtained from BEASY are compared with those obtained by He and Hutchison (2000), who modeled a semi-elliptical surface crack in the infinite body with an aspect ratios of a/c = 0.5 and 1 using the finite element method (FEM). A semi-elliptical surface crack in the infinite body with shapes of a/c = 0.5 & 1 are modeled in ABAQUS and a general purpose Finite. Same cracks on the surface of cylinder under tensile loading at the angle of 45^o where shear stress component on the crack front is maximum, are modeled in BEASY (in size of a/d =0.25). SIFs for each crack shape ($^a/_c$) have been normalized by the corresponding maximum values for the same crack shape which happens at Corner Point on Ellipse (CPE) for Mode II and Deepest Point on Ellipse (DPE) for Mode III. Results are plotted in Figure 4-4. BEASY shows good agreement with FEM in both Mode II and Mode III. However, in Mode III, as it mentioned before values are insignificantly different in the range of small φ due to corner singularity.

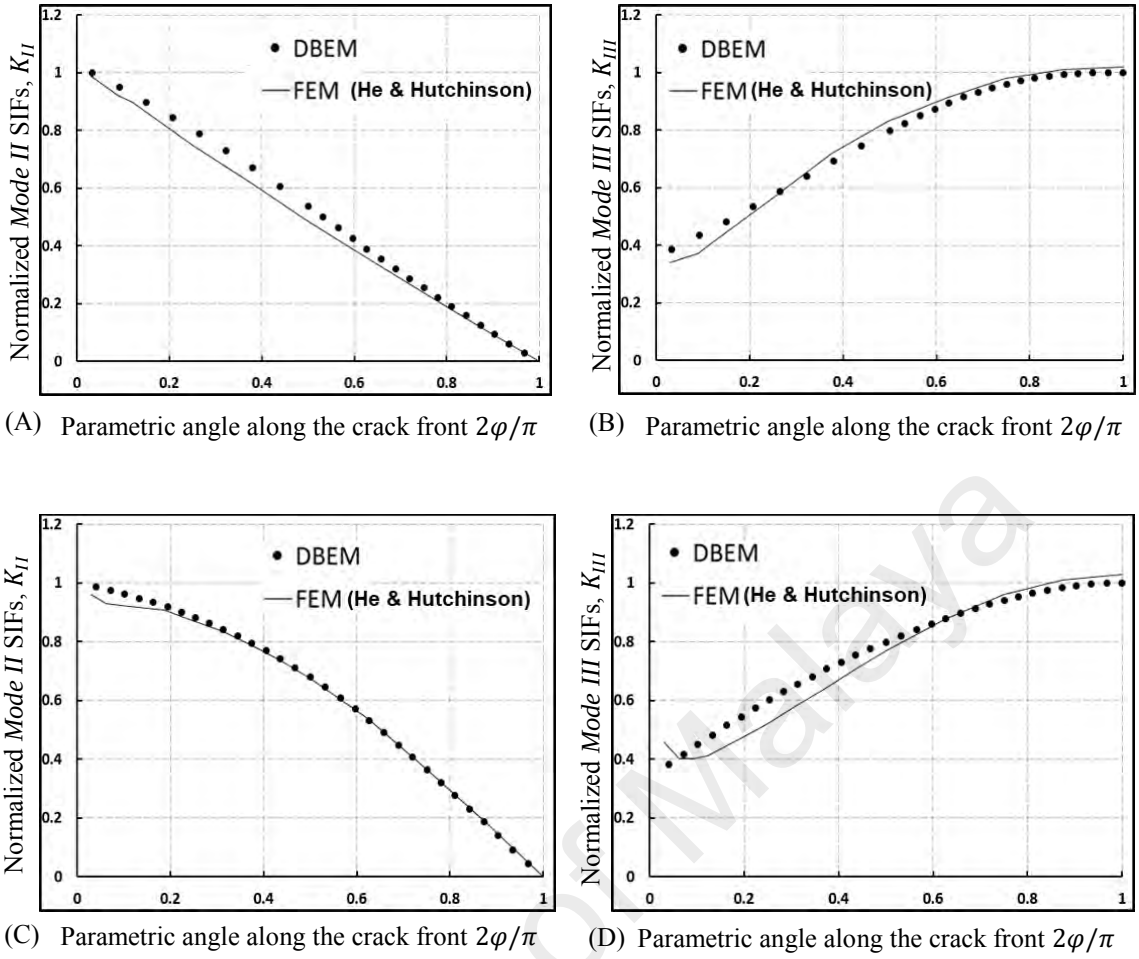

(A) Parametric angle along the crack front $2\varphi/\pi$ (B) Parametric angle along the crack front $2\varphi/\pi$

(C) Parametric angle along the crack front $2\varphi/\pi$ (D) Parametric angle along the crack front $2\varphi/\pi$

Figure 4-4: SIF distributions of semi-elliptical surface cracks modeled by DBEM in the cylinder bar under pure tension and obtained by FEM (He & Hutchinson, 2000) (A) Mode II for a/c=0.5; (B) Mode III for a/c=0.5; (C) Mode II for a/c=1; (D) Mode III for a/c =1.

4.1.2 Reference Solution for Cylinder Bar under Pure Torsion

An analytical solution for similarly aligned and loaded elliptical crack in an infinite solid is given by He and Hutchison (He & Hutchinson, 2000).

$$K_{II} = K_{II}^{0} + \delta K_{II} \quad \text{Eq. 4-17}$$

$$K_{III} = K_{III}^{0} + \delta K_{III} \quad \text{Eq. 4-18}$$

where

$$K_{II}^{0} = \frac{\tau_{xz}^{o}\sqrt{\pi a}k^{2}(a/c)\cos\varphi}{B[\sin^{2}\varphi + (a/c)^{2}\cos^{2}\varphi]^{1/4}} \quad \text{Eq. 4-19}$$

$$K_{III}^{0} = \frac{\tau_{xz}^{o}\sqrt{\pi a}k^{2}(1-\nu)\sin\varphi}{B[\sin^{2}\varphi + (a/c)^{2}\cos^{2}\varphi]^{1/4}} \quad \text{Eq. 4-20}$$

$$k^{2} = 1 - (a/c)^{2}, \quad B = (k^{2}-\nu)E(k) + \nu(a/c)^{2}K(k) \quad \text{Eq. 4-21}$$

With elliptical integrals defined by

$$E(k) = \int_{0}^{\pi/2}\sqrt{1-k^{2}\sin^{2}\varphi}\,d\varphi \quad \text{Eq. 4-22}$$

$$K(k) = \int_{0}^{\pi/2}\frac{d\varphi}{\sqrt{1-k^{2}\sin^{2}\varphi}} \quad \text{Eq. 4-23}$$

δK_{II} and δK_{III} for different cases are provided in (He & Hutchinson, 2000). Some cases are presented in Table 4-1.

4.1.2.1 Comparison Results from BEASY with Reference Solution

Semi-elliptical surface cracks are modeled in the cylinder bar subjected to pure torsion of 100 MPa in BEASY and results are compared with the same cracks evaluated in Eq. 4-17 and Eq. 4-18. Comparison of two methods for the stress intensity distributions are presented in Figure 4-5. It can be seen that BEASY is in good agreement on both Mode II and Mode III SIFs with analytical solution.

Table 4-1: Polynominal approximations for the SIF corrections in Eq. 4-17 & Eq. 4-18.

$$y = c_0 + c_1\left(\frac{2\varphi}{\pi}\right) + c_2\left(\frac{2\varphi}{\pi}\right)^2 + c_3\left(\frac{2\varphi}{\pi}\right)^3 + c_4\left(\frac{2\varphi}{\pi}\right)^4 + c_5\left(\frac{2\varphi}{\pi}\right)^5 + c_6\left(\frac{2\varphi}{\pi}\right)^6 + c_7\left(\frac{2\varphi}{\pi}\right)^7 + c_8\left(\frac{2\varphi}{\pi}\right)^8$$

$$y \equiv y_{II} = \delta K_{II}/\left(K_{II}^0\right)_{\varphi=0} \text{ or } y \equiv y_{III} = \delta K_{III}/\left(K_{III}^0\right)_{\varphi=\pi/2}$$

K	c/a	c_0	c_1	c_2	c_3	c_4	c_5	c_6	c_7	c_8
y_{II}	1	0.0153	-2.494	27.32	-143.5	421.1	-723.8	723.8	-3.897	87.34
y_{III}	1	0.5177	-4.421	22.59	-63.87	96.07	-71.99	21.13		
y_{II}	1.5	-0.047	-0.331	1.041	-1.063	0.4011				
y_{III}	1.5	0.3608	-2.528	10.62	-26.41	36.99	-26.72	7.715		
y_{II}	2	0.0239	-1.019	3.102	-3.975	2.401	-0.532			
y_{III}	2	0.3341	-2.406	8.369	-14.63	12.35	-3.991			

It is evident that when crack size is small and shape is high (where the crack in the cylinder bar is close to one in infinite body) BEASY shows more consistency on both mode II and Mode III SIFs. Mode II and Mode III SIF distributions of a crack with aspect ratio of a/c=0.5 and different size ratios are plotted in Figure 4-5A & B, respectively. For Mode III, BEASY shows higher accuracy in smaller crack sizes. Graphs in Figure 4-5C proves that Mode II SIFs of cracks with the same aspect ratios do not change considerably when their sizes increase. However, Mode III as it mentioned before is more responsive to crack size changes (Figure 4-5D). The effect of the corner singularity is evident in the vicinity of CPE where the differences between results obtained by two methods are relatively small.

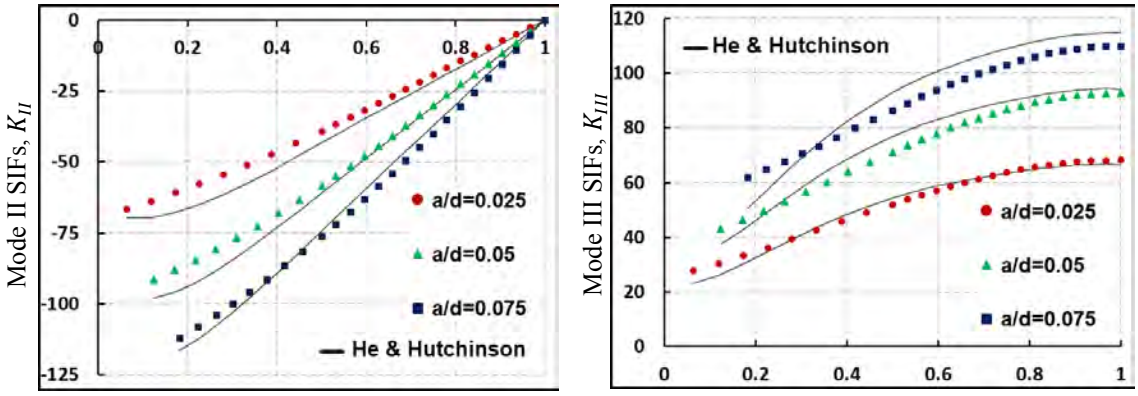

(A) Parametric angle along the crack front $2\varphi/\pi$ (B) Parametric angle along the crack front $2\varphi/\pi$

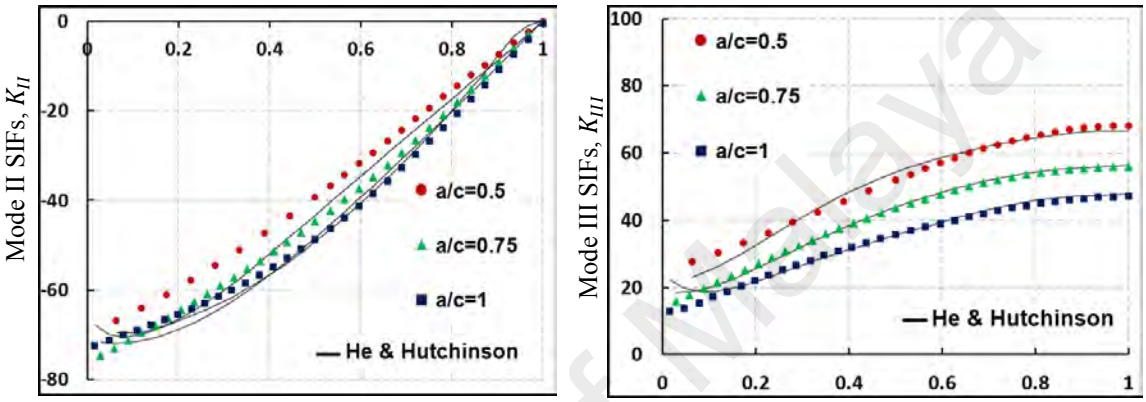

(C) Parametric angle along the crack front $2\varphi/\pi$ (D) Parametric angle along the crack front $2\varphi/\pi$

Figure 4-5: SIF distributions of semi-elliptical surface cracks on the cylinder bar under pure torsion calculated by BEASY and that obtained by analytical solution proposed by He and Hutchinson (2000) (A) Mode II for a/c=0.5; (B) Mode III for a/c=0.5; (C) Mode II for a/d=0.025; (D) Mode III for a/d =0.025.

4.1.2.2 Comparison Results from BEASY with Results from FEM

Comparison of SIFs distributions for semi-elliptical surface crack in the cylinder bar subjected to pure torsion between DBEM and Finite element Method (FEM) are given in Figure 4-6. A semi-elliptical surface crack in the infinite body with shapes of a/c = 0.5 & 1 are modeled in ABAQUS. A general purpose Finite element code was used for the analysis (He & Hutchinson, 2000). Same cracks on the surface of Cylinder under torsional loading are modeled in BEASY (in size of a/d =0.25). SIFs for each crack shape ($^{a}/_{c}$) have been normalized by the corresponding maximum values for the same crack shape which happens at CPE for Mode II and DPE for Mode III. BEASY shows acceptable

agreement with FEM in both Mode II and Mode III. The highest difference is seen in Mode II where it was within 7%. Moreover, in Mode III values are different in the range of small φ where K_{III} is relatively small.

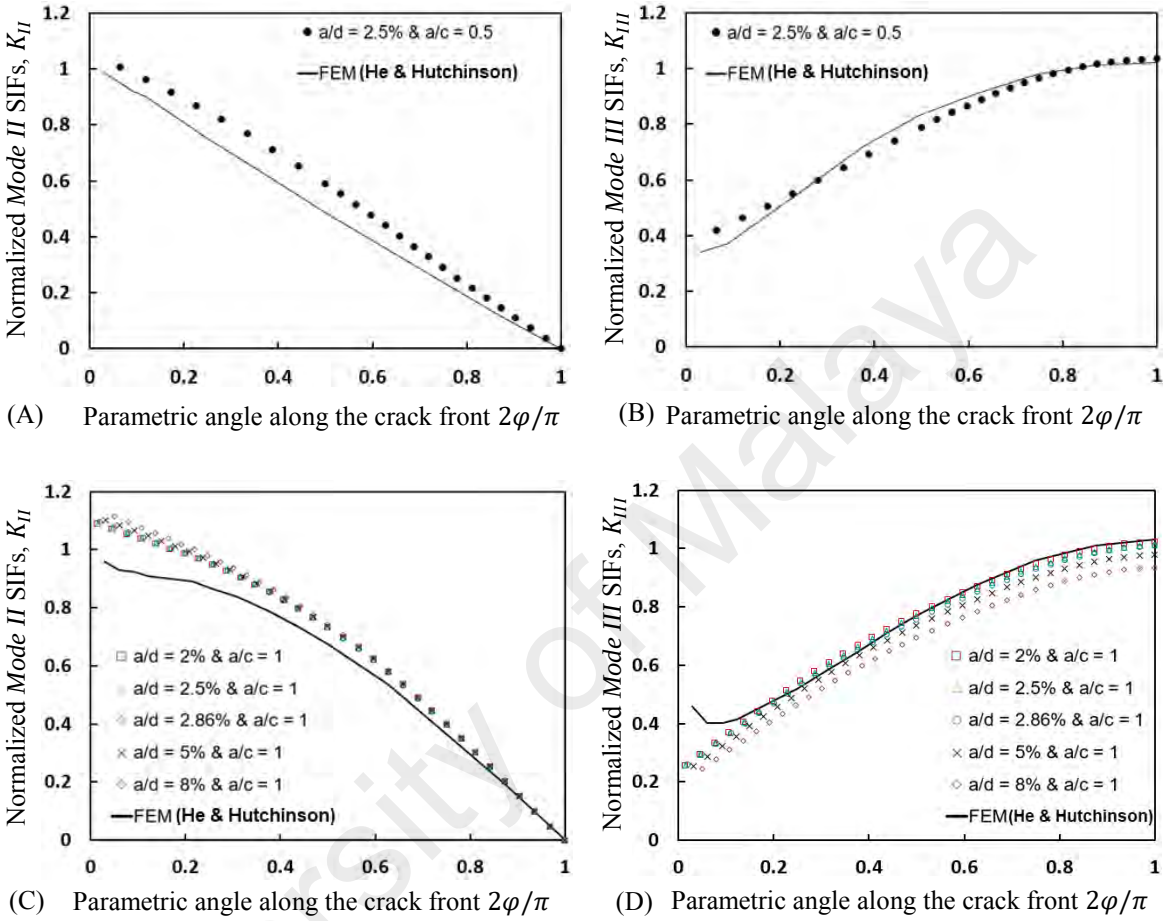

(A) Parametric angle along the crack front $2\varphi/\pi$ (B) Parametric angle along the crack front $2\varphi/\pi$

(C) Parametric angle along the crack front $2\varphi/\pi$ (D) Parametric angle along the crack front $2\varphi/\pi$

Figure 4-6: SIF distributions of semi-elliptical surface cracks modeled by DBEM in the cylinder bar under pure torsion and obtained by FEM (He & Hutchinson, 2000) (A) Mode II for a/c=0.5; (B) Mode III for a/c=0.5; (C) Mode II for a/c=1; (D) Mode III for a/c =1.

4.2 SIF Evaluation

4.2.1 Crack Size Evaluations

First set of simulations are performed to investigate on influence of crack size ratio $\left({}^{a}/_{d}\right)$ on SIF distributions. To evaluate crack size ratio, same crack with depth of $a = 2\,mm$ and shapes of ${}^{a}/_{c} = 0.75, 1$ & 1.5 are modelled in cylinders with different diameters

which vary from $d = 10$ mm to $d = 100$ mm and fixed lengths of $L = 4d$. Cylinder dimensions and respected crack ratios are given in Table 4-2.

Table 4-2: Cylinder diameter and respected crack ratios used to study crack size

$d(mm)$	a/d	a/c
10	0.2	0.75
10	0.2	1
10	0.2	1.5
15	0.1333	0.75
15	0.1333	1
15	0.1333	1.5
20	0.1	0.75
20	0.1	1
20	0.1	1.5
25	0.08	0.75
25	0.08	1
25	0.08	1.5
30	0.0667	0.75
30	0.0667	1
30	0.0667	1.5
35	0.0571	0.75

Table 4-2: Cont'd.

$d(mm)$	a/d	a/c
35	0.0571	1
35	0.0571	1.5
40	0.05	0.75
40	0.05	1
40	0.05	1.5
45	0.0444	0.75
45	0.0444	1
45	0.0444	1.5
50	0.04	0.75
50	0.04	1
50	0.04	1.5
60	0.0333	0.75
60	0.0333	1
60	0.0333	1.5
70	0.0286	0.75
70	0.0286	1
70	0.0286	1.5
80	0.025	0.75

Table 4-2: Cont'd.

$d(mm)$	a/d	a/c
80	0.025	1
80	0.025	1.5
90	0.0222	0.75
90	0.0222	1
90	0.0222	1.5
100	0.02	0.75
100	0.02	1
100	0.02	1.5

Figure 4-7 shows results for semi-elliptical surface cracks on the cylinder bar subjected to pure tension. It can be observed that cracks with higher size ratio receives higher values of SIF. However, when crack size ratio gets smaller than 0.1 Mode I SIFs do not change considerably. In other words, when cracks are relatively small in regards to cylinder sizes, cylinder turns into infinite solid body for those cracks so changing in crack size does not affect the Mode I SIF. It is evident that SIF values at $\varphi = \pi/2$ for a crack with depth of $a = 2mm$ and ratio of $a/d = 0.1$ are within 2% difference with the lower crack size ratios (Figure 4-7D) so this crack size ratio has been chosen as maximum crack size for crack shape evaluation in the cylinder bar under pure tension.

Same set of simulations have been performed on the cylinder with a semi-elliptical surface crack subjected to pure torsion. Results for Mode II SIFs are presented in Figure 4-8. Plots show that rate of changes in Mode II for crack ratios less than $a/d = 0.05$ is small. Again as it mentioned before when cracks are relatively small in regards to

cylinder sizes, model is really close to the infinite solid body so changing in crack size does not affect the Mode II SIF, as well.

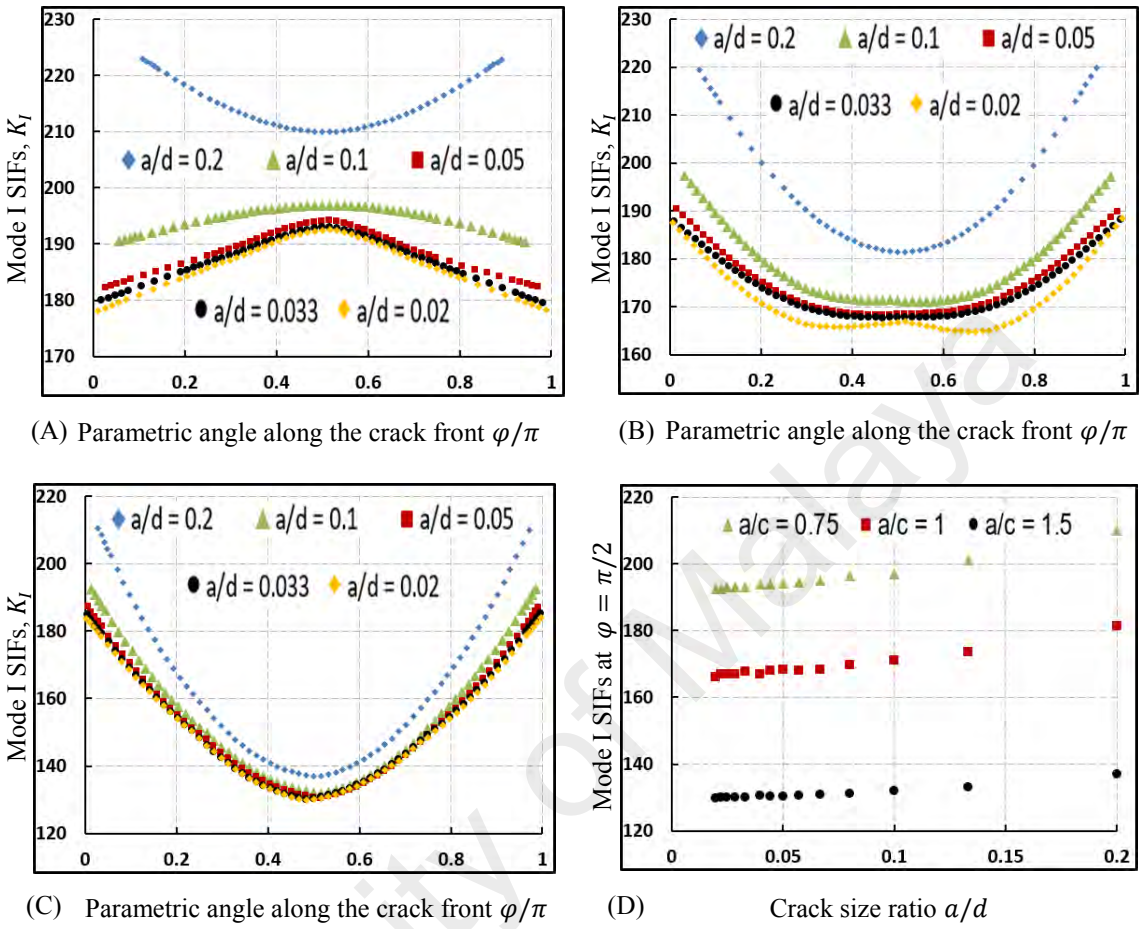

(A) Parametric angle along the crack front φ/π (B) Parametric angle along the crack front φ/π

(C) Parametric angle along the crack front φ/π (D) Crack size ratio a/d

Figure 4-7: Mode I SIF distributions for semi-elliptical surface cracks on the cylinder bar under pure tension (A) for a/c=0.75; (B) for a/c=1; (C) for a/c=1.5; (D) SIF values at $\varphi = \pi/2$.

Results for Mode III SIFs of semi-elliptical surface cracks in the cylinder bar subjected to pure torsion are provided in Figure 4-9. As it mentioned before, Mode III is more sensitive than Mode II and rate of changes for Mode III is more considerable. Same graphs are plotted for Mode III SIF values at $\varphi = \pi/2$ where the maximum value for Mode III SIF occurs (Figure 4-9D). Despite Mode II, Mode III SIF, acquires less values of SIF at a higher size ratio as it expected. It is shown that Mode III is more sensitive to crack size changes than Mode II. Graphs in Figure 4-9D confirm that for sizes less than 2-3% of cylinder diameter, Mode III is not considerably changed by changing in crack size.

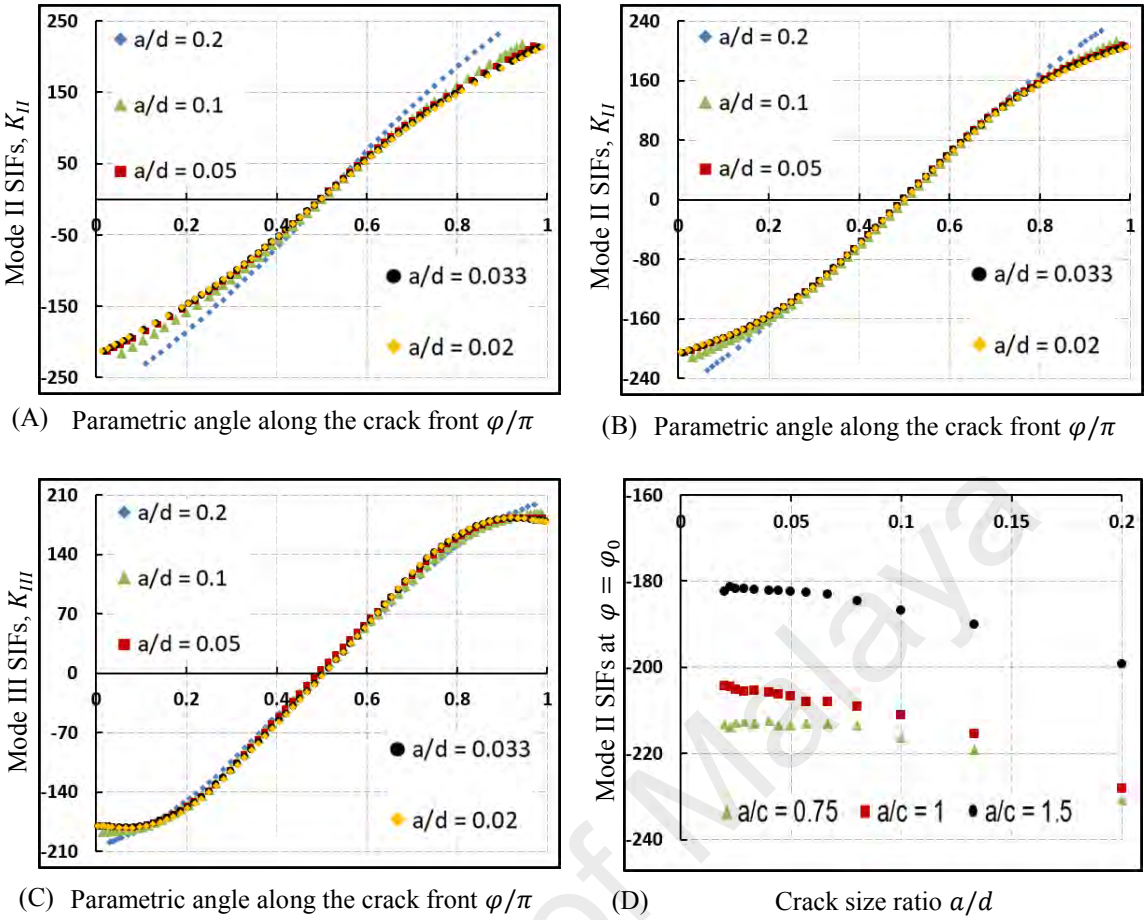

(A) Parametric angle along the crack front φ/π

(B) Parametric angle along the crack front φ/π

(C) Parametric angle along the crack front φ/π

(D) Crack size ratio a/d

Figure 4-8: Mode II SIF distributions for semi-elliptical surface cracks on the cylinder bar under pure torsion (A) for a/c=0.75; (B) for a/c=1; (C) for a/c=1.5; (D) SIF values at $\varphi = \varphi_0$.

4.2.2 Crack Shape Evaluation

In the second set of simulations, crack shape (a/c) is studied. Cylinder diameter is assumed $d = 10\text{mm}$ and its length $L = 40\text{mm}$. In the cylinder subjected to pure tension, four different crack size and five crack shapes are considered. Total number of simulations have been done for this set is 20. Crack ratios for second set in the cylinder subjected to pure tension are given in Table 4-3

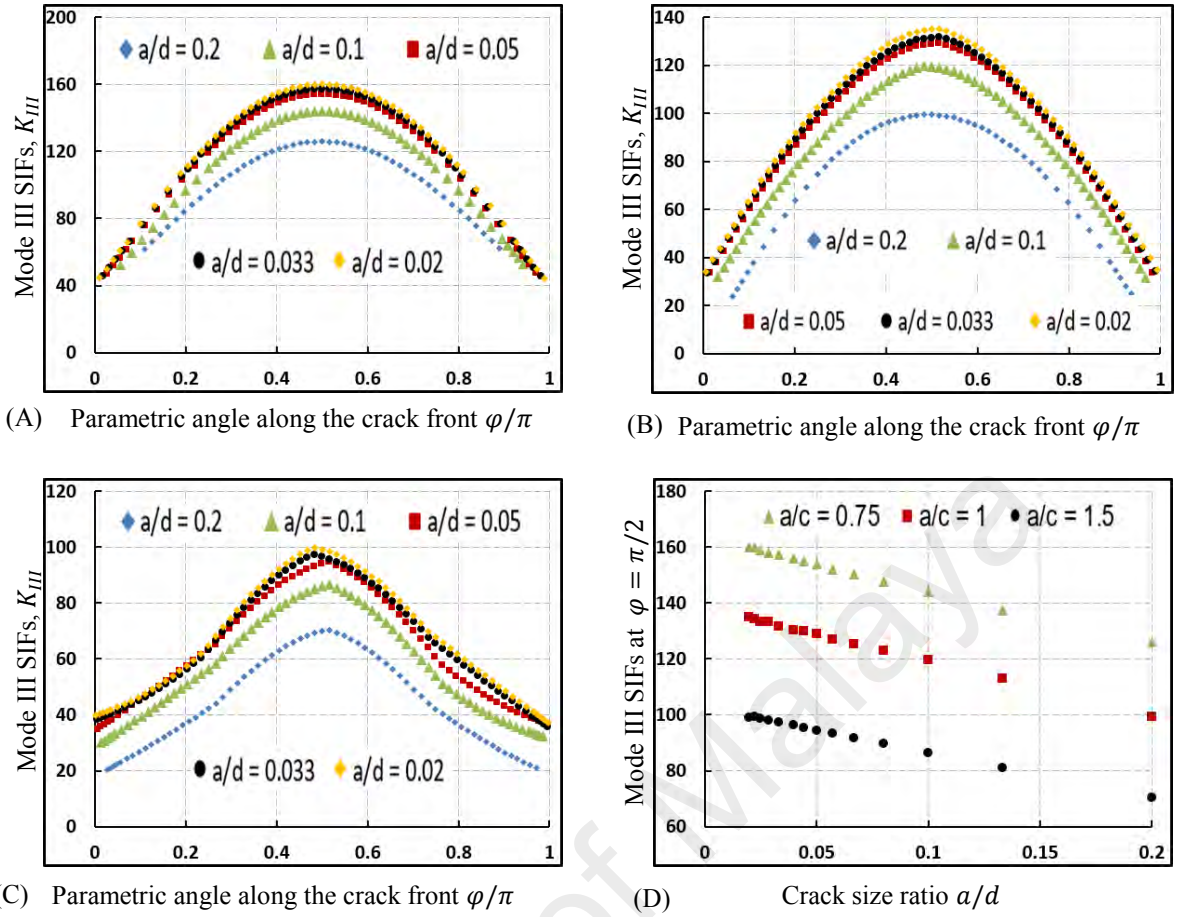

(A) Parametric angle along the crack front φ/π

(B) Parametric angle along the crack front φ/π

(C) Parametric angle along the crack front φ/π

(D) Crack size ratio a/d

Figure 4-9: Mode III SIF distributions for semi-elliptical surface cracks on the cylinder bar under pure torsion (A) for a/c=0.75; (B) for a/c=1; (C) for a/c=1.5; (D) SIF values at $\varphi = \pi/2$.

Table 4-3: Crack ratios used to study crack shape in the cylinder subjected to pure tension.

a/d	a/c
0.025	0.3333
0.05	0.5
0.075	1
0.1	1.5
	2

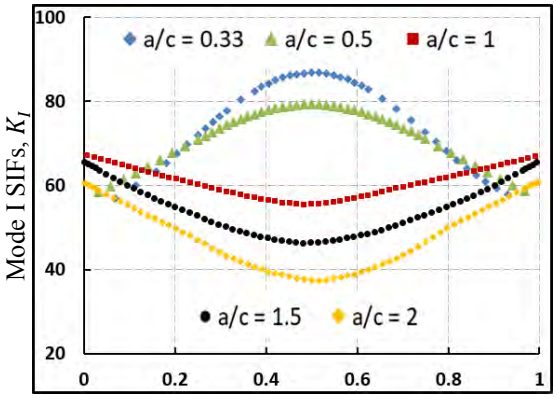

(A) Parametric angle along the crack front φ/π

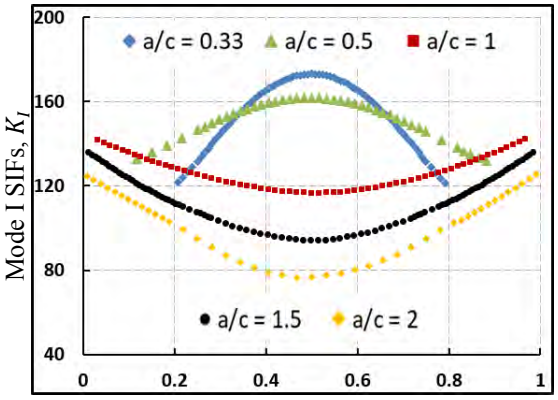

(B) Parametric angle along the crack front φ/π

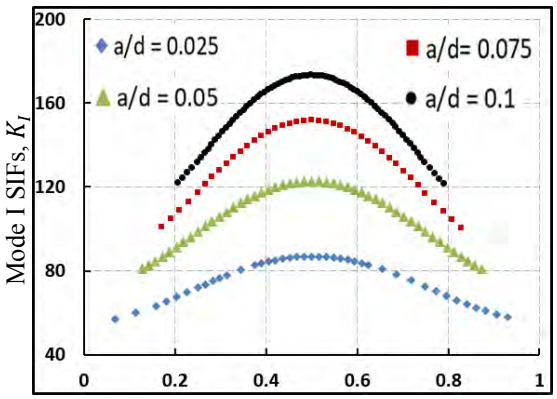

(C) Parametric angle along the crack front φ/π

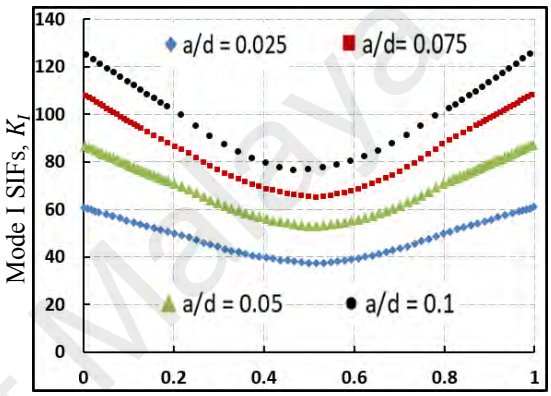

(D) Parametric angle along the crack front φ/π

Figure 4-10: Mode I SIF distributions for semi-elliptical surface cracks on the cylinder bar under pure tension (A) for a/d=0.025; (B) for a/d=0.1; (C) for a/c=1/3; (D) for a/c=2.

SIF distributions for crack shape evaluations in the cylinder subjected to pure tension are presented in Figure 4-10. SIF distributions for a crack with the same size of a/d=0.025 and a/d=0.1 for different crack shape are provided in Figure 4-10A & B, respectively. It can be seen that when crack shape is less than one maximum value of Mode I SIF along the crack front happens at DPE but for crack shapes higher than one CPE acquires the maximum. Influences of crack size ratio on Mode I SIF distributions presented in Figure 4-10C & D. Obviously, cracks with higher depths possess higher values of SIF.

In the cylinder bar subjected to pure torsion, four different crack size and seven crack shapes are evaluated. Total number of simulations have been done for this set is 28. Crack ratios for second set in the cylinder subjected to pure torsion are given in Table 4-4.

Table 4-4: Crack ratios used to study crack shape in the cylinder subjected to pure torsion.

a/d	a/c
0.025	0.3333
0.05	0.5
0.075	0.6
0.1	0.75
	1
	1.5
	2

Figure 4-11 provide Mode II SIF distributions on the cylinder bar subjected to pure torsion. Rising in crack size values causes increasing in Mode II SIFs but crack shape has different influences on SIFs. Increasing in crack shape values leads to higher values of Mode II SIFs until crack shape reaches a/c = 0.75-1 but when crack shape values exceed this limit, Mode II SIF will decrease around the CPE. It can be seen that even after a/c = 1 Mode II SIFs have higher values in the range of $\varphi \gg 0.08\pi$ but in the range of $\varphi_0 \ll \varphi \ll 0.08\pi$ values of Mode II SIFs get lower. This phenomenon is due to nature of Mode II SIFs.

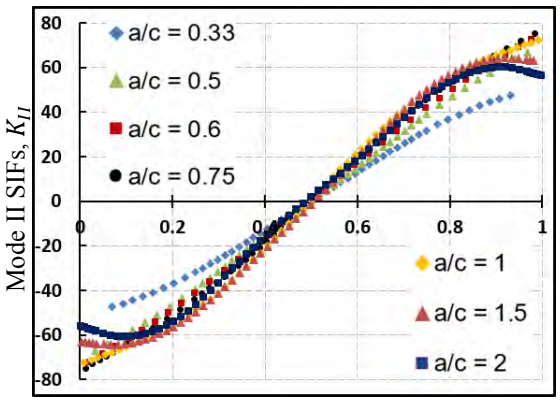

(B) Parametric angle along the crack front φ/π

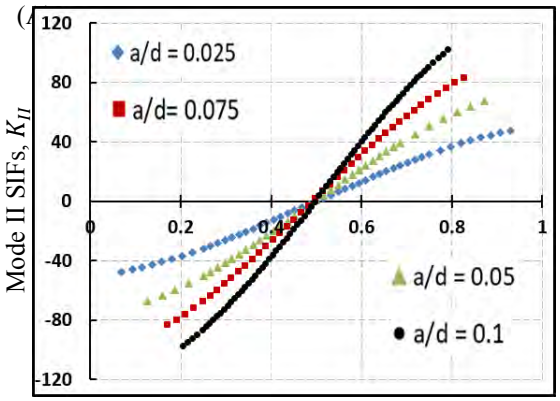

(C) Parametric angle along the crack front φ/π

(D) Parametric angle along the crack front φ/π

Figure 4-11: Mode II SIF distributions for semi-elliptical surface cracks on the cylinder bar under pure torsion (A) for a/d=0.025; (B) for a/d=0.1; (C) for a/c=1/3; (D) for a/c=2.

Mode III SIF distributions for a cylinder bar subjected to pure torsion is presented in Figure 4-12. Like Mode I, Mode III SIFs show the same changes according to crack size alterations. Higher crack sizes leads to higher SIF values but increasing in crack shape causes decreasing in SIF values. It can be observed that for cracks with aspect ratio higher than one, minimum values for Mode III SIFs happens at $\varphi \cong 0.08\pi$ instead of $\varphi = \varphi_0$ but differences in the range of $\varphi_0 \ll \varphi \ll 0.08\pi$ is negligible.

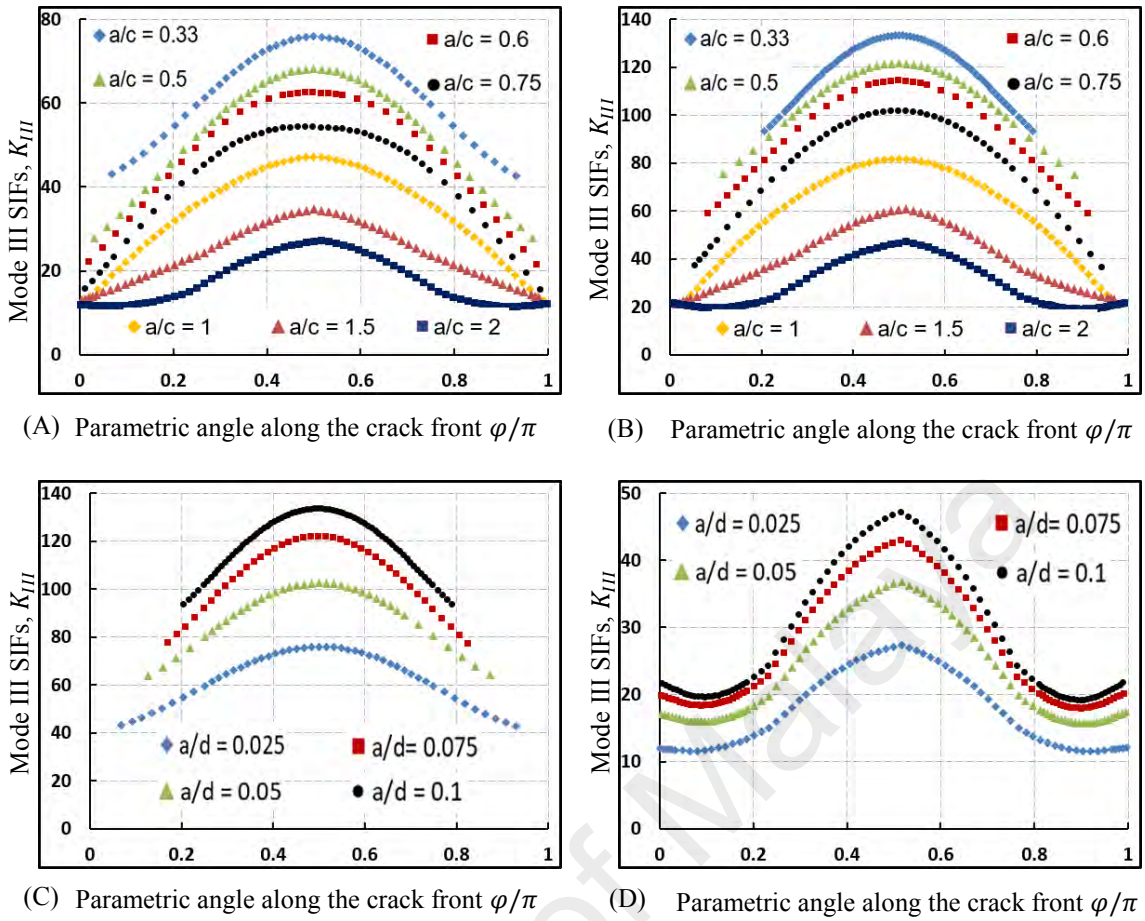

(A) Parametric angle along the crack front φ/π (B) Parametric angle along the crack front φ/π

(C) Parametric angle along the crack front φ/π (D) Parametric angle along the crack front φ/π

Figure 4-12: Mode III SIF distributions for semi-elliptical surface cracks on the cylinder bar under pure torsion (A) for a/d=0.025; (B) for a/d=0.1; (C) for a/c=1/3; (D) for a/c=2.

4.2.3 Crack Inclination Evaluation

4.2.3.1 Cylinder Bar Subjected to Pure Tension

For cylinder bar under pure tension four different angle of 0º, 22.5º, 45º and 67.5º are chosen to study effects of crack inclinations on SIFs. Total number of simulations have been performed in this section is 60 since the angle of 0º is studied in crack shape evaluations. As expected, Mode I is maximum at 0^o inclination due to pure tensile loading. Inclination alteration, as it discussed before, causes decrease in tension stress along the crack front until it gets to 90^o where Mode I SIFs get negligible. So the maximum values of Mode I is observed at 0^o it is negligible at 90^o.

Mode I SIF distributions for a crack with size of a/d=0.025 and shape of a/c=0.5 is presented in Figure 4-13 as an example. It can be seen that at the angle of 0º, Mode I SIFs have its maximum value and it decreases in value when inclination angle gets higher.

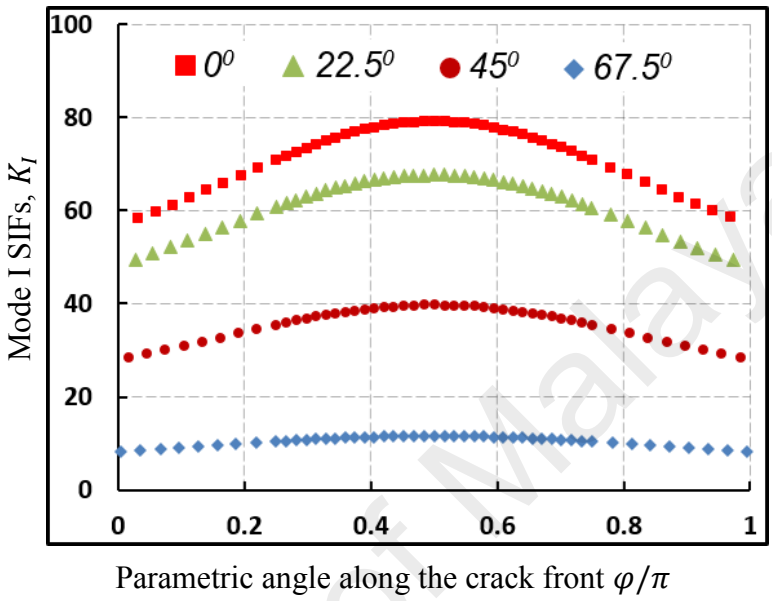

Figure 4-13: Mode I SIF distributions for semi-elliptical surface cracks on the cylinder bar subjected to pure tension a/d=0.025 and a/c=0.5.

At the angle of 0^o Mode II and Mode III SIFs are negligible due to lack of shear stresses but crack inclination leads to torsion component on the crack front. Mode II and Mode III SIFs experience their peak at angle of 45º where tension transform to pure torsion on the crack face at that angle. Figure 4-14A provides Mode II SIF distribution for a crack with size of a/d=0.025 and shape of a/c=0.5. It can be seen that at the angle of 45º Mode II SIFs reaches its maximum value. Effects of crack aspect ratio on Mode II SIFs in the cylinder bar under pure tension provided in Figure 4-14B.

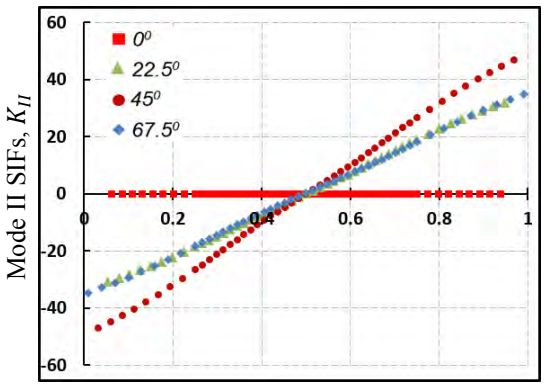

(A) Parametric angle along the crack front φ/π

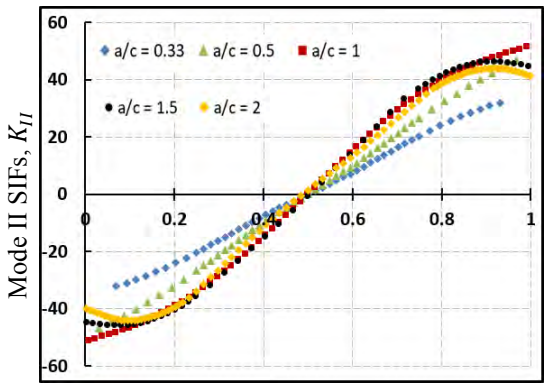

(B) Parametric angle along the crack front φ/π

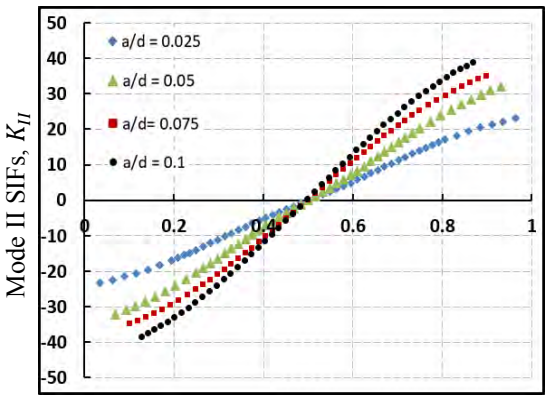

(C) Parametric angle along the crack front φ/π

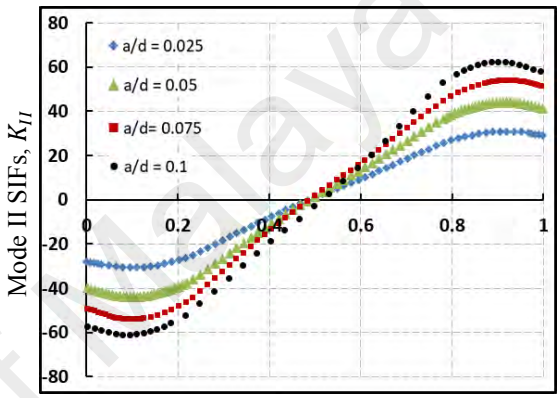

(D) Parametric angle along the crack front φ/π

Figure 4-14: Mode II SIF distributions for semi-elliptical surface cracks on the cylinder bar under pure tension (A) for a/d=0.025 & a/c=0.5 ; (B) for a/d=0.025 & $\theta = 45^o$; (C) for a/c=1/3 & $\theta = 45^o$; (D) for a/c=2 & $\theta = 45^o$.

Same patterns for cracks with shapes less and higher than one can be observed here. Influences of crack size on the Mode II SIF distributions are shown for minimum and maximum crack aspect ratio in Figure 4-14C & D, respectively. Cracks with higher depths receive higher Mode II SIFs.

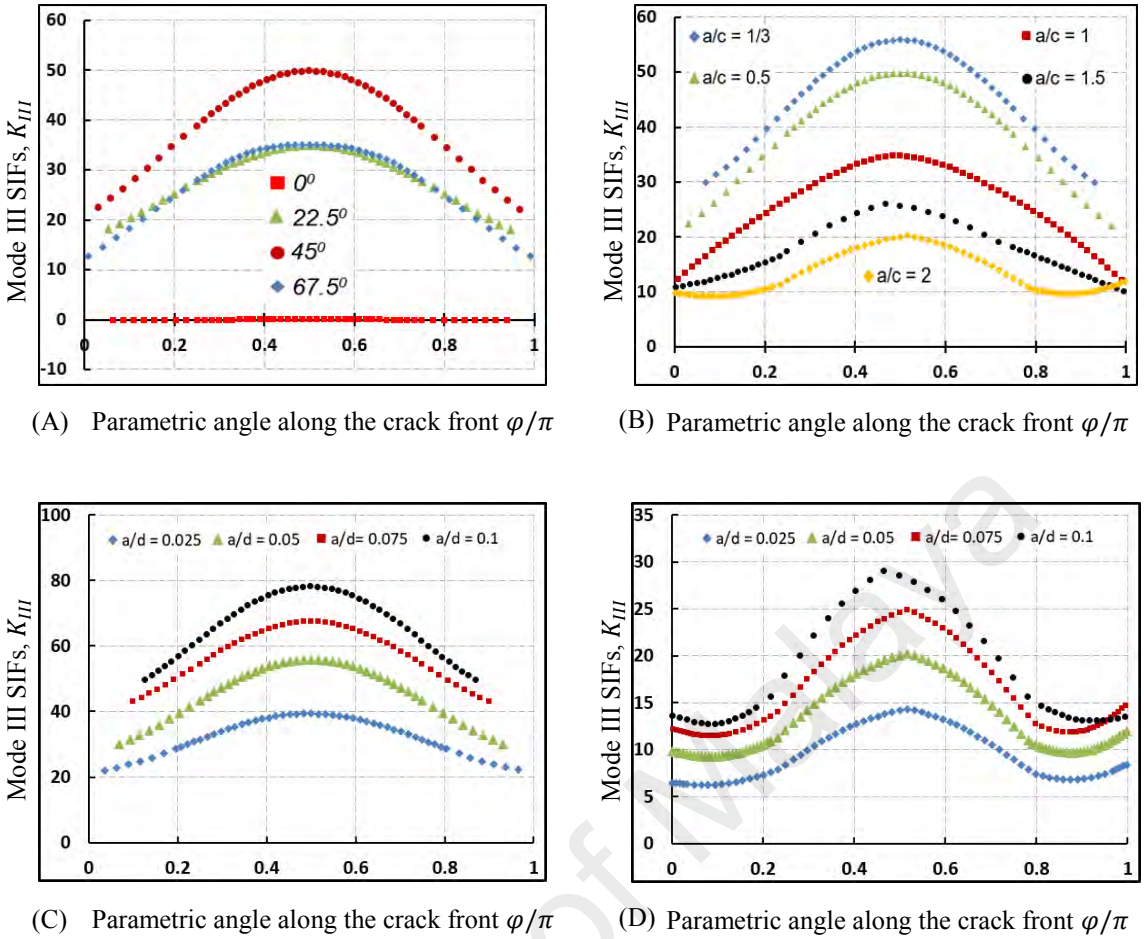

(A) Parametric angle along the crack front φ/π (B) Parametric angle along the crack front φ/π

(C) Parametric angle along the crack front φ/π (D) Parametric angle along the crack front φ/π

Figure 4-15: Mode III SIF distributions for semi-elliptical surface cracks on the cylinder bar under pure tension (A) when a/d=0.025 & a/c=0.5 ; (B) when a/d=0.025 & $\theta = 45^o$; (C) when a/c=1/3 & $\theta = 45^o$; (D) when a/c=2 & $\theta = 45^o$.

Same plots are presented for Mode III SIFs in Figure 4-15. Like Mode II, Mode III experience its maximum value at the angle of 45^o. Graphs for a crack with a same size and different crack aspect ratio confirms that cracks with less aspect ratio holds higher values of Mode III SIFs (Figure 4-15B). Mode III SIFs also show the same reaction to the crack size alterations. It increases when crack size gets higher.

4.2.3.2 Cylinder Bar Subjected to Pure Torsion

For cylinder bar under pure torsion five different angle of 0°, 22.5°, 45°, 67.5° and 90° are chosen to study effects of crack inclinations on SIFs. Total number of simulations have

been performed in this section is 48 since the angle of 0° is studied in crack shape evaluations and only 3 crack shapes of 0.75, 1 and 1.5 are chosen to evaluate. Despite Mode I, Mode II is maximum at 0^o inclination due to pure torsional loading. Inclination alteration, as it discussed before, causes decrease in shear stress along the crack front it gets to 45^o where it is negligible and it gains its maximum value again at the angle of 90^o. Mode I SIF distributions for a crack with size of a/d=0.025 and shape of a/c=0.5 is presented in Figure 4-16A as an example. At the angle of 0^o mode I SIFs are negligible due to lack of tensile stresses but crack inclination leads to tension component on the crack front. Mode I SIFs experience their peak at angle of 45° where torsion transform to pure tension on the crack face at that angle (Figure 4-16A). Crack shape and crack size contribute the same influences on Mode I SIFs in the cylinder bar under pure torsion as in the cylinder bar under pure tension (Figure 4-16).

Figure 4-17 provides Mode II SIF distribution for the same crack. It can be seen that maximum values of Mode II is observed at 0^o and 90^o with opposite sign and it is negligible at 45°. Same pattern can be seen in Mode III SIFs where absolute values at $\varphi = \pi/2$ in the angle of 90^o is a bit higher than the same one at 0^o. (Figure 4-18).

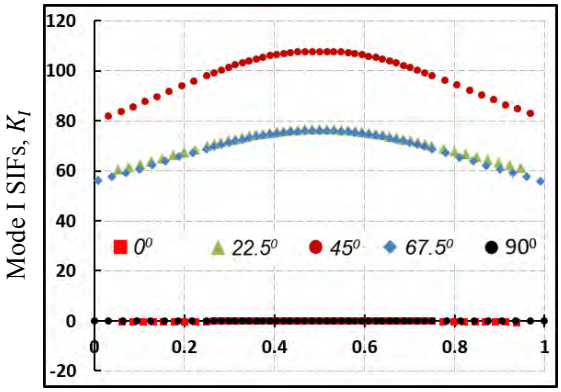

(A) Parametric angle along the crack front φ/π

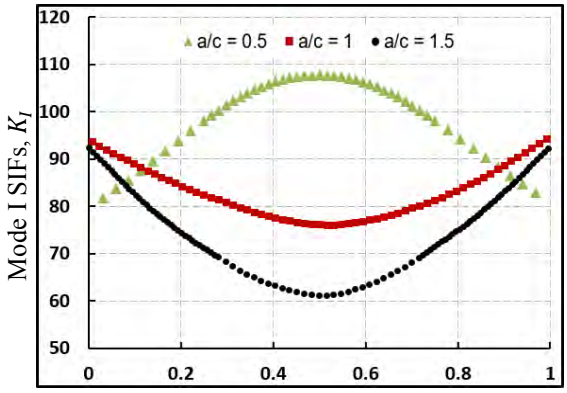

(B) Parametric angle along the crack front φ/π

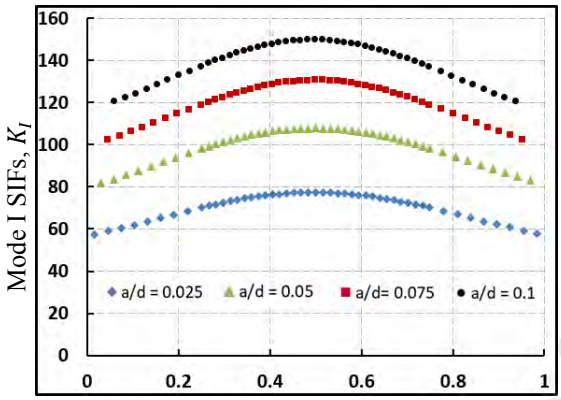

(C) Parametric angle along the crack front φ/π

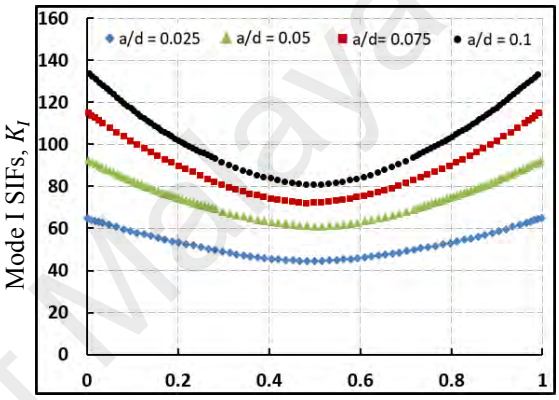

(D) Parametric angle along the crack front φ/π

Figure 4-16: Mode I SIF distributions for semi-elliptical surface cracks on the cylinder bar under pure torsion (A) for a/d=0.05 & a/c=0.5 ; (B) for a/d=0.05 & $\theta = 45^o$; (C) for a/c=0.5 & $\theta = 45^o$; (D) for a/c=1. & $\theta = 45^o$.

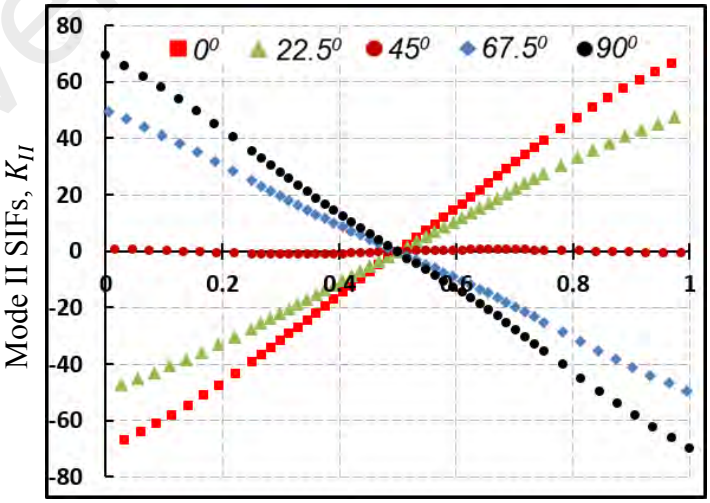

Parametric angle along the crack front φ/π

Figure 4-17: Mode II SIF distributions for semi-elliptical surface cracks on the cylinder bar subjected to pure torsion a/d=0.025 and a/c=0.5.

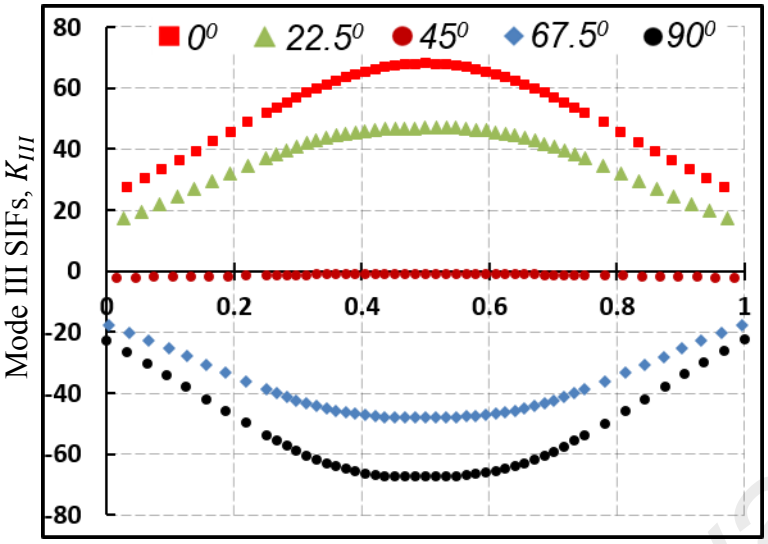

Figure 4-18: Mode III SIF distributions for semi-elliptical surface cracks on the cylinder bar subjected to pure torsion a/d=0.025 and a/c=0.5.

4.3 Closed-Form Solution

4.3.1 Cylinder Bar under Pure Tension

Stress intensity factors for a semi-elliptical surface crack in the cylinder subjected to the pure tension can be obtained from Eq. 4-24 (This solution works for materials which have Poisson's ratio close to $\nu \approx 0.3$). This solution is obtained through curve fitting approaches on the results produced by BEASY software.

$$K^0 = \sigma^0 \sqrt{\frac{\pi a}{Q}}\, F_{JM}\left(\frac{a}{d}, \frac{a}{c}, \frac{c}{r}, \theta, \varphi\right) \qquad \text{Eq. 4-24}$$

$0.02 \ll {}^{a}/_{d} \ll 0.2$, $0.33 \ll {}^{a}/_{c} \ll 2$, ${}^{c}/_{r} < 0.7$ and $\varphi_0 \ll \varphi \ll \pi - \varphi_0$

Q is shape factor for an ellipse and given as

$$Q = 1 + 1.464\left(\frac{a}{c}\right)^{1.65} \qquad for\ \frac{a}{c} \ll 1 \qquad \text{Eq. 4-25}$$

$$Q = 1 + 1.464\left(\frac{c}{a}\right)^{1.65} \qquad for\ \frac{a}{c} > 1 \qquad \text{Eq. 4-26}$$

The function F_{JM} accounts for influence of crack shape($^{a}/_{c}$), crack size$\left(^{a}/_{d}\right)$, crack inclination (θ) and parametric angle(φ), and is chosen as

$$F_{JM} = f_S\, f_\theta\, g \qquad \text{Eq. 4-27}$$

To achieve a reliable and practical approximation on available results, each function has been evaluated separately. Function f_S stands for normalized SIF values at $\varphi = {}^{\pi}/_{2}$ for Mode I and Mode III SIFs. As it discussed before, maximum or minimum values for Mode I SIF happens at the $\varphi = {}^{\pi}/_{2}$ and for Mode III this is the point which always acquires the maximum value of SIF.

However, for Mode II SIF, there is no single positon along the crack front where the maximum occurs due to corner singularity. In Mode II SIFs, maximum values of SIF at $\varphi_0 \ll \varphi \ll 0.08\pi$ according to the crack aspect ratio. Normalized values of maximum Mode II SIF are collected in each case and used to determine the function f_S for Mode II.

Function f_S for Mode I, Mode II and Mode III in the cylinder bar under pure tension can be written, respectively, as

$$f_{s,I} = 1.353 + 0.022\left(^{a}/_{d}\right) + 1.774\left(^{a}/_{d}\right)^{2} + 1.157\sin\left(-1.142\left(^{a}/_{c}\right)\right) + \left(0.8613\sin\left(1.478\left(^{a}/_{c}\right)\right)\right)^{2} \qquad \text{Eq. 4-28}$$

$$f_{s,II} = 0.1878 - 0.3766\left(\frac{a}{d}\right)\left(\frac{a}{c}\right) + 4.068\left(\frac{a}{d}\right)^2 + 1.772\sin\left(-0.845\left(\frac{a}{c}\right)\right) + \left(1.062\sin\left(0.8393\left(\frac{a}{c}\right)\right)\right)^3 \quad \text{Eq. 4-29}$$

$$f_{s,III} = 1.547 + 0.4245\left(\frac{a}{d}\right) - 3.21\left(\frac{a}{d}\right)^2 - 1.046e^{0.1412(a/c)} + \left(0.2783\sin\left(1.872\left(\frac{a}{c}\right)\right)\right)^2 \quad \text{Eq. 4-30}$$

The function f_θ accounts for influence of crack inclination θ on the SIFs. Since inclination leads to stress equilibrium modification on the crack face and arising new stress components. Inclination for a crack modelled in the cylinder bar prompts different φ_0 which means same crack with same size and ratio has different crack front arc length in different inclination.

The function f_θ for Mode I, Mode II and Mode III SIFs in the cylinder bar under pure tension proposed as:

$$f_{\theta,I} = (\cos\theta)^2 \quad \text{Eq. 4-31}$$

$$f_{\theta,II} = 1.023e^{-0.01205(a/c)} - 0.5477e^{-3.697(a/c)} \times \sin(2\theta) + \left(0.03936e^{-2.714(a/c)} - 1.039e^{-5.694(a/c)}\right) \times (\cos(2\theta) - 1) \quad \text{Eq. 4-32}$$

$$f_{\theta,III} = \sin(2\theta) \quad \text{Eq. 4-33}$$

Last function in the solution is fine-tuning curve-fitting g function. Few factors considered to derive the function g. The nature of each Mode and their distributions along the crack front in different crack size and ratio are studied to obtain a proper curve-fitting function. These function can be written as

$$g_I = p_I + (1 - q_I \sin\varphi)^2 \quad \text{Eq. 4-34}$$

$$g_{II} = p_{II} \cos\varphi + q_{II} \sin 2\varphi \quad \text{Eq. 4-35}$$

$$g_{III} = 1 - \left(p_{III} \cos\varphi + q_{III} \sin 2\varphi\right)^2 \quad \text{Eq. 4-36}$$

p and q are functions of crack aspect ratio and crack size ratio and presented in Table 4-5.

Table 4-5: Polynominal approximation formula for Eq. 4-34 - Eq. 4-36 and their coefficients.

$$p \equiv q = c_{00} + c_{10}\left(\frac{a}{d}\right) + c_{01}\left(\frac{a}{c}\right) + c_{20}\left(\frac{a}{d}\right)^2 + c_{11}\left(\frac{a}{d}\right)\left(\frac{a}{c}\right) + c_{02}\left(\frac{a}{c}\right)^2 + c_{30}\left(\frac{a}{d}\right)^3 + c_{21}\left(\frac{a}{d}\right)^2\left(\frac{a}{c}\right) + c_{12}\left(\frac{a}{d}\right)\left(\frac{a}{c}\right)^2 + c_{03}\left(\frac{a}{c}\right)^3 + c_{31}\left(\frac{a}{d}\right)^3\left(\frac{a}{c}\right) + c_{22}\left(\frac{a}{d}\right)^2\left(\frac{a}{c}\right)^2 + c_{13}\left(\frac{a}{d}\right)\left(\frac{a}{c}\right)^3 + c_{04}\left(\frac{a}{c}\right)^4$$

	c_{00}	c_{10}	c_{01}	c_{20}	c_{11}	c_{02}	c_{30}	c_{21}	c_{12}	c_{03}	c_{31}	c_{22}	c_{13}	c_{04}
p_I	-0.6171	-12.69	0.9844	33.4	29.38	-0.6003	19.32	-66.47	-18.79	0.4273	0.391	26.85	3.553	-0.1077
q_I	-0.2334	-6.1	0.2481	25.32	12.91	0.0018	-3.223	-47.65	-7.041	0.0467	16.13	18.27	1.013	-0.0149
p_{II}	0.9235	5.776	0.2709	-97.49	1.124	-0.7362	610.4	15.14	-3.089	0.6089	-292.3	16.65	0.471	-0.151
q_{II}	0.2921	0.2312	-2.23	87.53	-12.66	3.779	-485.9	-65.31	14.65	-2.353	375.5	1.405	-4.062	0.503
p_{III}	0.1613	6.796	1.947	-109.6	-5.332	-2.147	673.4	0.2147	7.555	0.8326	-362.4	32.6	-3.552	-0.0848
q_{III}	0.2246	-3.624	-0.7859	31.57	9.119	0.09398	-108.9	-24.43	-8.556	0.5522	-37.29	14.05	2.117	-0.2056

It is evident that parametric angle φ for cracks in infinite solid body start from zero and goes to π but as it mentioned before in the cylinder bar since it has curvature parametric angle does not have the same range. In the cylinder bar parametric angle is $\varphi_0 \leq \varphi \leq \pi - \varphi_0$ and φ_0 can be calculated by

$$\varphi_0 = \tan^{-1}\left(\frac{a}{\sqrt{4r^2 - a^2}}\right) \qquad \text{if} \quad a = c \;\&\; \theta = 0 \quad \text{Eq. 4-37}$$

Else

$$\varphi_0 = \left|\tan^{-1}\left(\frac{\cos(\theta)\left(\sqrt{a^2 {r_\theta}^4 + c^4 r^2 - a^2 c^2 {r_\theta}^2} - a{r_\theta}^2\right)}{\sqrt{a\left(2r^2\sqrt{a^2 {r_\theta}^4 + c^4 r^2 - a^2 c^2 {r_\theta}^2} + a^3 {r_\theta}^2 - ac^2 r^2 - 2ar^2 {r_\theta}^2\right)}}\right)\right| \quad \text{Eq. 4-38}$$

Where $r_\theta = {}^{r}/_{\cos(\theta)}$ and $r = d/2$.

However, in practical cases like existing cracks on the components it is impossible to define parameter c. According to Figure 4-19, it is easier to measure a and c'. In this case Equations Eq. 4-45 and Eq. 4-46 should be implemented to calculate φ_0 and c, respectively.

$$\beta = \cos^{-1}\left(\frac{c'}{r_\theta}\right) \quad \text{Eq. 4-39}$$

$$a' = r(1 - \sin\beta) \quad \text{Eq. 4-40}$$

$$\varphi_0 = \sin^{-1}\left(\frac{a'}{a}\right) \quad \text{Eq. 4-41}$$

$$c = \frac{c'}{\cos\varphi_0} \quad \text{Eq. 4-42}$$

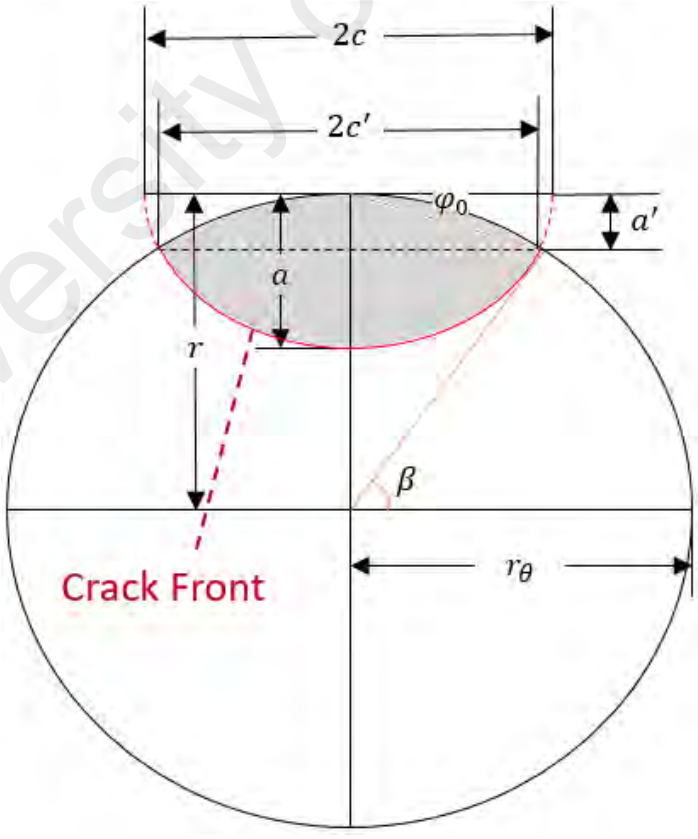

Figure 4-19: Schematic diagram of a semi-elliptical surface crack in a solid cylinder bar at any inclination θ.

4.3.1.1 Evaluations of Crack Size Ratio

Figure 4-20 shows Mode I SIF values at DPE for a crack with same aspect ratio on different cylinders under pure tension. All results are normalized by $\tau^0\sqrt{\pi a/Q}$ factor. Proposed solution shows good agreement in Mode I and differences between BEASY and solution do not exceed 3%.

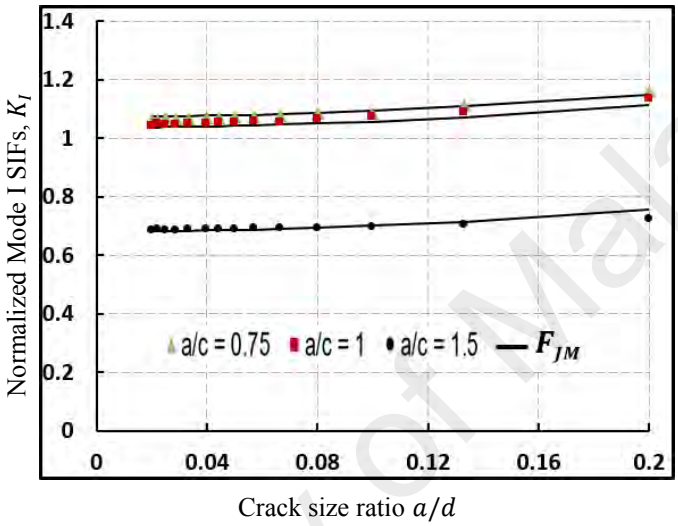

Figure 4-20: Normalized SIF values at $\varphi = \pi/2$ for Mode I SIFs in the cylinder bar under pure tension.

4.3.1.2 Evaluations of Crack Aspect Ratio

Normalized Mode I SIFs for a semi-elliptical surface crack with size of a/d = 0.025 & 0.1 are plotted in Figure 4-21A & B. Results for a semi-elliptical surface crack with size of a/c = 1/3 & 2 are plotted in Figure 4-21C & D. clearly solution shows acceptable accuracy in Mode I in all ranges.

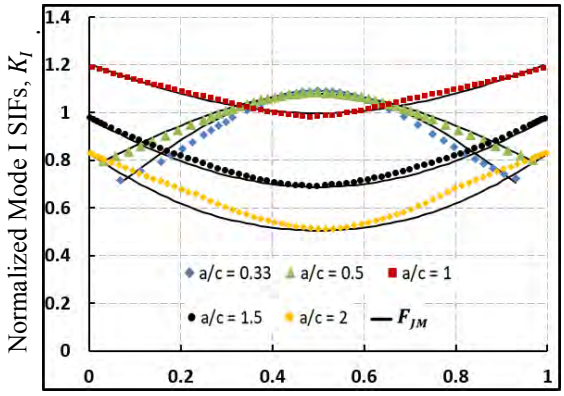

(A) Parametric angle along the crack front φ/π

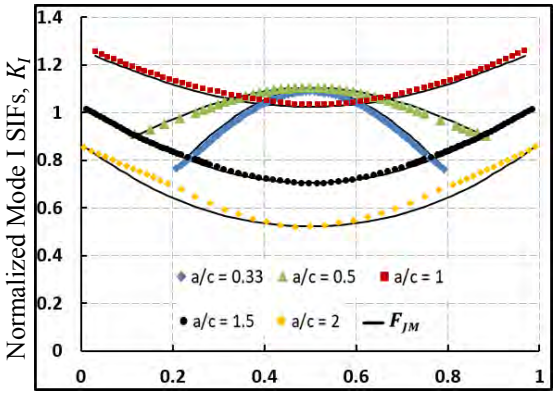

(B) Parametric angle along the crack front φ/π

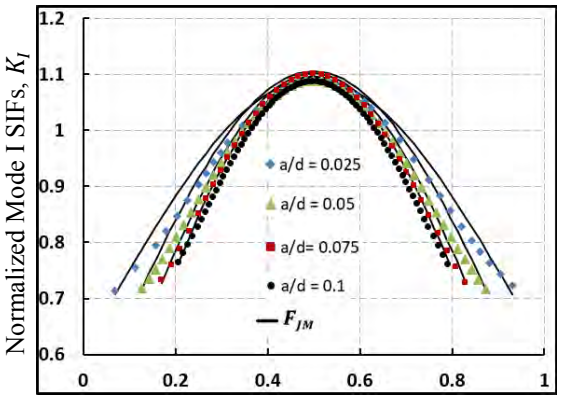

(C) Parametric angle along the crack front φ/π

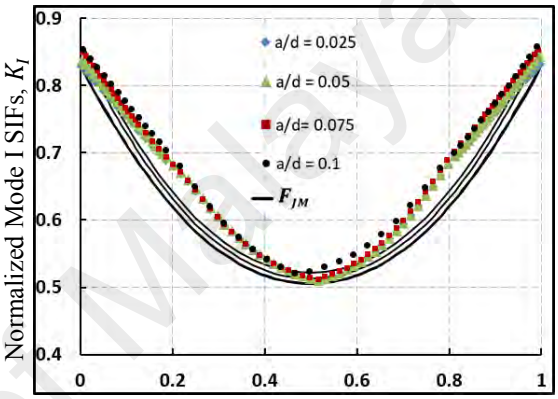

(D) Parametric angle along the crack front φ/π

Figure 4-21: Normalized Mode I SIF distributions for semi-elliptical surface crack on the cylinder under tension (A) for a/d = 0.025; (B) for a/d = 0.1; (C) for a/c = 1/3; (D) for a/c = 2.

4.3.1.3 Evaluations of Crack Inclination Angle

Typical normalized Mode I SIFs for a semi-elliptical surface crack with size of a/d = 0.05 and crack shape of a/c = 0.5 at different inclination angle is plotted in Figure 4-22. It can be seen that proposed solution shows good consistency with BEASY at different angles. Figure 4-23 provides results for Mode II SIFs in the cylinder bar under pure tension along with proposed solution. Solution shows good accuracy in different crack sizes, shapes and inclinations and the differences are within 5%.

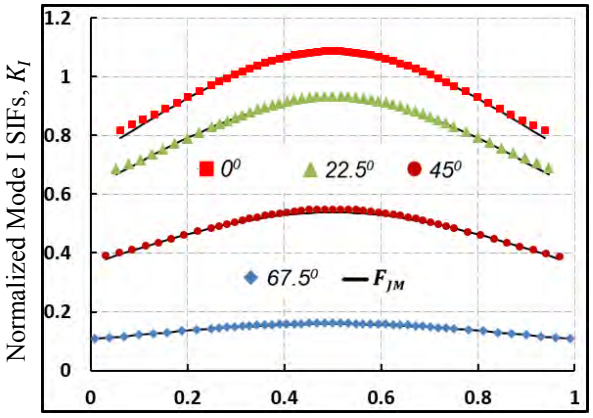

Figure 4-22: Normalized Mode I SIF distributions for semi-elliptical surface crack with size of a/d = 0.05 & a/c = 0.5 on the cylinder bar under pure tension.

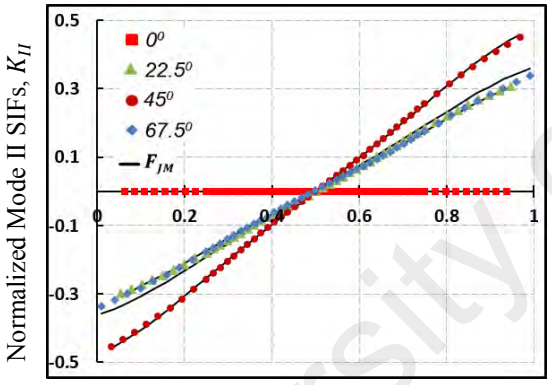

(A) Parametric angle along the crack front φ/π

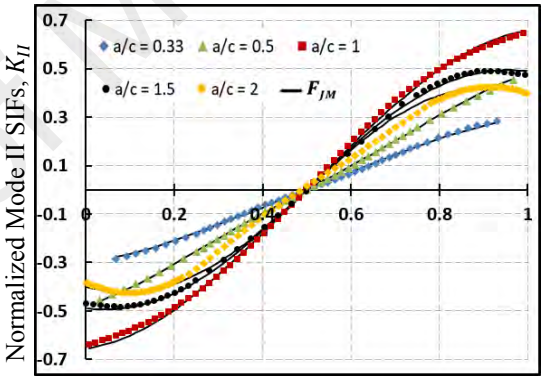

(B) Parametric angle along the crack front φ/π

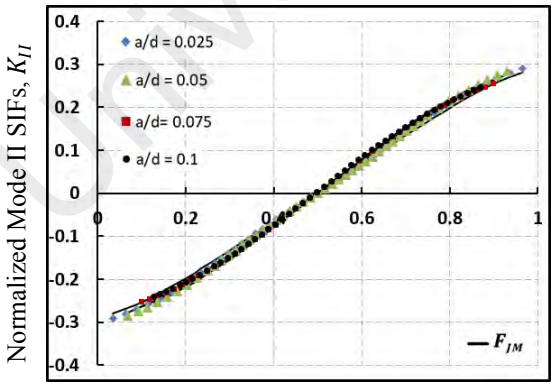

(C) Parametric angle along the crack front φ/π

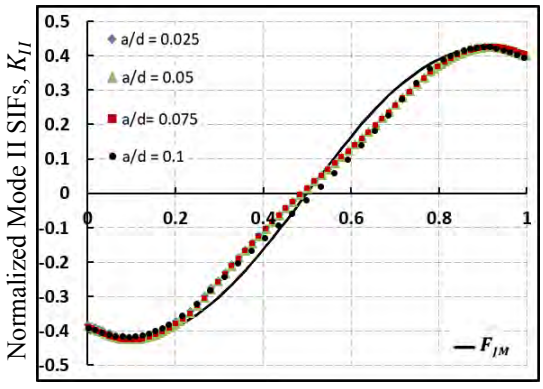

(D) Parametric angle along the crack front φ/π

Figure 4-23: Normalized Mode II SIF distributions for semi-elliptical surface crack on the cylinder under tension (A) for a/d = 0.05 & a/c = 0.5; (B) for a/d = 0.05 & $\theta = 45^o$; (C) for a/c = 1/3 & $\theta = 45^o$; (D) for a/c = 2 & $\theta = 45^o$.

Same verification for Mode III SIFs in the cylinder bar under pure tension is presented in Figure 4-24. Solution also exhibits high accuracy in all different crack ratios and inclinations.

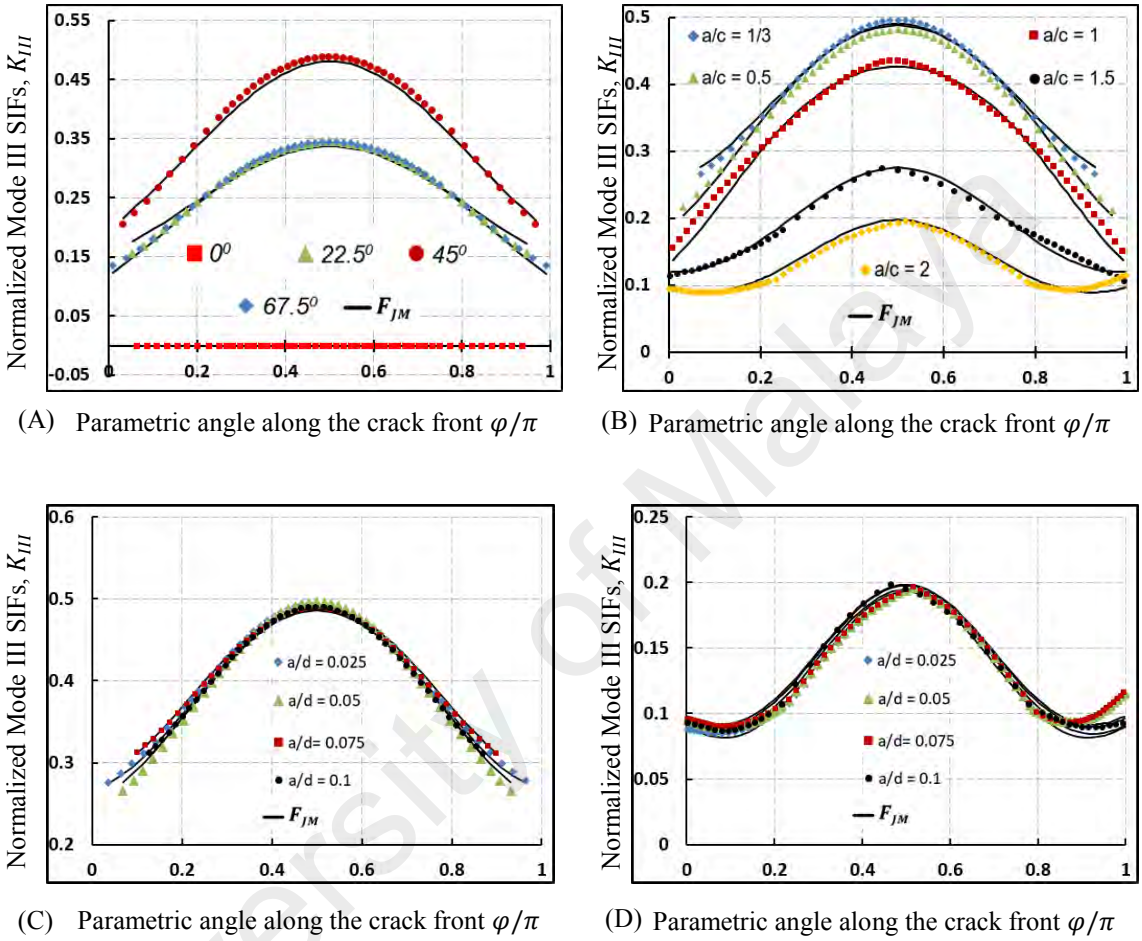

(A) Parametric angle along the crack front φ/π

(B) Parametric angle along the crack front φ/π

(C) Parametric angle along the crack front φ/π

(D) Parametric angle along the crack front φ/π

Figure 4-24: Normalized Mode III SIF distributions for semi-elliptical surface crack on the cylinder under tension (A) for a/d = 0.05 & a/c = 0.5; (B) for a/d = 0.05 & $\theta = 45^o$; (C) for a/c = 1/3 & $\theta = 45^o$; (D) for a/c = 2 & $\theta = 45^o$.

4.3.2 Cylinder bar under Pure Torsion

Stress intensity factors for a semi-elliptical surface crack in the cylinder subjected to the pure torsion can be obtained from Eq. 4-43 (This solution works for ductile materials which have Poisson's ratio close to $\nu \approx 0.3$). This solution is obtained through curve fitting approaches on the results produced by BEASY software.

$$K^0 = \tau^0 \sqrt{\frac{\pi a}{Q}}\, F_{JM}\left(\frac{a}{d}, \frac{a}{c}, \frac{c}{r}, \theta, \varphi\right) \quad \text{Eq. 4-43}$$

$0.02 \ll {}^{a}/_{d} \ll 0.2$, $0.33 \ll {}^{a}/_{c} \ll 2$, ${}^{c}/_{r} < 0.7$ and $\varphi_0 \ll \varphi \ll \pi - \varphi_0$ when $\theta = 0$

$0.02 \ll {}^{a}/_{d} \ll 0.2$, $0.5 \ll {}^{a}/_{c} \ll 2$, ${}^{c}/_{r} < 0.7$ and $\varphi_0 \ll \varphi \ll \pi - \varphi_0$ when $\theta > 0$

Q can be obtained by Eq. 4-25 and Eq. 4-26.

Function f_S for Mode I, Mode II and Mode III in the cylinder bar under pure torsion can be written, respectively, as

$$f_{s,I} = 0.8876 + 0.1288e^{0.1623({}^{a}/_{d})} + 0.1335e^{-20.72({}^{a}/_{d})} - 0.005913e^{2.86({}^{a}/_{c})} \quad \text{Eq. 4-44}$$

$$f_{s,II} = -0.6591 + 0.3114\left(\frac{a}{d}\right) - 4.974\left(\frac{a}{d}\right)^2 + 3.986\left(\frac{a}{d}\right)^3 - 0.5521\sin\left(1.386\left(\frac{a}{c}\right)\right) + \left(-0.3238\sin\left(4.193\left(\frac{a}{c}\right)\right)\right)^2 + \left(0.5895\sin\left(5.028\left(\frac{a}{c}\right)\right)\right)^3 \quad \text{Eq. 4-45}$$

$$f_{s,III} = 0.3633 - 1.187\left(\frac{a}{d}\right) + 0.8775\left(\frac{a}{d}\right)^2 - 0.9186\left(\frac{a}{d}\right)^3 + 0.4616e^{-0.3482({}^{a}/_{c})} + 0.1853\sin\left(2.479\left(\frac{a}{c}\right)\right) + \left(-0.2319\sin\left(4.652\left(\frac{a}{c}\right)\right)\right)^2 \quad \text{Eq. 4-46}$$

The function f_θ for Mode I, Mode II and Mode III SIFs in the cylinder bar under pure torsion proposed as

$$f_{\theta,I} = \sin(2\theta) \quad \text{Eq. 4-47}$$

$$f_{\theta,II} = \left(0.4366e^{-5.654(a/c)} + 0.9955e^{-0.00078(a/c)}\right)\cos(2\theta) - 7.552e^{-3.989(a/c)} + 7.16e^{-3.918(a/c)} \quad \text{Eq. 4-48}$$

$$f_{\theta,III} = \cos(2\theta) \quad \text{Eq. 4-49}$$

Function g for Mode I, Mode II and Mode III SIFs in the cylinder bar under pure torsion proposed as

$$g_I = p_I + (1 - q_I \sin\varphi)^2 \quad \text{Eq. 4-50}$$

$$g_{II} = p_{II}\cos\varphi + q_{II}\sin 2\varphi \quad \text{Eq. 4-51}$$

$$g_{III} = 1 - \left(p_{III}\cos\varphi + q_{III}\sin 2\varphi\right)^2 \quad \text{Eq. 4-52}$$

p and q are functions of crack aspect ratio and crack size ratio and presented in Table 4-6.

Table 4-6: Polynominal approximation formula for Eq. 4-50 - Eq. 4-52 and their coefficients.

$$p \equiv q = c_{00} + c_{10}\left(\frac{a}{d}\right) + c_{01}\left(\frac{a}{c}\right) + c_{20}\left(\frac{a}{d}\right)^2 + c_{11}\left(\frac{a}{d}\right)\left(\frac{a}{c}\right) + c_{02}\left(\frac{a}{c}\right)^2 + c_{30}\left(\frac{a}{d}\right)^3 + c_{21}\left(\frac{a}{d}\right)^2\left(\frac{a}{c}\right) + c_{12}\left(\frac{a}{d}\right)\left(\frac{a}{c}\right)^2 + c_{03}\left(\frac{a}{c}\right)^3 + c_{31}\left(\frac{a}{d}\right)^3\left(\frac{a}{c}\right) + c_{22}\left(\frac{a}{d}\right)^2\left(\frac{a}{c}\right)^2 + c_{13}\left(\frac{a}{d}\right)\left(\frac{a}{c}\right)^3 + c_{04}\left(\frac{a}{c}\right)^4$$

	c_{00}	c_{10}	c_{01}	c_{20}	c_{11}	c_{02}	c_{30}	c_{21}	c_{12}	c_{03}	c_{31}	c_{22}	c_{13}	c_{04}
p_I	-0.9407	0.4848	1.408	-5.707	1.706	-0.3389								
q_I	-0.3865	-0.077	0.5135	-4.6	1.55	-0.0717								
p_{II}	1.103	5.529	-0.4552	3.444	-13.36	0.7323	-15.77	2.821	9.822	-0.463	11.43	-3.953	-2.144	0.09452
q_{II}	0.2121	2.898	-1.671	-9.058	-4.35	2.403	16.89	9.314	2.168	-1.243	-9.774	-3.473	-0.4617	0.23
p_{III}	0.4359	2.414	0.8051	-39.9	-4.375	-0.134	26.44	68.72	1.81	-0.3877	-21.45	-26.36	-0.0509	0.1455
q_{III}	0.06701	1.543	-0.3278	2.763	-2.453	-0.2913	41.77	-15.8	1.99	0.5969	-50.62	12.22	-0.7232	-0.1809

4.3.2.1 Evaluations of Crack Size Ratio

Normalized maximum SIF values for Mode II and Mode III are presented in Figure 4-25A & B, respectively along the proposed solution. Maximum differences between results and solution is observed at crack sizes 20% of cylinder diameter which is within 7-8%.

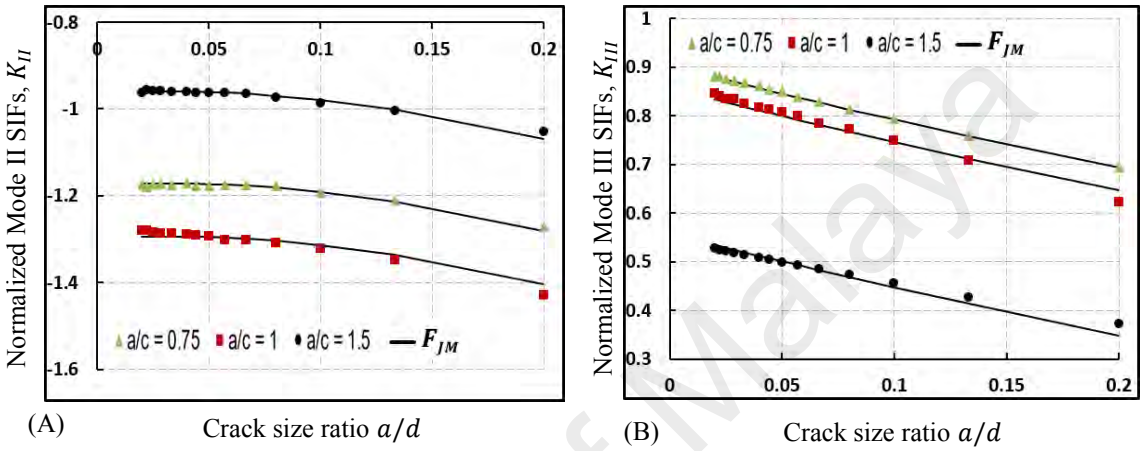

Figure 4-25: Normalized SIF values at (A) $\varphi = \varphi_0$ for Mode II; (B) $\varphi = \pi/2$ Mode III.

4.3.2.2 Evaluations of Crack Aspect Ratio

Verifications of solution for Mode II and Mode III SIFs in the cylinder bar under pure torsion are provided in Figure 4-26 and Figure 4-27, respectively. Solution exhibits consistency on both Mode II and Mode III SIFs. Maximum differences are observed in Mode III SIFs which is within 5%.

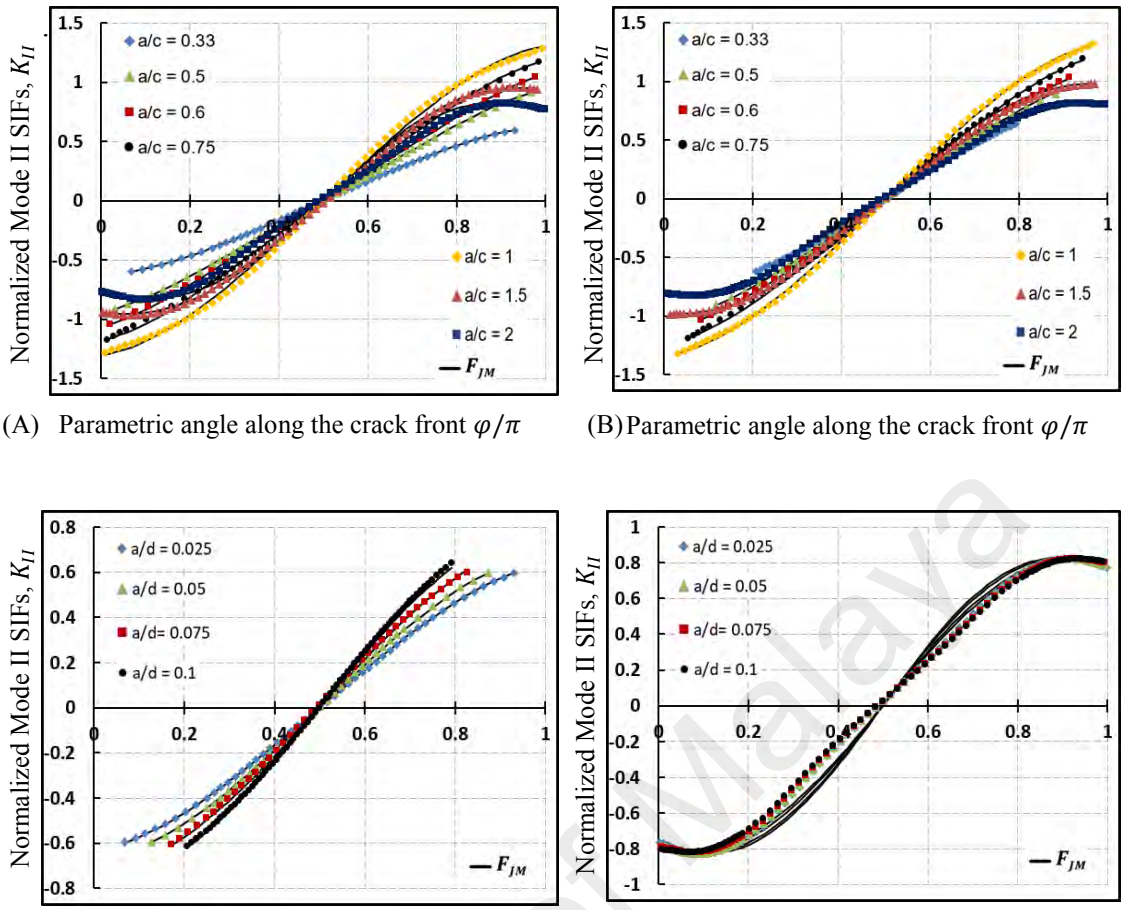

(A) Parametric angle along the crack front φ/π (B) Parametric angle along the crack front φ/π

(C) Parametric angle along the crack front φ/π (D) Parametric angle along the crack front φ/π

Figure 4-26: Normalized Mode II SIF distributions for semi-elliptical surface crack on the cylinder under torsion (A) for a/d = 0.025; (B) for a/d = 0.1; (C) for a/c = 1/3; (D) for a/c = 2.

4.3.2.3 Evaluations of Crack Inclination Angle

Results for different inclinations in the cylinder bar under pure torsion are shown in Figure 4-28A & B for Mode II and Mode III SIFs, respectively, along with proposed solution. The solution shows consistency in all inclination angles as it expected. Same verification for Mode I SIFs in the cylinder bar under pure torsion is shown in Figure 4-29, as well.

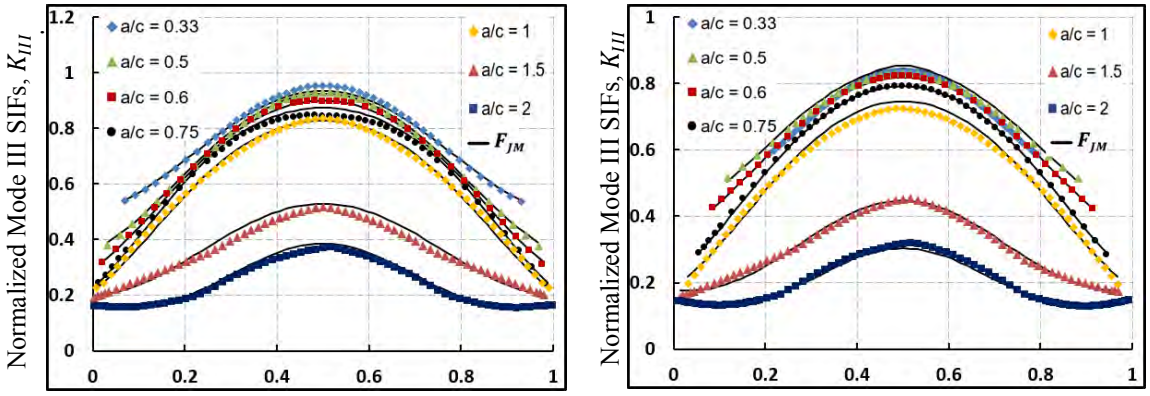

(A) Parametric angle along the crack front φ/π (B) Parametric angle along the crack front φ/π

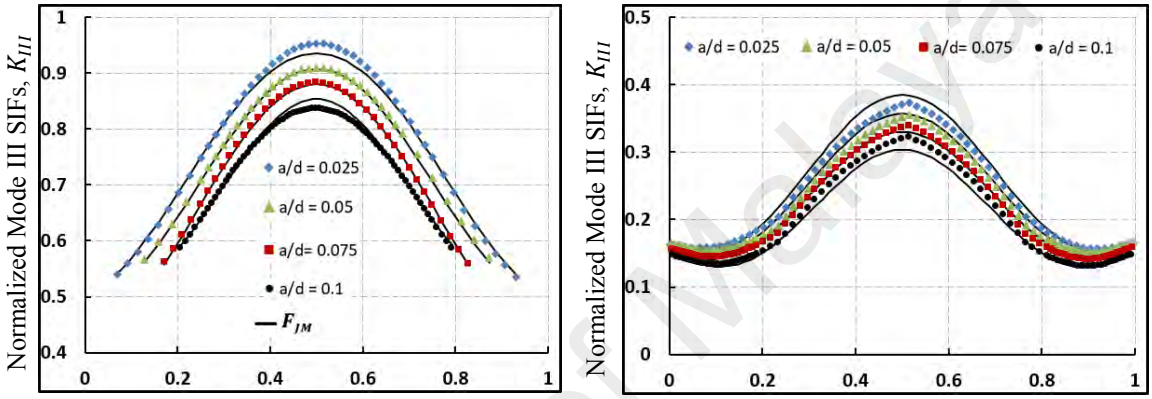

(C) Parametric angle along the crack front φ/π (D) Parametric angle along the crack front φ/π

Figure 4-27: Normalized Mode III SIF distributions for semi-elliptical surface crack on the cylinder under torsion (A) for a/d = 0.025; (B) for a/d = 0.1; (C) for a/c = 1/3; (D) for a/c = 2.

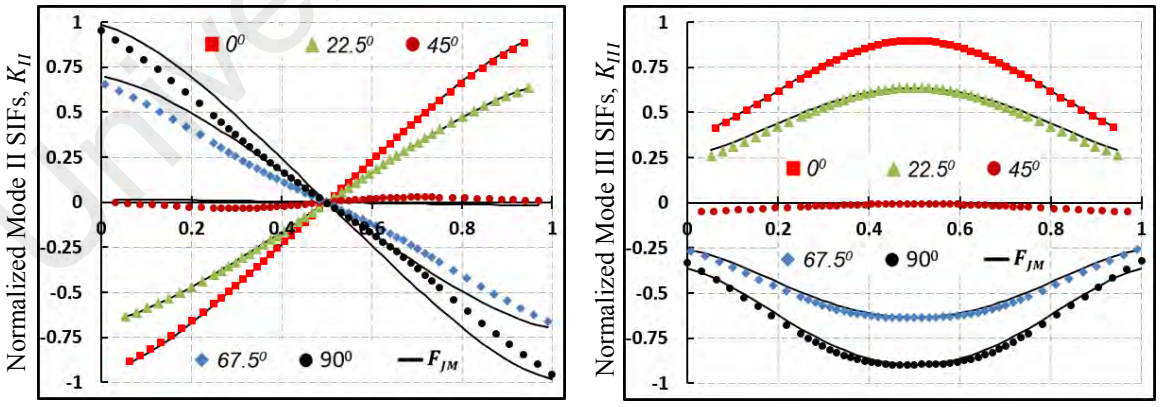

(A) Crack size ratio a/d (B) Crack size ratio a/d

Figure 4-28: Normalized SIF distributions for semi-elliptical surface crack on the cylinder bar under pure torsion (A) Mode II for a/d = 0.05 & a/c = 0.5; (B) Mode III for a/d = 0.05 & a/c = 0.5.

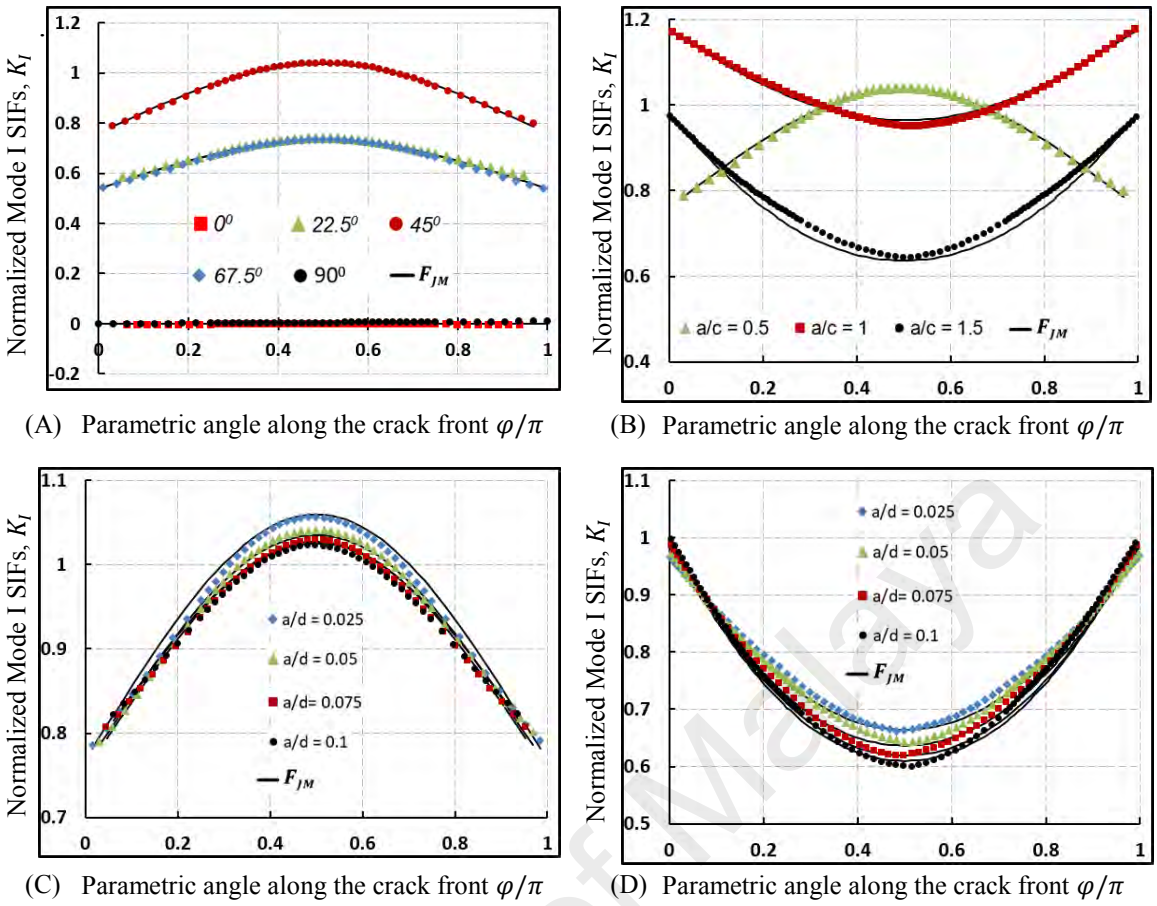

(A) Parametric angle along the crack front φ/π (B) Parametric angle along the crack front φ/π

(C) Parametric angle along the crack front φ/π (D) Parametric angle along the crack front φ/π

Figure 4-29: Normalized Mode I SIF distributions for semi-elliptical surface crack on the cylinder under torsion (A) for $a/d = 0.05$ & $a/c = 0.5$; (B) for $a/d = 0.1$ & $\theta = 45^o$; (C) for $a/c = 0.5$ & $\theta = 45^o$; (D) for $a/c = 1.5$ & $\theta = 45^o$.

4.4 Discussion

As it is mentioned in previous chapters, the aim of this work was achieve a comprehensive closed-form solutions which can predict stress intensity factor distribution along the crack front of an inclined semi-elliptical surface crack in the solid cylinder subjected to pure tension and pure torsion. To reach this goal, three main parameter of crack aspect size ratio, crack aspect ratio and crack inclination angle have been considered as variables of proposed solution. A distinct set of simulations has been performed to study the influence of each variable properly and a DBEM based-software BEASY is implemented to generate the SIFs.

Results obtained from BEASY, separately compared with different analytical solutions in the literature for each loading and findings proved the reliability of BEASY.

Raw collected data from BEASY showed that crack size ratio has positive effect on all SIF in regards to fracture Modes or boundary conditions. However, crack aspect ratio shows complicated influences on each fracture Modes. In Mode I, when aspect ratio increases, SIF distribution along the crack front will change significantly. The maximum values of Mode I SIFs happens at DPE for cracks with aspect ratio less than one. However, when aspect ratio increases to higher than one, maximum values of Mode I SIFs occurs at the CPE. For Mode II, SIF will increase when crack aspect ratio increases, until it reaches one and after that increasing in crack aspect ratio does not highly affected the maximum values of SIF. On the other hand, increasing in crack aspect ratio will lead to decrease in Mode III SIF values.

Changes in crack inclination angle causes arising of new fracture mode which were negligible at the crack inclination angle of 0^o. For instance, in cylinder bar under pure tension, the only non-zero SIF is Mode I SIF. However, by increasing in crack inclination angle the value of Mode I SIF is decreasing and Mode II and Mode III which were negligible start increasing. On the other hand, in cylinder bar under pure torsion, Mode I is zero at the angle of 0^o and it will increase when inclination angle increases. After collecting data from BEASY, results have been processed in MATLAB according to changes on each parameter precisely and solutions have been extracted by curve-fitting approach.

Proposed solution can predict SIF distribution at any point along the crack front for any arbitrary crack in any arbitrary solid cylinder only by measuring three distinct parameter. This method is comparatively faster than any other FEM or DBEM -based numerical methods and can be solved in few seconds without need of machines or computers.

CHAPTER FIVE: CONCLUSION AND FURTHER WORK

5.1 Conclusion

Mode I, Mode II and Mode III SIFs of semi-elliptical cracks in the cylinder bar under pure tension and pure torsion have been evaluated by using DBEM based software of BEASY. In the cylinder subjected to pure tension, Mode I SIFs were at maximum at the crack inclination of 0^o and it was negligible at 45^o. On the other hand, Mode II and Mode III, acquired their minimum absolute values at the crack inclination angle of 0^o and maximum values at 45^o. However, in the cylinder bar subjected to pure torsion, Mode I was negligible at the angle of 0^o and 90^o and possessed the maximum value at the angle of 45^o. Mode II and Mode III, were maximum where Mode I was negligible and minimum at the crack inclination angle of 45^o. Mode III SIF was strongly affected by both crack size and crack shape alterations and even at small crack sizes, the differences were considerable. However, at small crack size ratios ($a/d \leq 0.1$), Mode I and Mode II, showed slight changes according to crack size changes. Crack aspect ratio exhibited distinctive influences on Mode I, Mode II and Mode III SIFs. In Mode I SIF, maximum value occured at DPE when crack aspect ratio is less than one but it moves to CPE for ratios higher than one. Mode II, showed different reaction to aspect ratio changes. It got higher until aspect ratio reached one and after that it decreased. Mode III declined when aspect ratio got lower but after ratio of one rate of reduction was higher. Effects of aspect ratio on SIF distributions along the crack front was evident on Mode II and Mode III SIFs when crack aspect ratio was higher than one. Closed-form solutions to predict Mode I, Mode II and Mode III SIFs in cylinder bar under pure tension and pure torsion for cracks with different sizes, shapes and inclinations were derived from collected data. Proposed solution showed good agreement with collected results from BEASY and the deviation

did not exceed 5% except for high crack inclinations angle ($\theta \geq 60^{o}$) in Mode II SIFs which was 7-8%.

5.2 Further Work

1- In order to gain the solution, research went through plenty of analytical and mathematical works. In the cylinder bar under pure tension, reference solution was Newman-Raju's (1981). Since that solution (Equation 4-1) is applicable for cracks in infinite plate, it needs some Modifications. On the other hand, solutions seemed to be inaccurate compared to other investigations in the literature have been done afterwards. So introducing a correction factor to their solution can be an acceptable research study.

2- Apart from that, during this study some investigations have been done on width correction factor (Equation 4-16). To evaluate width factor same crack is modelled on the prismatic bars with different geometries. Geometry changed from square to cylinder in 6-7 stages and changes on SIFs have been studied. Research on this section can be titled as a "new width correction factor for cylinder bars".

3- Cracks in this study were considered semi-elliptical which in reality they may have jagged edges instead of smooth flat line. Mathematical approached like interpolation can be applied to proposed solution and find more accurate results for jagged crack fronts.

5.3 Publications

This research has resulted in the following two ISI publications:

1- Empirical solutions for stress intensity factors of a surface crack in a solid cylinder under pure torsion. Engineering Fracture Mechanics, 193, 122-136. (2018)

2- Analysis of surface cracks in cylinder bars using dual boundary element method. Engineering Analysis with Boundary Elements, 93, 112-123. (2018)

REFERENCES

Alatawi, I. A., & Trevelyan, J. (2014). A direct evaluation of stress intensity factors using the Extended Dual Boundary Element Method. *Engineering Analysis with Boundary Elements, 52*, 56-63.

Aliabadi, M. H., Hall, W. S., & Phemister, T. G. (1985). Taylor expansions for singular kernels in the boundary element method. *Int. J. Num. Meth. Eng., 21*, 2221-2236.

Anderson, T. L., & Glinka, G. (2006). A closed-form method for integrating weight functions for part-through cracks subject to Mode I loading. *Engineering Fracture Mechanics, 73*, 2153-2165.

Anderson, W. E., Paris, P. C., & Gomez, M. P. (1961). A rational analytic theory in fatigue. *The trend of engineering, 13*(11), 9-14.

Andersson, R., Larsson, F., & Kabo, E. (2018). Evaluation of stress intensity factors under multiaxial and compressive conditions using low order displacement or stress field fitting. *Engineering Fracture Mechanics, 189*, 204-220.

Arnold, S. M., & Binienda, W. K. (1995). Driving force analysis in an infinite anisotropic plate with multiple crack interactions. *International Journal of Fracture, 71*(3), 213-245.

Astiz, M. A. (1986). An incompatible singular elastic element for two- and three-dimensional crack problems. *Int J Fracture, 31*, 105-124.

Atluri, S. N., & Nishioka, T. (1983). Analytical solution for embedded elliptical cracks, and finite element-alternating method for elliptical surface cracks, subjected to arbitrary loadings. *Engineering Fracture Mechanics, 17*, 247-268.

Atroshchenko, E., Potapenko, S., & Glinka, G. (2009). Stress intensity factor for an embedded elliptical crack under arbitrary normal loading. *International Journal of Fatigue, 31*(11-12), 1907-1910.

Bao, R., Zhang, X., & Yahaya, N. A. (2010). Evaluating stress intensity factors due to weld residual stresses by the weight function and finite element methods. *Engineering Fracture Mechanics, 77*(13), 2550-2566.

Barroso, A., Graciani, E., Mantič, V., & París, F. (2012). A least squares procedure for the evaluation of multiple generalized stress intensity factors at 2D multimaterial corners by BEM. *Engineering Analysis with Boundary Elements, 36*(3), 458-470.

Beer, F. P., & Johnston, J. E. R. (1981). *Mechanics of Materials*. New York: McGraw-Hill, Inc.

Benthem, J. P., & Koiter, W. T. (1973). *Mechanics of Fracture 1*: Noordhoff Int Pub 1.

BEASY 10 Release 14, BEASY Ashurst Lodge, Ashurst, Southampton SO40 7AA, United Kingdom.

Blackburn, W. S. (1976). Calculation of stress intensity factors for straight cracks in grooved and ungrooved shafts. *Eng Fract Mech, 8*(4), 731-736.

Bush, A. J. (1981). Stress intensity factors for single-edge-crack solid and hollow round bars loaded in tension. *J Test Eval, 9*(4), 731-736.

Campagnolo, A., Meneghetti, G., Berto, F., & Tanaka, K. (2017). Crack initiation life in notched steel bars under torsional fatigue: Synthesis based on the averaged strain energy density approach. *International Journal of Fatigue, 100*, 563-574.

Carpinteri, A. (1992A). Stress intensity factors for straight-fronted edge cracks in round bars. *Eng Fract Mech, 42*(6), 1035-1040.

Carpinteri, A. (1992B). Elliptical-arc surface cracks in round bars. *Fatigue Fract Eng Mater Struct, 15*(11), 1141-1153.

Chakraborty, D., Murthy, K. S. R. K., & Chakraborty, D. (2017). Experimental determination of mode I stress intensity factor in orthotropic materials using a single strain gage. *Engineering Fracture Mechanics, 173*, 130-145.

Chandra, D., Purbolaksono, J., Nukman, Y., Liew, H. L., Ramesh, S., & Hamdi, M. (2014). Fatigue crack growth of a corner crack in a square prismatic bar under combined cyclic torsion–tension loading. *International Journal of Fatigue, 64*, 67-73.

Chapuliot, S. (2016). Stress intensity factor calculation in sharp and beveled edge nozzle corners. *International Journal of Pressure Vessels and Piping, 141*, 11-18.

Chauhan, M. M., Sharma, D. S., & Dave, J. M. (2016). Stress intensity factor for hypocycloidal hole in finite plate. *Theoretical and Applied Fracture Mechanics, 82*, 59-68.

Chen, C.-D. (2015). Analytical solutions of stress singularities in a sectorial plate based on Reissner–Mindlin plate theory. *Applied Mathematical Modelling, 39*(23), 7657-7679.

Chen, Y. Z. (2016A). Evaluation of stress intensity factors from stress concentration factors for a crack embedded in dissimilar elliptic inclusion. *Theoretical and Applied Fracture Mechanics*, 177-182.

Chen, Y. Z. (2016B). Solution for a crack embedded in thermal dissimilar elliptic inclusion. *Engineering Fracture Mechanics, 160*, 15-21.

Cheng, W. (1999). Determination of the mode I stress intensity factors for an edge-cracked beam with fixed ends. *Engineering Fracture Mechanics, 63*(2), 193-208.

Chudinovich, I., & Constanda, C. (2002). Variational and Potential Methods in the Theory of Bending of Plates with Transverse Shear Deformation: *Chapman & Hall/CRC, Boca Raton, FL*.

Ciarlet, P. G. (1988). Mathematical Elasticity, Volume I: Three-dimensional Elasticity. *Retrieved from Amsterdam, New York, Oxford.*

Cirello, A., Furgiuele, F., Maletta, C., & Pasta, A. (2008). Numerical simulations and experimental measurements of the stress intensity factor in perforated plates. *Engineering Fracture Mechanics, 75*(15), 4383-4393.

Cisilino, A. P., & Ortiz, J. E. (2005). Boundary element analysis of three-dimensional mixed-mode cracks via the interaction integral. *Computer Method in Applied Mechanics and Engineering, 194*, 935-956.

Citarella, R., Sepe, R., Giannella, V., & Ishtyryakov, I. (2016). Multiaxial Fatigue Crack Propagation of an Edge Crack in a Cylindrical Specimen Undergoing Combined Tension-Torsion Loading. *procedia structural integrity, 2*, 2706-2717.

Constanda, C. (1990). A Mathematical Analysis of Bending of Plates with Transverse Shear Deformation: *Longman-Wiley, Harlow-New York*.

Cortínez, V. H., & Dotti, F. E. (2013). Mode I stress intensity factor for cracked thin-walled open beams. *Engineering Fracture Mechanics, 110*, 249-257.

Cotterell, B., & Rice, J. R. (1980). Slightly curved or kinked cracks. *International Journal of Fracture, 16*(2), 155-169.

Courtin, S., Gardin, C., Bézine, G., & Ben Hadj Hamouda, H. (2005). Advantages of the J-integral approach for calculating stress intensity factors when using the commercial finite element software ABAQUS. *Engineering Fracture Mechanics, 72*(14), 2174-2185.

Cui, X., Li, H., Cheng, G., Tang, C., & Gao, X. (2017). Contour integral approaches for

the evaluation of stress intensity factors using displacement discontinuity method. *Engineering Analysis with Boundary Elements, 82*, 119-129.

D., F. M. M. F. (1995). Analysis of fatigue crack growth in rotary bend specimens and railway axles. *Fatigue Fract Engng Mater Struct, 18*, 171–178.

Dao, N. H., & Sellami, H. (2012). Stress intensity factors and fatigue growth of a surface crack in a drill pipe during rotary drilling operation. *Engineering Fracture Mechanics, 96*, 629-640.

Daoud, O., Cartwright, D. J., & Carney, M. (1978). Strain-energy release rate for a single-edge-cracked circular bar in tension. *J Strain Anal Eng Des, 13*(2), 83-89.

Datta, S., Chattopadhyay, A., Iyyer, N., & Phan, N. (2018). Fatigue crack propagation under biaxial fatigue loading with single overloads. *International Journal of Fatigue, 109*, 103-113.

Delale, F., Binienda, W., & Wang, A. S. D. (1991). Analysis of bent crack in unidirectional fiber reinforced composites. *International Journal of Fracture, 47*(1), 1-24.

Dempsey, J. P., & Mu, Z. (2014). Weight function for an edge-cracked rectangular plate. *Engineering Fracture Mechanics, 132*, 93-103.

Deschênes, P. A., Lanteigne, J., Verreman, Y., Paquet, D., Lévesque, J. B., & Brochu, M. (2017). A new experimental method to study the influence of welding residual stresses on fatigue crack propagation. *International Journal of Fatigue, 100*, 444-452.

Dhakad, S., Saxena, S., Purohit, R., & Pandey, U. (2017). Life Prediction and Stress Intensity Factor (SIF) analysis for the base straight component and weld straight component (Pipes) used in the nuclear power plant. *Materials Today: Proceedings, 4*(4, Part D), 5429-5434.

Dirgantara, T., & Aliabadi, M. H. (2002). Stress intensity factors for cracks in thin plates. *Engineering Fracture Mechanics, 69*(13), 1465-1486.

Dong, P., Hong, J. K., & Cao, Z. (2003). Stresses and stress intensities at notches: 'anomalous crack growth' revisited. *International Journal of Fatigue, 25*(9), 811-825.

Dosiyev, A. A., & Buranay, S. C. (2015). One-block method for computing the generalized stress intensity factors for Laplace's equation on a square with a slit

and on an L-shaped domain. *Journal of Computational and Applied Mathematics, 289*, 400-411.

Dotti, F. E., Cortínez, V. H., & Reguera, F. (2013). Mode I stress intensity factor for cracked thin-walled composite beams. *Theoretical and Applied Fracture Mechanics, 67-68*, 38-45.

Dunn, M. L., Suwito, W., & Hunter, B. (1997). Stress intensity factors for cracked I-beams. *Engineering Fracture Mechanics, 57*(6), 609-615.

Dyja, H., Szota, P., & Mroz, S. (2004). 3D FEM modelling and its experimental verification of the rolling of reinforcement rod. *Journal of Materials Processing Technology, 153-154*, 115-121.

Elfakhakhre, N. R. F., Long, N. M. A. N., & Eshkuvatov, Z. K. (2018). Stress intensity factor for an elastic half plane weakened by multiple curved cracks. *Applied Mathematical Modelling, 60*, 540-551.

Elices, M., Perez-Guerrero, M., Iordachescu, M., & Valiente, A. (2017). Fracture toughness of high-strength steel bars. *Engineering Fracture Mechanics, 170*, 119-129.

Erdogan, F. (1983). Stress intensity factors. *Journal of Applied Mechanics, Transactions of the ASME, 50*, 992-1002.

Fabrikant, V. I. (1989). *Applications of Potential Theory in Mechanics, A selection of New Results*.

Fillery, B. P., & Hu, X. Z. (2010). Compliance based assessment of stress intensity factor in cracked hollow cylinders with finite boundary restraint: Application to thermal shock part I. *Engineering Fracture Mechanics, 77*(14), 2662-2681.

Fonte, M. A., & Freitas, M. M. (1997). Semi-elliptical crack growth under rotating or reversed bending combined with steady torsion. *Fatigue & Fracture of Engineering Materials & Structures, 20*(6), 895–906.

Fonte, M. d., Gomes, E., & Freitas, M. d. (1999A). Stress Intensity Factors for Semi-Elliptical Surface Cracks in Round Bars Subjected to Mode I (Bending) and Mode III (Torsion) Loading. *European Structural Integrity Society, 25*, 249-260.

Fonte, M. d., & Freitas, M. d. (1999B). Stress Intensity Factors for semi-elliptical surface cracks in round bars under bending and torsion. *International Journal of Fatigue, 21*, 457-463.

Forman, R. G., & Shivakumar, V. (1986). Growth behavior of surface cracks in the circumferential plane of solid and hollow cylinders. *Fracture mechanics: seventeenth volume, ASTM STP, 905*, 59-74.

Freese, C. E., & Baratta, F. I. (2006). Single edge-crack stress intensity factor solutions. *Engineering Fracture Mechanics, 73*(5), 616-625.

Freitas, M. M., Fonte, M. D. (1995). Analysis of fatigue crack growth in rotary bend specimens and railway axles. *Fatigue Fract Engng Mater Struct, 18*, 171–178.

Fu, G., Yang, W., & Li, C.-Q. (2017). Stress intensity factors for mixed mode fracture induced by inclined cracks in pipes under axial tension and bending. *Theoretical and Applied Fracture Mechanics, 89*, 100-109.

Galin, L. A. (1961). *Contact Problems in the Theory of Elasticity*.

Gao, Y. L., Tan, C. L., & Selvadurai, A. P. S. (1992). Stress intensity factors for cracks around or penetrating an elliptic inclusion using the boundary element method. *Engineering Analysis with Boundary Elements, 10*(1), 59-68.

Gintalas, M., Ainsworth, R. A., & Scenini, F. (2017). T-stress solutions for through-wall circumferential cracks in straight pipes under bending. *International Journal of Pressure Vessels and Piping*, *152*, 27-37.

Ghafoori, E., & Motavalli, M. (2011). Analytical calculation of stress intensity factor of cracked steel I-beams with experimental analysis and 3D digital image correlation measurements. *Engineering Fracture Mechanics, 78*(18), 3226-3242.

Gonzáles, G. L. G., González, J. A. O., Castro, J. T. P., & Freire, J. L. F. (2017). A J-integral approach using digital image correlation for evaluating stress intensity factors in fatigue cracks with closure effects. *Theoretical and Applied Fracture Mechanics, 90*, 14-21.

Griffith, A. A. (1920). The phenomena of rupture and flow in solids. *Philosophical Transactions of the Royal Society of London, A221*, 163-197.

Guiggiani, M., Krishnasamy, G., Rizzo, F. J., & Rudolphi, T. J. (1991). Hypersingular boundary integral equations. A new approach to their numerical treatment, in Boundary Integral Methods, Theory and Applications. *L. Morino & R. Piva, Springer-Verlag, Berlin*, 211-220.

Guo, K., Bell, R., & Wang, X. (2007). The stress intensity factor solutions for edge cracks in a padded plate geometry under general loading conditions. *International*

Journal of Fatigue, 29(3), 481-488.

Guo, W., Shen, H., & Li, H. (2003). Stress intensity factors for elliptical surface cracks in round bars with different stress concentration coefficient. *International Journal of Fatigue, 25*, 733-741.

Guozhong, C., Kangda, Z., & Dongdi, W. (1995). Stress intensity factors for semi-elliptical surface cracks in plates and cylindrical pressure vessels using the hybrid boundary element method. *Engineering Fracture Mechanics, 52*(6), 1035-1054.

Gupta, P., Duarte, C. A., & Dhankhar, A. (2017). Accuracy and robustness of stress intensity factor extraction methods for the generalized/eXtended Finite Element Method. *Engineering Fracture Mechanics, 179*, 120-153.

Hammond, M. J., & Fawaz, S. A. (2016). Stress intensity factors of various size single edge-cracked tension specimens: A review and new solutions. *Engineering Fracture Mechanics, 153*, 25-34.

Hashimoto, S., Komata, H., & Matsunaga, H. (2017A). Quantitative Evaluation of the Flaking Strength of Rolling Bearings with Small Defects: (Part 1: FEM Analyses of the Stress Intensity Factor, KII, under Rolling Contact). *procedia structural integrity, 7*, 453-459.

He, J. W., & Hutchinson, M. Y. (2000). Surface crack subject to mixed mode loading. *Engineering Fracture Mechanics, 65*, 1-14.

He, X., Dong, Y., Yang, B., & Li, Y. (2018). A wide range stress intensity factor solution for an eccentrically cracked middle tension specimen with clamped ends. *Engineering Fracture Mechanics, 191*, 461-475.

He, Z., Kotousov, A., Fanciulli, A., Berto, F., & Nguyen, G. (2016). On the evaluation of stress intensity factor from displacement field affected by 3D corner singularity. *International Journal of Solids and Structures, 78-79*, 131-137.

Hermann, S., & Sosa, H. (1986). On bars with cracks. *Engineering Fracture Mechanics, 24*, 889-894.

Holdbrook, S. J., & Dove, W. D. (1979). The stress intensity factor for a deep surface crack in a finite plate. *Engng Fracture Mech, 12*, 347-364.

Hosseini, A., & Mahmoud, M. A. (1985). Evaluation of stress intensity factor and fatigue growth of surface cracks in tension plates. *Engng Fracture Mech, 22*, 957-974.

Hou, C., Wang, Z., Liang, W., Yu, H., & Wang, Z. (2017). Investigation of the effects of

confining pressure on SIFs and T-stress for CCBD specimens using the XFEM and the interaction integral method. *Engineering Fracture Mechanics, 178*, 279-300.

Iida, J., & Hasebe, N. (2016). Stress intensity factors of a rhombic hole with symmetric cracks under uniform transverse thin plate bending. *Engineering Fracture Mechanics, 156*, 16-24.

Imachi, M., Tanaka, S., & Bui, T. Q. (2018). Mixed-mode dynamic stress intensity factors evaluation using ordinary state-based peridynamics. *Theoretical and Applied Fracture Mechanics, 93*, 97-104. Irwin, G. R. (1957). Analysis of stresses and strains near the end of a crack traversing a plate. *Journal of Applied Mechanics, 24*, 236-364.

Isida, M., Noguchi, H., & Yoshida, T. (1984). Tension and bending of finite thickness plates with a semi-elliptical surface crack. *Int J Fracture, 26*, 157-188.

Isidoroa, J., & Martins, R. F. (2016). Calculation of stress intensity factors KI, KII and KIII of cracked components submitted to flexural and torsional loads. *Procedia Engineering, 160*, 131-136.

Ismail, A., Ariffin, A. K., Abdullah, S., & Ghazali, M. J. (2012). Stress intensity factors for surface cracks in round bar under single and combined loadings. *Meccanica, 47*(5), 1141-1156.

J. ROYER, A. L. V. (1994). Stress Intensity Factor Variations Along Crack Fronts under Three Modes in a Round Bar. *Advances in Fracture Resistance and Structural Integrity, A volume in International Series on the Strength and Fracture of Materials and Structures*, 99–106.

James, L. A., & Mills, W. J. (1988). Review and synthesis of stress intensity factor solutions applicable to cracks in bolts. *Eng Fract Mech, 30*, 641-654.

James, L. E., & Anderson, W. E. (1969). A simple experimental procedure for stress intensity factor calibration *Engineering Fracture Mechanics, 1*, 565-568.

Jia, L.-J., Ikai, T., Shinohara, K., & Ge, H. (2016). Ductile crack initiation and propagation of structural steels under cyclic combined shear and normal stress loading. *Construction and Building Materials, 112*, 69-83.

Jiang, Z.-C., Tang, G.-J., & Li, X.-F. (2015). Effect of initial T-stress on stress intensity factor for a crack in a thin pre-stressed layer. *Engineering Fracture Mechanics,*

150, 19-27.

Jin, X., Shah, S., Roegiers, J.-C., & McLennan, J. (2016). Weight function of stress intensity factor for symmetrical radial cracks emanating from hollow cylinder. *Engineering Fracture Mechanics, 159*, 144-154.

Jin, X., Zeng, Y., Ding, S., Zhang, B., McLennan, J., Roegiers, J.-C. Bian, X. (2017). Weight function of stress intensity factor for single radial crack emanating from hollow cylinder. *Engineering Fracture Mechanics, 170*, 77-86.

Jing, Z., & Wu, X. R. (2015). Wide-range weight functions and stress intensity factors for arbitrarily shaped crack geometries using complex Taylor series expansion method. *Engineering Fracture Mechanics, 138*, 215-232.

Joseph, R. P., Purbolaksono, J., Liew, H. L., Ramesh, S., & Hamdi, M. (2014). Stress intensity factors of a corner crack emanating from a pinhole of a solid cylinder. *Engineering Fracture Mechanics, 128*, 1-7.

Kaklara, J. A., & Googarchin, H. S. (2018). Approximate stress intensity factors for a semi-circular crack in an arbitrary structure under arbitrary mode I loading. *Theoretical and Applied Fracture Mechanics, 94*, 71-83.

Kassir, M. K., & Sih, G. C. (1966). Three dimensional stress distributions around an elliptical crack under arbitrary loadings. *J Appl Mech, 33*, 601-611.

Kastratovic, G., Grbovic, A., & Vidanovic, N. (2015). Approximate method for stress intensity factors determination in case of multiple site damage. *Applied Mathematical Modelling, 39*, 6050-6059.

Kazarinov, N., Smirnov, I., Sudenkov, Y., Petrov, Y., & Slesarenko, V. (2017). Experimental investigation of dynamic crack propagation in PMMA plates. *procedia structural integrity, 6*, 83-89.

Keprate, A., Ratnayake, R. M. C., & Sankararaman, S. (2017). Adaptive Gaussian process regression as an alternative to FEM for prediction of stress intensity factor to assess fatigue degradation in offshore pipeline. *International Journal of Pressure Vessels and Piping, 153*, 45-58.

Kienzler, R., & Herrmann, G. (1986). An elementary theory of defective beams. *Acta Mech, 62*, 37-46.

Kim, S. H., Lee, K. Y., & Park, M. B. (1998). Stress intensity factors for interlaminar cracked composites under arbitrary normal crack surface loading. *International*

Journal of Solids and Structures, 35(33), 4355-4367.

Kobayashi, A. S., & Shah, R. C. (1971). Stress intensity factor for an elliptical crack under arbitrary normal loading. *Engineering Fracture Mechanics, 3*, 71-96.

Kobayashi, A. S., & Shah, R. C. (1973). Stress intensity factors for an elliptical crack approaching the surface of a semi-elliptical solid. *International Journal of Fracture, 9*(2), 133-146.

Kolitsch, S., Gänser, H.-P., & Pippan, R. (2017). Approximate stress intensity factor solutions for semi-elliptical cracks with large a/W and c/B under tension and bending. *Theoretical and Applied Fracture Mechanics, 92*, 167-177.

Kondo, T., Kurabe, Y., Sasaki, T., Kurahashi, T., & Miyashita, Y. (2014). Use of strain gages for determining generalized stress intensity factors of sharp V-notched plates under transverse bending. *Engineering Fracture Mechanics, 124-125*, 248-261.

Kou, K. P., & Burdekin, F. M. (2006). Closed-form solution for stress intensity factors of semi-elliptical surface cracks with different inclinations in a cylinder bar under pure tension and pure torsion. *Engineering Fracture Mechanics, 73*, 1693-1710.

Krylov, V. I., & Kantorovich, L. V. (1964). *Approximate method of higher analysis*. New York: Interscience Publishers, Inc.

Kupradze, V. D. (1979). *Three-Dimensional Problems of the Mathematical Theory of Elasticity and Thermoelasticity*: North-Holland publishing company Amsterdam, Oxford, New York.

Lan, X., Ji, S., Noda, N.-A., & Cheng, Y. (2017). Stress intensity factor solutions for several crack problems using the proportional crack opening displacements. *Engineering Fracture Mechanics, 171*, 35-49.

Lawn, B. R., & Wilshaw, T. R. (1975). *Fracture of brittle solids*. Cambridge: Cambridge University Press.

Lazzarin, P., & Filippi, S. (2006). A generalized stress intensity factor to be applied to rounded V-shaped notches. *International Journal of Solids and Structures, 43*(9), 2461-2478.

Lebahn, J., Heyer, H., & Sander, M. (2013). Numerical stress intensity factor calculation in flawed round bars validated by crack propagation tests. *Engineering Fracture Mechanics, 108*, 37-49.

Levan, A., & Royer, J. (1993). Part-circular surface cracks in round bars under tension, bending and twisting. *Int J Fract, 61*, 71-99.

Li, C.-Q., Fu, G., & Yang, W. (2016). Stress intensity factors for inclined external surface cracks in pressurised pipes. *Engineering Fracture Mechanics, 165*, 72-86.

Li, S., & Wang, J. (2018). The stress intensity factor and propagation of an inclined crack in the central layer of a composite laminate under tension. *Theoretical and Applied Fracture Mechanics, 93*, 128-136.

Li, W., Zhao, H., Nehila, A., Zhang, Z., & Sakai, T. (2017). Very high cycle fatigue of TC4 titanium alloy under variable stress ratio: Failure mechanism and life prediction. *International Journal of Fatigue, 104*, 342-354.

Li, Y., Sun, T., Gao, Q., & Tan, C. (2018A). A stress intensity factor estimation method for kinked crack. *Engineering Fracture Mechanics, 188*, 202-216.

Li, Y., Sun, T., Tian, Y., Gao, Q., & Tan, C. (2018B). A stress intensity factor estimation method for the kinked crack under anti-plane load. *Theoretical and Applied Fracture Mechanics, 93*, 319-325.

Likeb, A., Gubeljak, N., & Matvienko, Y. (2014). Stress Intensity Factor and Limit Load Solutions for New Pipe-ring Specimen with Axial Cracks. *Procedia Materials Science, 3*, 1941-1946.

Lin, P. C., & Pan, J. (2008). Closed-form structural stress and stress intensity factor solutions for spot welds under various types of loading conditions. *International Journal of Solids and Structures, 45*(14), 3996-4020.

Lin, X. B., & Smith, R. A. (1999A). Finite element modelling of fatigue crack growth of surface cracked plates Part III: Stress intensity factor and fatigue crack growth life. *Engineering Fracture Mechanics, 63*, 541-556.

Lin, X. B., & Smith, R. A. (1999B). Stress intensity factors for corner cracks emanating from fastener holes under tension. *Engineering Fracture Mechanics, 62*(6), 535-553.

Liu, W., Wang, S., & Yao, X. (2016). Experimental study on stress intensity factor for an axial crack in a PMMA cylindrical shell. *Polymer Testing, 56*, 36-44.

Livieri, P. (2016). Stress intensity factors from stress analysis of an equivalent hole. *Theoretical and Applied Fracture Mechanics, 84*, 119-128.

Livieri, P., & Segala, F. (2012). Evaluation of Stress Intensity Factors from elliptical

notches under mixed mode loadings. *Engineering Fracture Mechanics, 81*, 110-119.

Livieri, P., & Segala, F. (2016). Stress intensity factors for embedded elliptical cracks in cylindrical and spherical vessels. *Theoretical and Applied Fracture Mechanics*.

Love, A. (1929). On stress produced in a semi-infinite solid by pressure on part of the boundary. *Phylosophical Transactions of the Royal Society, Series A*, 228:378-395.

M Shiratori, T. M., Y Sakay, G.R Zhang. (1987). Analysis and application of influence coefficients for round bar with a semi-elliptical surface crack. In *Y Murakami (Ed.), Stress Intensity Factors Handbook, Vol II* (pp. 659–665). Oxford: Pergamon Press.

M.A Fonte, M. M. F. (1994). *Fatigue crack growth under rotating bending and steady torsion.* Paper presented at the Proc Fourth Int Conf on Biaxial/Multiaxial Fatigue 94, Paris.

Madia, M., Beretta, S., Schödel, M., Zerbst, U., Luke, M., & Varfolomeev, I. (2011). Stress intensity factor solutions for cracks in railway axles. *Engineering Fracture Mechanics, 78*(5), 764-792.

Mahbadi, H. (2017). Stress intensity factor of radial cracks in isotropic functionally graded solid cylinders. *Engineering Fracture Mechanics, 180*, 115-131.

Mahmoud, M. A., & Hosseini, A. (1986). Assessment of stress intensity factor and aspect ratio variability of surface cracks in bending plates. *Engng Fracture Mech, 24*, 207-221.

Maltis, P. (2009). Torsion of a cylinder with a shallow external crack. *International Journal of Solids and Structures, 46*(16), 3061-3067.

Man, K. W., Aliabadi, M. H., & Rooke, D. P. (1995). Stress intensity factors in the presence of contact stresses. *Engineering Fracture Mechanics, 51*(4), 591-601.

Mangalgiri, P. D., Ramamurthy, T. S., & Dattaguru, B. (1984). Stress intensity factors at the tips of cracks emanating from holes with misfit fasteners. *Paper presented at the Fracture 84, Proceedings of the 6th International Conference on Fracture (ICF6), New Delhi, India.*

Martin, P. A. (1986). Orthogonal polynomial solutions for pressurized elliptical cracks. *Mech. appl. Math.*, 39.

Matsumto, T., Tanaka, M., & Obara, R. (2000). Computation of stress intensity factors of interface cracks based on interaction energy release rates and BEM sensitivity analysis. *Engineering Fracture Mechanics, 65*(6), 683-702.

Matsunaga, H., Hashimoto, S., & Komata, H. (2017B). Quantitative Evaluation of the Flaking Strength of Rolling Bearings with Small Defects: (Part 2: Evaluation of the Flaking Strength of Rolling Bearings with Small Drilled Holes, based on the Stress Intensity Factor). *procedia structural integrity, 7*, 460-467.

Mattheck, C., Morawietz, P., Müller, S., Munz, D., & Kober, A. (1984). Bruchmekanik an Rissen in Wellen and Schrauben. *Der Machinenschaden, 57*(3), 73-76.

Mavrothanasis, F. I., & Pavlou, D. G. (2007). Mode-I stress intensity factor derivation by a suitable Green's function. *Engineering Analysis with Boundary Elements, 31*(2), 184-190.

Meneghetti, G., Campagnolo, A., & F.Berto. (2016). Averaged strain energy density estimated rapidly from the singular peak stresses by FEM: Cracked bars under mixed-mode (I + III) loading. *Engineering Fracture Mechanics, 167*, 20-33.

MESHII, T., & WATANABE, K. (1998). Closed-form stress intensity factor for an arbitrarily located inner circumferential surface crack in a cylinder subjected to axisymmetric bending loads. *Engineering Fracture Mechanics, 59*(5), 589-597.

Mi, & Aliabadi, M. H. (1992). Dual boundary element method for three-dimensional fracture mechanics analysis. *Engineering Analysis with Boundary Elements, 10*(2), 161-171.

Mi, Y., & Aliabadi, M. H. (1994). THREE-DIMENSIONAL CRACK GROWTH SIMULATION USING BEM. *Computers & Structures, 52*(5), 871-878.

Miura, N., Takahashi, Y., Shibamoto, H., & Inoue, K. (2008). Comparison of stress intensity factor solutions for cylinders with axial and circumferential cracks. *Nuclear Engineering and Design, 238*(2), 423-434.

Moftakhar, A. A., & Glinka, G. (1992). Calculation of Stress Intensity Factors by Efficient Integration of Weight Functions. *Engineering Fracture Mechanics, 43*, 749-756.

Mokhtarishirazabad, M., Lopez-Crespo, P., Moreno, B., Lopez-Moreno, A., & Zanganeh, M. (2017). Optical and analytical investigation of overloads in biaxial fatigue cracks. *International Journal of Fatigue, 100*(2), 583-590.

Moreira, P. M. G. P., Pastrama, S. D., & de Castro, P. M. S. T. (2009). Three-dimensional stress intensity factor calibration for a stiffened cracked plate. *Engineering Fracture Mechanics, 76*(14), 2298-2308.

Munz, D., Bubsey, R. T., & Srawley, J. E. (1980). Compliance and stress intensity coefficients for short bar specimens with chevron notches. *International Journal of Fracture, 16*(4), 359-374.

Murakami, Y. (1987). *Stress Intensity Factors Handbook* (Vol. 1): Pergamon Press.

Murakami, Y., & Tsuru, H. (1987). Stress-Intensity Factor Equations for semi-elliptical surface crack in a shaft under bending. In *Y Murakami (Ed.), Stress Intensity Factors Handbook* (pp. 657–658). Oxford: Pergamon Press.

Nabavi, S. M., & Ghajar, R. (2010). Analysis of thermal stress intensity factors for cracked cylinders using weight function method. *International Journal of Engineering Science, 48*(12), 1811-1823.

Nagai, M., Miura, N., & Shiratori, M. (2015). Stress intensity factor solution for a surface crack with high aspect ratio subjected to an arbitrary stress distribution using the influence function method. *International Journal of Pressure Vessels and Piping, 131*, 2-9.

Newman, J. C. J., & Raju, I. S. (1981). Stress intensity factor equations for cracks in three-dimensional finite bodies. *Retrieved from Virginia*: *Nasa*.

Newman, J. J., & Raju, I. S. (1981). An empirical stress intensity factor equation for the surface crack. *Engng Fracture Mech, 15*, 185-192.

Niasani, M. A., Ghajar, R., Googarchin, H. S., & Hossein Sharifi, S. M. (2017). Crack growth pattern prediction in a thin walled cylinder based on closed form thermo-elastic stress intensity factors. *Journal of Mechanical Science and Technology, 31*(4), 1603-1610.

Nisitani, H., & Murakami, Y. (1974). Stress intensity factors of an elliptical crack or a semi-elliptical crack subject to tension. *International Journal of Fracture, 10*, 353-368.

Noda, N.-A., & Takase, Y. (2003). Generalized stress intensity factors of V-shaped notch in a round bar under torsion, tension, and bending. *Engineering Fracture Mechanics, 70*, 1447-1466.

Noury, P., & Eriksson, K. (2017). Determination of stress intensity factors for cracked

bridge roller bearings using finite element analyses. *Engineering Fracture Mechanics, 169*, 67-73.

Okada, H., Koya, H., Kawai, H., Li, Y., & Osakabe, K. (2016). Computations of stress intensity factors for semi-elliptical cracks with high aspect ratios by using the tetrahedral finite element (fully automated parametric study). *Engineering Fracture Mechanics, 158*, 144-166.

Olsen, P. C. (1994). Determining the stress intensity factors KI, KII and the T-term via the conservation laws using the boundary element method. *Engineering Fracture Mechanics, 49*(1), 49-60.

Oore, M., & Burns, D. J. (1980). Estimation of stress intensity factors for embedded irregular cracks subjected to arbitrary normal stress fields. *J. Press. Vessel Technol. ASME, 102*, 202-211.

Ortega-Herrera, F. J., Lozano-Luna, A., Razón-González, J. P., García-Guzmán, J. M., & Figueroa-Godoy, F. (2017). *Mathematical Model to Predict the Stress Concentration Factor on a Notched Flat Bar in Axial Tension*, Cham.

Ortiz, J. E., Mantič, V., & París, F. (2006). A domain-independent integral for computation of stress intensity factors along three-dimensional crack fronts and edges by BEM. *International Journal of Solids and Structures, 43*(18-19), 5593-5612.

Ozturk, D., Pilchak, A. L., & Ghosh, S. (2017). Experimentally validated dwell and cyclic fatigue crack nucleation model for α–titanium alloys. *Scripta Materialia, 127*, 15-18.

Pachoud, A. J., Manso, P. A., & Schleiss, A. J. (2017). Stress intensity factors for axial semi-elliptical surface cracks and embedded elliptical cracks at longitudinal butt welded joints of steel-lined pressure tunnels and shafts considering weld shape. *Engineering Fracture Mechanics, 179*, 93-119.

Peng, D., & Jones, R. (2016). A simple method for calculating the stress intensity factors for complex 3D cracks at a notch. *Engineering Fracture Mechanics, 158*, 81-86.

Peng, D., Wallbrink, C., & Jones, R. (2005). An assessment of stress intensity factors for surface flaws in a tubular member. *Engineering Fracture Mechanics, 72*(3), 357-371.

Perl, M., & Steiner, M. (2017). The beneficial effect of full or partial autofrettage on the

combined 3-D stress intensity factors for inner radial crack arrays in a spherical pressure vessel. *Engineering Fracture Mechanics, 175*, 46-56.

Petroski, H. J., & Achenbach, J. D. (1978). Computation of the weight function from a stress intensity factor. *Engineering Fracture Mechanics, 10*(2), 257-266.

Pineau, A., Benzerga, A. A., & Pardoen, T. (2016). Failure of metals I: Brittle and ductile fracture. *Acta Materialia, 107*, 424-483.

Pommier, S., Sakae, C., & Murakami, Y. (1999). An empirical stress intensity factor set of equations for a semi-elliptical crack in a semi-infinite body subjected to a polynomial stress distribution. *International Journal of Fatigue, 21*(3), 243-251.

Pourheidar, A., Beretta, S., Ragazzi, D., & Baykara, C. (2018). Comparison of SIF solutions for cracks under rotating bending and their impact upon propagation lifetime of railway axles. *procedia structural integrity, 8*, 610-617.

Predan, J., Mocilnik, V., & Gubeljak, N. (2013). Stress intensity factors for circumferential semi-elliptical surface cracks in a hollow cylinder subjected to pure torsion. *Engineering Fracture Mechanics, 105*, 152-168.

Purbolaksono, J., Ali, A. A., Khinani, A., & Rashid, A. Z. (2009). Evaluation of stress intensity factors for multiple surface cracks in bi-material tubes. *Engineering Analysis with Boundary Elements, 33*(11), 1339-1343.

Rajaram, H., Socrate, S., & Parks, D. M. (2000). Application of domain integral methods using tetrahedral elements to the determination of stress intensity factors. *Engineering Fracture Mechanics, 66*(5), 455-482.

Raju, I. S., & Newman, J. C. (1986). Stress intensity factors for circumferential surface cracks in pipes and rods under tension and bending loads. *Fracture Mechanics, ASTM STP 905, 17*, 789–805.

Raju, I. S., & Newman, J. J. (1979). Stress intensity factors for a wide range of semi-elliptical surface cracks in finite thickness plates. *Engng Fracture Mech, 11*, 817-829.

Ribeiro, R. L., & Hil, M. R. (2016). A benchmark fracture mechanics solution for a two-dimensional eigenstrain problem considering residual stress, the stress intensity factor, and superposition. *Engineering Fracture Mechanics, 163*, 313-326.

Ricci, P., & Viola, E. (2006). Stress intensity factors for cracked T-sections and dynamic behaviour of T-beams. *Engineering Fracture Mechanics, 73*(1), 91-111.

Rigby, R., & Aliabadi, M. H. (1997). Stress intensity factors for cracks at attachment lugs. *Engineering Failure Analysis, 4*(2), 133-146.

Roiko, A., Solin, J., & Hänninen, H. (2017). Behavior of small cracks under negative stress ratio fatigue loading. *International Journal of Fatigue, 104*, 379-388.

Rozumek, D., Marciniak, Z., Lesiuk, G., Correia, J. A., & de Jesus, A. M. P. (2018). Experimental and numerical investigation of mixed mode I + II and I + III fatigue crack growth in S355J0 steel. *International Journal of Fatigue, 113*, 160-170.

Rozumek, D., Marciniak, Z., Lesiuk, G., & Correia, J. A. F. O. (2017). Mixed mode I/II/III fatigue crack growth in S355 steel. *procedia structural integrity, 5*, 896-903.

Rubio, P., Sanz, Y., Rubio, L., & Muñoz-Abella, B. (2017). Stress Intensity Factor and propagation of an open sickle shaped crack in a shaft under bending. *Theoretical and Applied Fracture Mechanics*.

Saboori, B., Torabi, A. R., Ayatollahi, M. R., & Berto, F. (2017). Experimental verification of two stress-based criteria for mixed mode I/III brittle fracture assessment of U-notched components. *Engineering Fracture Mechanics, 182*, 229-244.

Saimoto, A., Fujikawa, M., Makabe, C., Yamanaka, T., & Rana, M. S. (2010). Stress intensity factors for cracks initiated from a center-holed plate with unsymmetrical lengths under tension. *Engineering Failure Analysis, 17*(4), 838-847.

Salah el din, A. S., & Lovegrove, J. M. (1981). Stress intensity factors for fatigue cracking of round bars. *Int J Fatigue, 3*(3), 117-123.

Scott, P. M., & Thorpe, T. W. (1981). A critical review of crack tip stress intensity factors for semi-elliptical cracks. *Fatigue Fract Engng Mater Struct, 4*, 291-309.

Seifi, R. (2015). Stress intensity factors for internal surface cracks in autofrettaged functionally graded thick cylinders using weight function method. *Theoretical and Applied Fracture Mechanics, 75*, 113-123.

Seitl, S., Miarka, P., Sobek, J., & Klusák, J. (2017). A numerical investigation of the stress intensity factor for a bent chevron notched specimen: Comparison of 2D and 3D solutions. *procedia structural integrity, 5*, 737-744.

Shahani, A. R., & Habibi, S. E. (2007). Stress intensity factors in a hollow cylinder containing a circumferential semi-elliptical crack subjected to combined loading.

International Journal of Fatigue, 29(1), 128-140.

Shahani, A. R., & Nabavi, S. M. (2006). Closed-form stress intensity factors for a semi-elliptical crack in a thick-walled cylinder under thermal stress. *International Journal of Fatigue, 28*(8), 926-933.

Shen, G., & Glinka, G. (1991). Weight functions for a surface semi-elliptical crack in a finite thickness plate. *Theoretical Applied Fracture Mechanics, 15*(3), 247-255.

Shih, Y. S., & Chen, J. J. (2002). The stress intensity factor study of an elliptical cracked shaft. *Nuclear Engineering and Design, 214*, 137-145.

Shin, C. S., & Cai, C. Q. (2004). Experimental and finite element analyses on stress intensity factors of an elliptical surface crack in a circular shaft under tension and bending. *International Journal of Fracture, 129*, 239-264.

Shivakumar, K. N., & Newman, J. C. J. (1991). Stress intensity factors for large aspect ratio surface and corner cracks at a semicircular notch in a tension specimen. *Engineering Fracture Mechanics, 38*, 467-473.

Shlyonnikov, V. (2016). Nonlinear stress intensity factors in fracture mechanics and their applications. *procedia structural integrity, 2*, 744-752.

Sih, G. C., & Hartranft, R. J. (1973). Alternating method applied to the edge and surface crack problems in Mechanics of Fracture I: Methods of analysis and solutions of crack problems: *Edited by G.C.Sih. Noordhoff International Publishing Leyden*.

Sih, G. C., & Kassir, M. K. (1975). *Three-dimensional crack problems*. Retrieved from Leyden.

Sih, G. C., & Liebowitz, H. (1998). *Mathematical theories of brittle fracture. In: Treatise on fracture*. Retrieved from New York.

Siow, Y. W., Tan, C. J., Purbolaksono, J., & Andriyana, A. (2016). Numerical simulation of a corner crack growth in metals under multiaxial fatigue loading. *Key Engineering Materials, 701*, 235-240.

Sneddon, I. N. (1946). The distribution of stress in the neighbourhood of a crack in an elastic solid. *Retrieved from Series A., 187.*

Sodeifi, H., & Hosseini, M. (2015). Experimental and numerical studies for determining the mode I critical stress intensity factor using thick-walled hollow cylindrical marly specimens. *Arabian Journal of Geosciences, 8*(10), 8283-8293.

Song, C., Ooi, E. T., & Natarajan, S. (2018). A review of the scaled boundary finite element method for two-dimensional linear elastic fracture mechanics. *Engineering Fracture Mechanics, 187*, 45-73.

Sorensen, D. R., & Smith, F. W. (1976). The semi-elliptical surface crack - a solution by the alternating method. *Int. Journal of Fracture, 12*(1), 47-57.

Sripichai, K., & Pan, J. (2012). Closed-form structural stress and stress intensity factor solutions for spot welds in square overlap parts of cross-tension specimens. *Engineering Fracture Mechanics, 96*, 307-327.

Stäcker, C., & Sander, M. (2017). Experimental, analytical and numerical analyses of constant and variable amplitude loadings in the very high cycle fatigue regime. *Theoretical and Applied Fracture Mechanics, 92*, 394-409.

Stephan, P., & Costabel, M. (1987). An improved boundary element galerkin method for threedimensional crack problems. *Integral Equations and Operator Theory*, 10.

Sung, H. K., Kang, Y. L., & Moon, B. P. (1996). Mode II stress intensity factor for layered material under arbitrary shear crack surface loading. *Engineering Fracture Mechanics, 55*(1), 85-94.

Sung, S.-J., & Pan, J. (2017). Accurate analytical structural stress and stress intensity factor solutions for similar and dissimilar spot welds in lap-shear specimens. *Engineering Fracture Mechanics, 182*, 265-286.

Tada, H., Paris, P. C., & Irwin, G. R. (2000). *The stress analysis of cracks handbook, 3rd ed*. New York: ASME.

Tan, H. Q., Xu, M. H., Biniendal, W. K., & Arnold, S. M. (1993). Stress intensity factors in a fully interacting, multicracked, isotropic plate. *Computational Mechanics, 12*(5), 1-18.

Tao, Y., Fang, Q., Liu, Y., Liu, F., & Wen, P. (2015). Stress intensity factor of a mode I crack inside a nanoscale cylindrical inhomogeneity. *Engineering Fracture Mechanics, 141*, 44-56.

Toribio, J., Sanchez-Galvez, V., Astiz, M. A., & Campos, J. M. (1991). Stress intensity factor solutions for a cracked bolt under tension, bending and residual stress loading. *Engineering Fracture Mechanics, 39*(2), 359-371.

Uslu, M., Demir, O., & Ayhan, A. O. (2014). Surface cracks in finite thickness plates under thermal and displacement-controlled loads – Part 1: Stress intensity factors.

Engineering Fracture Mechanics, 115, 284-295.

Valiente, A. (1980). Fracture Criteria for Wires. *PhD thesis, Polytechnic University of Madrid, Spain*.

Wang, Q., & Zhang, X. (1999). A closed form solution about stress intensity factors of shear modes for 3-D finite bodies with eccentric cracks by the energy release rate method. *International Journal of Solids and Structures, 36*(7), 971-998.

Wang, Q. Z., Gou, X. P., & Fan, H. (2012). The minimum dimensionless stress intensity factor and its upper bound for CCNBD fracture toughness specimen analyzed with straight through crack assumption. *Engineering Fracture Mechanics, 82*, 1-8.

Wang, W., Zhou, A., Fu, G., Li, C.-Q., Robert, D., & Mahmoodian, M. (2017). Evaluation of stress intensity factor for cast iron pipes with sharp corrosion pits. *Engineering Failure Analysis, 81*, 254-269.

Wearing, J. L., & Ahmadi-Brooghani, S. Y. (1999). The evaluation of stress intensity factors in plate bending problems using the dual boundary element method. *Engineering Analysis with Boundary Elements, 23*(1), 3-19.

Weili, C., & Finnie, I. (1989). Stress intensity factors for radial cracks in circular cylinders and other simply closed cylindrical bodies. *Engineering Fracture Mechanics, 32*(5), 767-774.

Weißgraeber, P., Felger, J., Geipel, D., & Becker, W. (2016). Cracks at elliptical holes: Stress intensity factor and Finite Fracture Mechanics solution. *European Journal of Mechanics - A/Solids, 55*, 192-198.

Westgaard, H. M. (1939). Bearing pressures and crack. *J.Appl.Maths Mech., 6*, 49-53.

Wu, X. R. (1984). Approximate weight functions for center and edge cracks in finite bodies. *Engineering Fracture Mechanics, 20*(1), 35-49.

Wu, X. R. (1992). Analytical wide-range weight functions for various finite cracked bodies. *Engineering Analysis with Boundary Elements, 9*(4), 307-322.

Wu, X. R., Zhao, X. C., Xu, W., & Tong, D. H. (2018). Discussions on weight functions and stress intensity factors for radial crack(s) emanating from a circular hole in an infinite plate. *Engineering Fracture Mechanics, 192*, 192-204.

Xie, Y. J., Wang, X. H., & Wang, Y. Y. (2007). Stress intensity factors for cracked homogeneous and composite multi-channel beams. *International Journal of Solids and Structures, 44*(14-15), 4830-4844.

Xie, Y. J., Xu, H., & N., L. P. (1998). Crack mouth energy-release rate and its application. *Theoretical and Applied Fracture Mechanics, 29*(3), 195-203.

Xu, X. S., Zhou, Z. H., & Leung, A. Y. T. (2010). Analytical stress intensity factors for edge-cracked cylinder. *International Journal of Mechanical Sciences, 52*, 892-903.

Yan, F., Feng, X.-T., Lv, J.-H., & Li, S.-J. (2017). A continuous–discontinuous hybrid boundary node method for solving stress intensity factor. *Engineering Analysis with Boundary Elements, 81*, 35-43.

Yang, K., He, C., Huang, Q., Huang, Z. Y., Wang, C., Wang, Q., Zhong, B. (2017). Very high cycle fatigue behaviors of a turbine engine blade alloy at various stress ratios. *International Journal of Fatigue, 99*, 35-43.

Yin, Y., Wang, M., Han, Q., Wang, D., & Zhou, L. (2017). Stress intensity factors for L-shaped corner cracks in steel members with rectangular hollow section. *Engineering Fracture Mechanics, 170*, 107-118.

Yu, H., Sumigawa, T., Wu, L., & Kitamura, T. (2015). Generalized domain-independent interaction integral for solving the stress intensity factors of nonhomogeneous materials. *International Journal of Solids and Structures, 67-68*, 151-168.

Yu, P., Wang, Q., Zhang, C., & Zhao, J. (2018). Elastic T-stress and I-II mixed mode stress intensity factors for a through-wall crack in an inner-pressured pipe. *International Journal of Pressure Vessels and Piping, 159*, 67-72.

Zamani, N. G., & Sun, W. (1993). A direct method for calculating the stress intensity factor in BEM. *Engineering Analysis with Boundary Elements, 11*(4), 285-292.

Zareei, A., & Nabavi, S. M. (2016). Calculation of stress intensity factors for circumferential semi-elliptical cracks with high aspect ratio in pipes. *International Journal of Pressure Vessels and Piping, 146*, 32-38.

Zerbst, U., Ainsworth, R. A., Beier, H. T., Pisarski, H., Zhang, Z. L., Nikbin, K., Klingbeil, D. (2014). Review on fracture and crack propagation in weldments – A fracture mechanics perspective. *Engineering Fracture Mechanics, 132*, 200-276.

Zhang, R., & Guo, R. (2018). Determination of crack tip stress intensity factors by singular Voronoi cell finite element model. *Engineering Fracture Mechanics*.

Zhao, B., Liu, T., Pan, J., Peng, X., & Tang, X. (2017). A stress analytical solution for

Mode III crack within modified gradient elasticity. *Mechanics Research Communications, 84*, 142-147.

Zhao, J., Xie, L., Liu, J., & Zhao, Q. (2012). A method for stress intensity factor calculation of infinite plate containing multiple hole-edge cracks. *International Journal of Fatigue, 35*(1), 2-9.

Zhao, X., Zhao, X., Liu, C., Wen, Z., & Jin, X. (2016). A study on dynamic stress intensity factors of rail cracks at high speeds by a 3D explicit finite element model of rolling contact. *Wear, 366-367*, 60-70.

Zheng, X. J., Kiciak, A., & Glinka, G. (1997). Weight functions and stress intensity factors for internal surface semi-elliptical crack in thick-walled cylinder. *Engineering Fracture Mechanics, 58*, 207-221.